Agenzia nazionale per le nuove tecnologie,
l'energia e lo sviluppo economico sostenibile

MINISTERO DELLO SVILUPPO ECONOMICO

Modeling and Analysis of Nuclear Fuel Pin Behavior for Innovative Lead Cooled FBR

L. Luzzi, S. Lorenzi, D. Pizzocri, D. Rozzia, A. Aly, A. Del Nevo

Report RdS/PAR2013/022

Modeling and Analysis of Nuclear Fuel Pin Behavior for Innovative Lead Cooled FBR

L. Luzzi, S. Lorenzi, D. Pizzofri - CIRTEN POLIMI, D. Rozzia, A. Aly, A. Del Nevo - ENEA

Settembre 2014

Report Ricerca di Sistema Elettrico
Accordo di Programma Ministero dello Sviluppo Economico - ENEA
Piano Annuale di Realizzazione 2013
Area: Produzione di energia elettrica e protezione dell'ambiente
Progetto: Sviluppo competenze scientifiche nel campo della sicurezza nucleare e collaborazione ai programmi internazionali per il nucleare di IV Generazione
Obiettivo: Sviluppo competenze scientifiche nel campo della sicurezza nucleare
Responsabile del Progetto: Mariano Tarantino, ENEA

Il presente documento descrive le attività di ricerca svolte all'interno dell'Accordo di collaborazione "Sviluppo competenze scientifiche nel campo della sicurezza e collaborazione ai programmi internazionali per il nucleare di IV generazione"

Responsabile scientifico ENEA: Mariano Tarantino

Responsabile scientifico CIRTEN: Giuseppe Forasassi

ENEA Ricerca Sistema Elettrico	Sigla di identificazione	Distrib.	Pag.	di
	ADPFISS – LP2 – 054	L	1	75

Titolo

Modeling and analysis of nuclear fuel pin behavior for innovative lead cooled FBR

Descrittori

Tipologia del documento: Rapporto Tecnico

Collocazione contrattuale: Accordo di programma ENEA-MSE su sicurezza nucleare e Reattori di IV generazione

Argomenti trattati: Reattori Nucleari Veloci, Sicurezza nucleare, Analisi incidentale

Sommario

In relazione alle attuali linee di ricerca su sicurezza e reattori veloci di IV generazione, l'attività svolta si è posta l'obiettivo di sviluppo ed estensione del codice di fuel pin performance TRANSURANUS per l'analisi di reattori innovativi raffreddati a piombo. La suddetta versione estesa del codice, denominata LFR-oriented, permette la modellazione e l'analisi termo-meccanica delle barrette di combustibile adottate nel reattore a piombo scelto come riferimento (ALFRED - Advanced Lead-cooled Fast Reactor), al fine di ottimizzarne il design e le caratteristiche di sicurezza. L'attività descritta nel presente report si divide in 2 parti.

Una prima parte ha riguardato una revisione critica dei principali modelli fenomenologici per il piombo e per gli acciai austenitici della classe 15-15Ti, materiale di guaina che si prevede di adottare in ALFRED. In particolare, sulla base dei dati sperimentali disponibili in letteratura, tale lavoro ha permesso di conseguire i seguenti risultati principali: 1) condurre una revisione critica delle correlazioni disponibili per i suddetti materiali nella versione originaria di TRANSURANUS (versione v1m3j12); 2) mettere a punto correlazioni specifiche per la modellazione sia dell'acciaio di guaina AIM1, sia di un generico acciaio della classe 15-15Ti, focalizzando l'attenzione sulle problematiche relative allo swelling, allo scorrimento viscoso e ai tempi di rottura per interazione meccanica guaina-combustibile (aspetto cruciale, che era assente nella versione v1m3j12); 3) realizzare la versione estesa di TRANSURANUS, adatta per le analisi termo-meccaniche delle barrette di combustibile impiegate nei reattori a piombo.

La seconda parte ha una revisione critica dei principali modelli di conduzione per combustibili MOX con aggiunta di percentuali di attinidi minori, per predisporre la fase di sviluppo e implementazione nel codice TRANSURANUS di tali modelli. L'attività, dopo aver identificato tutti principali parametri e processi che influenzano la conducibilità, ha riguardato la valutazione delle correlazioni disponibili del codice TRANSURANUS, riportando le correlazioni, le dipendenze ed i range di validità. Successivamente si è fatta una rassegna dei modelli disponibili in letteratura, rilevanti allo scopo dell'attività e derivabili dalle attività sperimentali effettuate nell'ambito del progetto FP7 PELGRIMM.

Note:

Autori:

L. Luzzi, S. Lorenzi, D. Pizzocri (CIRTEN-POLIMI)
D. Rozzia, A. Aly A. Del Nevo (ENEA)

Copia n. In carico a:

REV.	DESCRIZIONE	DATA		REDAZIONE	CONVALIDA	APPROVAZIONE
1			NOME			
			FIRMA			
0	EMISSIONE	26/09/14	NOME	A. Del Nevo	M. Tarantino	M. Tarantino
			FIRMA			

(This page has been intentionally left blank)

CIRTEN

Consorzio **I**nteruniversitario per la **R**icerca **TE**cnologica **N**ucleare

POLITECNICO DI MILANO

DIPARTIMENTO DI ENERGIA, Sezione INGEGNERIA NUCLEARE - CeSNEF

Part1

Modeling and analysis of nuclear fuel pin behavior for innovative lead cooled FBR

Lelio Luzzi, **Stefano Lorenzi, Davide Pizzocri**

CERSE-POLIMI RL 1493/2013

Milano, Agosto 2014

Lavoro svolto in esecuzione dell'Attività LP2.A.3_A
AdP MSE-ENEA sulla Ricerca di Sistema Elettrico - Piano Annuale di Realizzazione 2013
Progetto B.3.1 "Sviluppo competenze scientifiche nel campo della sicurezza nucleare e collaborazione ai programmi internazionali per il nucleare di IV generazione"

(this page is intentionally left blank)

LIST OF CONTENTS

(this page is intentionally left blank)

1 Introduction

The Lead-cooled Fast Reactor (LFR) has been selected by the Generation IV International Forum as one of the candidates for the next generation of nuclear power plants (GIF, 2002). Advanced reactor concepts cooled by Heavy Liquid Metals (HLMs) ensure a great potential for plant simplifications and higher operating efficiencies compared to other coolants, nevertheless introducing additional safety concerns and design challenges (Cacuci, 2010). Reactor conditions of HLM-cooled reactor designs (e.g., extended exposure to neutron irradiation, high temperature, corrosive environment) impose challenges for engineers and designers concerning the selection of structural and cladding materials. Key guidance on material behavior and help to improve the design can be achieved by means of fuel pin performance codes. Since the fuel pin behavior is determined by the synergy of several phenomena (heat transfer to the coolant, creep, swelling and corrosion of the cladding, relocation, densification, creep, and swelling of the fuel, fission gas release, etc.), a fuel pin analysis can be adequately accomplished by means of integral performance codes. In the present work, the TRANSURANUS code (Lassmann *et al.*, 2013) developed at JRC-ITU (Karlsruhe) has been extended for the analysis of nuclear fuel pin behavior of the LFR employing 15-15Ti austenitic steels as cladding material.

This work is grafted in the research activity of the Nuclear Reactor Group of the Politecnico di Milano on LFRs. The particular features of this innovative reactor concepts attained the attention of the European Commission and the LEADER Project (LEad Advanced DEmonstration Reactor) has been introduced in the 7th Framework Program (FP7 – http://wwpw.leader-fp7.eu/). As a part of the LEADER Project, the design of a demonstrator reactor is forecasted. This is a small (300 MWth) reactor called ALFRED (Advanced Lead-cooled Fast Reactor) whose aim is to prove the technical and economic feasibility of the Generation IV lead reactor concept (Alemberti *et al.*, 2013). The 15-15Ti austenitic steel is considered to be the cladding material in the ALFRED reactor, as well as for other fast reactor systems like the Accelerator-Driven System MYRRHA (Aït Abderrahim *et al.*, 2012) and the Sodium Fast Reactor ASTRID (Gavoille *et al.*, 2013). Despite the lower resistance to void swelling compared to the ferritic-martenstic steel T91 (the former candidate material for the cladding), the 15-15Ti austenitic steel has been selected due to the better thermal creep resistance, the good mechanical strength and because it has been already qualified and licensed in fast reactors.
This report presents a critical review of the main LFR material properties (except for the fuel, which is out of the scope of the present deliverable), aimed at the extension and validation of the fuel pin performance code TRANSURANUS (TU) for modeling and analyzing the fuel pin integral behavior in innovative LFRs, specifically referring to the ALFRED reactor.
Actually, an *LFR-oriented version* of TRANSURANUS represents the first, necessary step in a more general process of analysis and optimization (see Figure 1), finalized to support the design and the construction of ALFRED by means of the following actions:

i) critical analysis of the fuel pin behavior in reactor through the study of a "reference case" (based on "best estimate" models) to verify the respect of design limits;
ii) identification of possible critical issues through an extensive sensitivity analysis on the most significant phenomena (both in normal operation and accident conditions) affected by a considerable modeling uncertainty, and oriented to the definition of a "worst case scenario" for the fuel pin performance;

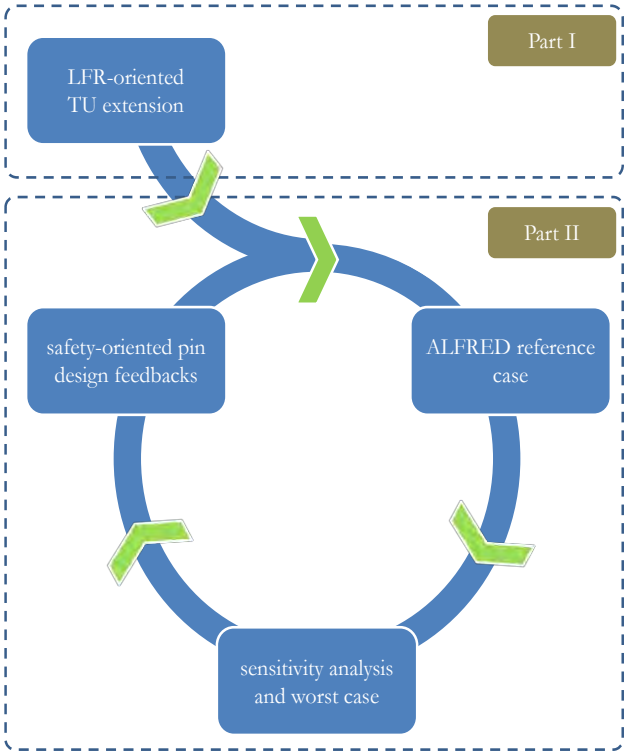

Figure 1: Scheme of the optimization process that can be carried out by means of the extended TRANSURANUS version to give feedbacks on the ALFRED conceptual design.

iii) optimization of the fuel pin design, in order to improve the performance and safety-by-design features of the ALFRED reactor;

iv) identification of design solutions aimed at achieving enlarged safety margins and of the most adequate FA geometrical configuration from the thermo-mechanical point of view (e.g., optimization of the radial power peak factor in the reactor core).

The *v1m3j12 version* of the TRANSURANUS code has to be considered as the starting point of the work, which has permitted the development of an *LFR-oriented version* that includes an updating of the correlations for the thermo-physical properties of the lead and introduces new correlations for swelling, thermal creep and heat capacity of the 15-15Ti austenitic steels. As first step of this process, a review of the main properties of lead as a coolant is carried out, making a comparison with literature data. Afterwards, a critical review of the correlations for the 15-15Ti austenitic steels is performed.

In this report, on the basis of the information available in literature, the correlations included in the LFR-oriented version of TRANSURANUS, for evaluating the thermo-physical properties of lead, the thermo-mechanical properties and the treatment of the in-reactor behavior of 15-15Ti steels, are reported.

LIST OF SYMBOLS

Latin symbols

A, B, C	materials constants
c_p	specific heat (at constant pressure) [J kg^{-1} K^{-1}]
CDF	cladding cumulative damage function [-]
D	pin diameter [m]
E	Young's modulus [GPa]
$\overline{E}$	mean neutron energy [MeV]
EAB	elongation at break [%]
LMP	Larson-Miller Parameter
Nu	Nusselt number [-]
Nu_{lam}	laminar Nusselt number (Ushakov correlation) [-]
p	pin pitch [m]
P	P parameter (thermal creep)
Pe	Peclet number [-]
R	perfect gas constant [cal mol^{-1} K^{-1}]
t	temperature [°C]
t_R	rupture time [h]
T	temperature [K]
T_{boil}	boiling temperature [K]
T_l	*liquidus* temperature [K]
T_{melt}	melting temperature [K]
T_s	*solidus* temperature [K]

Greek symbols

ΔH	specific activation energy [cal mol^{-1}]
Δt	time interval [h]
$\frac{\Delta V}{V}$	volume swelling strain [%]
ε	equivalent thermal creep strain [%]
$\dot{\varepsilon}$	equivalent creep strain rate [% h^{-1}]
ε_{th}	equivalent thermal creep cladding hoop strain [%]
$\varepsilon_{th,R}$	equivalent thermal creep cladding rupture strain [%]
λ	thermal conductivity [W m^{-1} K^{-1}]
ρ	density [kg m^{-3}]
ρ_0	density at 20°C [kg m^{-3}]
σ	stress (Von Mises equivalent) [MPa]
σ_{UT}	ultimate tensile strength [MPa]
$\sigma_{Y,0.2\%}$	yield strength [MPa]
φ	fast neutron flux [n cm^{-2} s^{-1}]
Φ	fast neutron fluence [10^{22}]
ζ	linear thermal expansion coefficient [%]
ω	Ushakov correlation parameter [-]

Δ indicates variations

LIST OF ACRONYMS

AIM	Austenitic Improved Material
ALFRED	Advanced Lead-cooled Fast Reactor European Demonstrator
ASTRID	Advanced Sodium Technological Reactor for Industrial Demonstration
CEA	Commisariat à l'Energie Atomique
CDF	Cumulative Damage Function
FA	Fuel Assembly
FAE	Fuel Adjacency Effect
FBR(s)	Fast Breeder Reactor(s)
FP7	7th Framework Program
GESA	Gepulste ElektronenStrahlAnlage
GIF	Generation IV International Forum
HLM	Heavy Liquid Metals
INL	Idaho National Laboratory
ITU	Institute for TransUranium elements
JOG	Joint Oxide-Gain
JRC	Joint Research Center
LEADER	Lead-cooled European Advanced DEmonstration Reactor
LFR(s)	Lead-cooled Fast Reactor(s)
LMFR(s)	Liquid Metal-cooled Fast Reactor(s)
LMP	Larson-Miller Parameter
MYRRHA	Multipurpose hYbrid Research Reactor for High-tech Applications
MOX	Mixed OXyde
NEA	Nuclear Energy Agency
OECD	Organization for Economic Co-operation and Development
P	Parameter, cladding thermal creep
PCMI	Pellet Cladding Mechanical Interaction
PLD	Pulsed Laser Deposition
POLIMI	Politecnico di Milano
POLITO	Politecnico di Torino
SFR	Sodium Fast Reactor(s)
TU	TRANSURANUS
UT	Ultimate Tensile strength
YS	Yield Strength

LIST OF FIGURES

LIST OF TABLES

2 Lead as a coolant in fast reactors

In this section, the properties of lead are presented, focusing in particular on its use as a coolant in fast reactors. The OECD-NEA Handbook (OECD-NEA, 2007) has been used as summarized and reasoned reference.

2.1 General considerations

Pure lead is an interesting coolant in fast reactors due to its high mass number and its low absorption cross-section, which are fundamental properties for a fast reactor coolant. It has good thermal characteristics for heat removal. With respect to sodium and lead-bismuth eutectic (the other metals proposed as coolants in innovative LMFRs), it has high melting temperature (327°C, 600 K) and an high boiling point (1749°C, 2022 K) allowing a wide range of operation.

Compared to sodium, it does not present the problem of strong exothermic reaction with air and water, while with respect to the lead-bismuth eutectic, it is less corrosive, it does not present the problem of activation issue typical of bismuth (polonium production) and does not present the issue of solidification volume growth. Nevertheless, it is steel-aggressive for the core materials both for erosion and corrosion issues (therefore, a flow velocity of less than 2 m s^{-1} is envisaged, and an oxygen control and/or a coating for cladding are required, respectively) and it is very toxic and polluting, requiring particular attention from production to disposal or recycling.

2.2 Heat exchange correlation for Nusselt number

Liquid lead is meant to be the coolant of LFRs. Therefore, its heat exchange properties are fundamental. The heat exchange correlation has been developed by Ushakov *et al.* (1977) for regular hexagonal fuel elements, far from spacing grids.
The correlation that is called in the TRANSURANUS routine is the following:

$$\mathrm{Nu} = 7.55\frac{\mathrm{p}}{\mathrm{D}} - 20\left(\frac{\mathrm{p}}{\mathrm{D}}\right)^{-13} + \frac{3.67}{90}\left(\frac{\mathrm{p}}{\mathrm{D}}\right)^{-2}\mathrm{Pe}^{\left(0.56+0.19\frac{\mathrm{p}}{\mathrm{D}}\right)} \quad (1)$$

$1.2 \leq \frac{\mathrm{p}}{\mathrm{D}} \leq 2.0$ (1.3 < p/D < 2.0 in TU)

$1 < Pe < 4000$

In Figure 2, Ushakov correlation is plotted (Nu as a function of Pe) for three different pitch parameters (p/D = 1.30, 1.35 and 1.40).

It should be noted that this correlation is just an approximation of the Ushakov complete correlation for triangular lattice, acceptable in the range of pin-pitch over diameter indicated above. The complete correlation is reported in Equation (2).

$$\mathrm{Nu}_{\mathrm{lam}} = \left(7.55\frac{\mathrm{p}}{\mathrm{D}} - 6.3\left(\frac{\mathrm{p}}{\mathrm{D}}\right)^{-17\frac{\mathrm{p}}{\mathrm{D}}\left(\frac{\mathrm{p}}{\mathrm{D}}-0.81\right)}\right)\left(1 - \frac{3.6\frac{\mathrm{p}}{\mathrm{D}}}{\left(\frac{\mathrm{p}}{\mathrm{D}}\right)^{20}(1+2.5\omega^{0.86})+3.2}\right) \quad (2)$$

$$Nu = Nu_{lam} + \frac{3.67}{90\left(\frac{p}{D}\right)^2}\left(1 - \frac{1}{\frac{1}{6}\left(\left(\frac{p}{D}\right)^{30} - 1\right) + \sqrt{1.15 + 1.24\omega}}\right) Pe^{0.56+0.19\frac{p}{D}-0.1\left(\frac{p}{D}\right)^{-80}}$$

$$\omega = \frac{\text{conductivity of coolant}}{\text{conductivity of cladding}}$$

$$1 < Pe < 4000$$

$$1.0 \leq \frac{\text{p}}{\text{D}} \leq 2.0$$

$$\omega > 0.01$$

The complete correlation is implemented in TRANSURANUS, and called only when $\frac{\text{p}}{\text{D}}$ is out of the validity range for the simplified one.

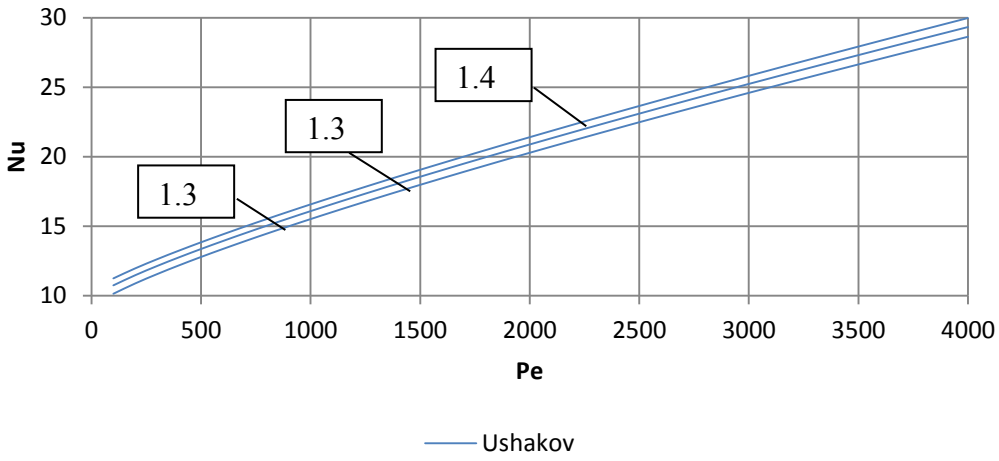

Figure 2: Nusselt number dependence on Peclet number and on pitch parameters for liquid pure lead in a triangular lattice (far from spacers) according to simplified Ushakov correlation. The three curves are plotted with p/D = 1.30, 1.35 and 1.40.

2.3 Corrosion of the cladding

The problem of keeping a stainless steel in the aggressive environment represented by liquid lead is not yet solved, but certainly maintaining flow velocity under 2 m s^{-1} reduces the erosion effect. Nevertheless, the stainless steel of which the cladding is made requires further protection, and different coating layers are under development. Among the proposed solutions, the most promising are the FeCrAlY alloy, realized through the so-called GESA (Gepulste ElektronenStrahlAnlage) treatment (Weisenburger *et al.*, 2008) and the Al_2O_3 coating realized through Pulse Laser Deposition (PLD) (Garcia Ferrè *et al.*, 2013)[1]. For our purposes, the modeling solution that can be adopted is substitute an external layer of the cladding (40 μm) by a coating which is not affected by

[1] The lead corrosion and erosion of the cladding is a critical issue for LFR development. A complete review of this research field goes beyond the scope of this work.

corrosion and is featured by a thermal conductivity of 16 W m^{-1} K^{-1} (Agosti *et al.*, 2013). Mechanical and irradiation effects on the coating are presently not taken into account.

2.4 Other relevant properties of lead

The other properties of liquid lead are less problematic for this work, and therefore they are simply reported with their correlation according to OECD-NEA (2007).

Melting point

OECD-NEA (2007) indicates an interpolation value between the ones available in literature. The dependence on pressure is in the order of a 0.08 K increase per 1 MPa increase and thus it has been disregarded.

$$T_{melt} = 600.6 \pm 0.1 \text{ K} \quad (3)$$

Boiling point

For boiling point, uncertainties are higher than for melting point. The value recommended in the OECD-NEA (2007) is the following:

$$T_{boil} = 2016 \pm 10 \text{ K} \quad (4)$$

Density

The density of liquid lead can be related to temperature with a simple linear correlation. Even if purity is not well specified in single references, agreement within data is very strong, with uncertainty under 1%. This is shown in Figure 3. The correlation is reported in Table 1.

Table 1: Liquid lead density correlation.

[T]	[ρ]	Reference
K	kg m^{-3}	OECD-NEA, 2007
Correlation		
$\rho = 11367 - 1.1944\ T$		

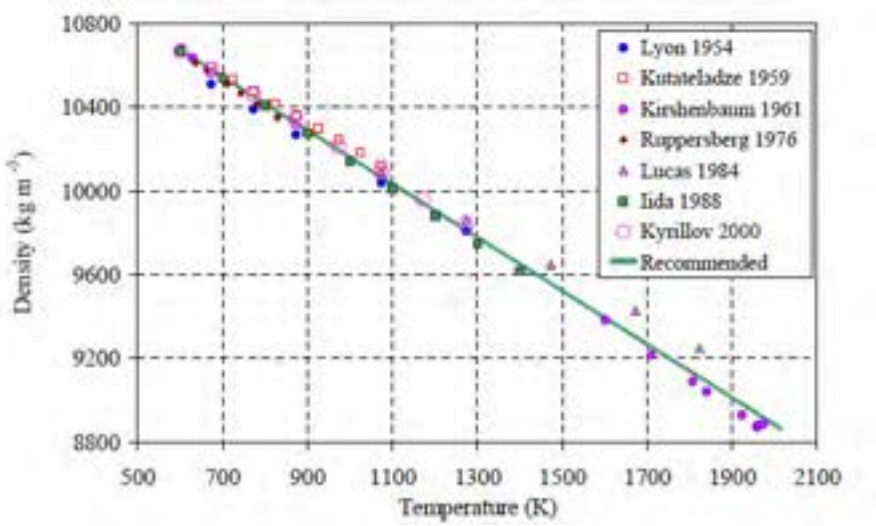

Figure 3: Liquid lead density (OECD-NEA, 2007).

Specific heat capacity at constant pressure

According to OECD-NEA (2007), Gurvich and Veyts (1991) correlation is suggested as a reasonable choice between available data (Table 2). Both data and correlation are plotted in Figure 4.

Table 2: Liquid lead specific heat capacity correlation.

[T]	$[c_p]$	Reference
K	$J\,kg^{-1}K^{-1}$	OECD-NEA, 2007
Correlation		
$c_p = 175.1 - 4.961\,10^{-2}\,T + 1.985\,10^{-5}\,T^2 - 2.099\,10^{-9}\,T^3 - 1.524\,10^{6}\,T^{-2}$		

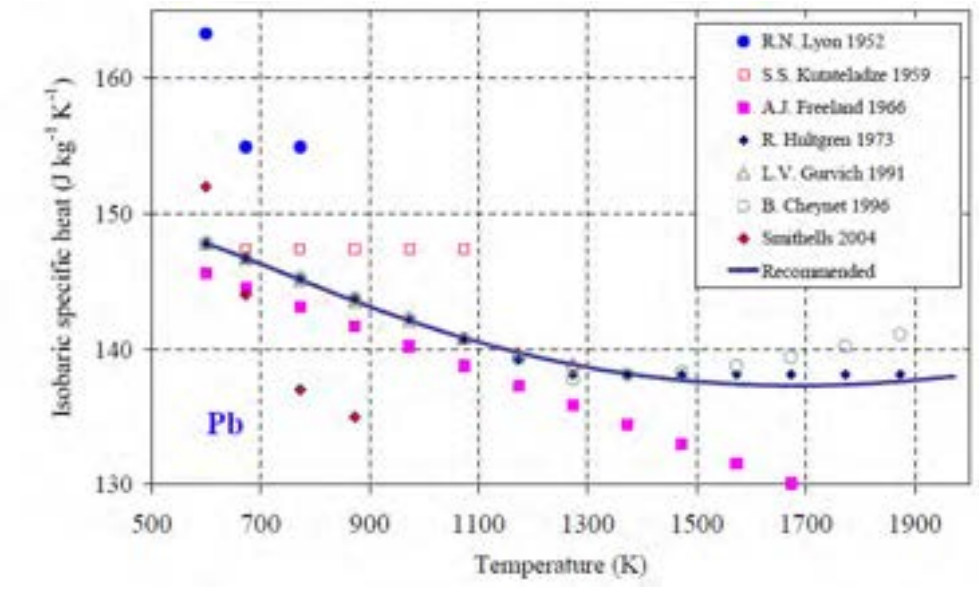

Figure 4: Gurvich correlation for isobaric specific heat of liquid lead as presented in OECD-NEA (2007).

Thermal conductivity

The data regarding the thermal conductivity of liquid lead are very dispersed. Therefore, in this case, the recommendation by OECD-NEA (2007) is particularly useful (Table 3). The proposed correlation is linear and fits well recent data, as is shown in Figure 5.

Table 3: Liquid lead thermal conductivity correlation.

[T]	[λ]	Reference
K	$W\,m^{-1}K^{-1}$	OECD-NEA, 2007
Correlation		
$\lambda = 9.2 + 0.011\,T$		

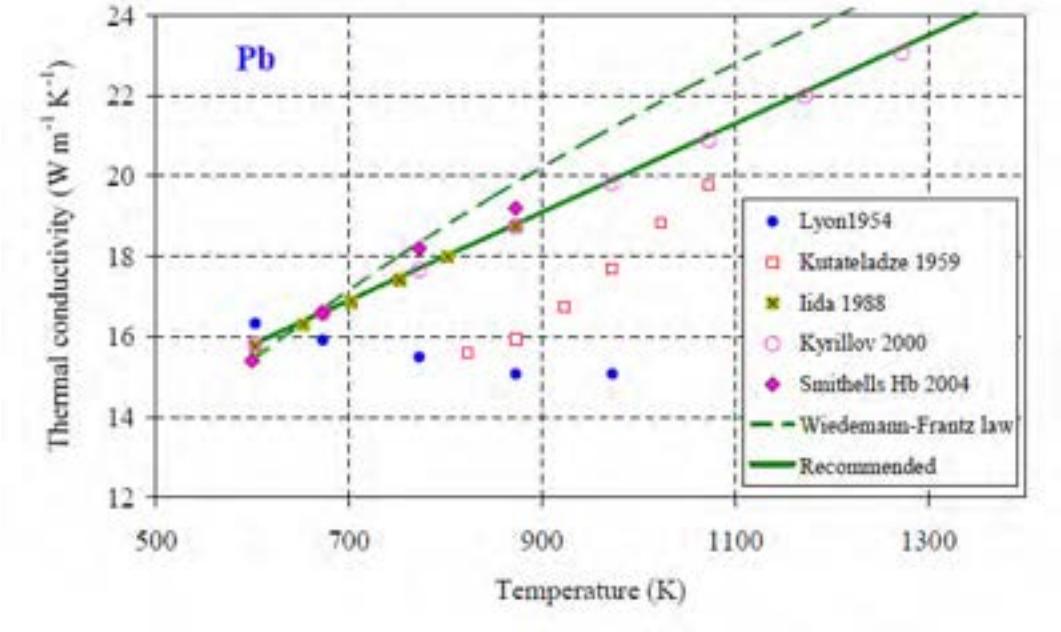

Figure 5: Liquid lead thermal conductivity (OECD-NEA, 2007).

3 Austenitic stainless steels for Lead-cooled Fast Reactors

This section presents the correlations for the main thermal and mechanical properties of 15-15Ti austenitic stainless steels adopted as cladding material for some lead-cooled fast nuclear reactors (e.g., ALFRED, MYRRHA).

Specific austenitic stainless steels have been developed to be used as cladding materials in fast reactors. The main advantages of these materials are their good thermal creep behavior and their excellent mechanical properties. The main issue for these materials is to resist swelling, avoiding the risk of gap reopening during fuel life and hence the occurrence of the so-called "thermal feedback effect" (Lombardi, 2006). This is achieved through the inclusion of titanium, whose little TiC precipitates are able to increase the incubation time of the phenomena interacting with the voids created by fast neutrons irradiation. Also silicon seems to play an important role in contrasting swelling. Moreover, the presence of boron goes in the direction of improving creep ductility (Frost, 1994). The characteristics of these steels may justify their use as structural materials also for other components, such as the Fuel Assemblies (FAs) wrapper.

Following this concept, a certain number of 15-15Ti steels has been developed in different countries: D9 in the US, AIM1 in France, DIN 1.4970 in Germany. The chemical compositions of these alloys is summarized in Table 4. All these materials are cold worked at 20%.

Table 4: Chemical composition of some austenitic stainless steels of the 15-15Ti family. Compositions are expressed in weight percentage [wt. %] (Gavoille et al., 2013; Banerjee et al., 2007).

	C	Cr	Ni	Mo	Si	Mn	Ti	Nb	P	B
AIM1	0.1	15	15	1.2	0.6	1.5	0.4	-	0.03	0.0060
DIN 1.4970	0.1	15	15	1.2	0.4	1.5	0.5	-	-	0.0045
D9	0.05	14	15	1.5	0.9	1.7	0.23	-	-	0.0015

In the following subsections, a review of the main properties of 15-15Ti will be presented, all described by out-of-pile correlations. The properties of the austenitic steels (Többe, 1975) are compared with other literature data in order to assess their validity. On the other hand, the specific heat (Banejree, 2007), the swelling and the thermal creep have been updated. In particular, these last two properties have been carefully evaluated since the different composition of the alloying material has a great impact on these material features.

3.1 Thermo-physical properties

Here below, the fundamental out-of-pile thermal properties of 15-15Ti austenitic stainless steels are reported. For all these properties, the effect of specific alloyed elements is minimum, and therefore the difference between the specific alloys (AIM1, 1.4970 and D9) is practically negligible. On the other hand, for some mechanical properties, swelling and thermal creep, the different percentage of the alloying elements has a relevant impact on these properties.

Melting temperature

In the TRANSURANUS code, the melting temperature is set in the SOLIMT subroutine at:

$$T_{melt} = 1673 \text{ K} \quad (5)$$

From literature data, the melting temperature (*liquidus*) and solidification temperature (*solidus*) have been measured for 1.4970 steel by Nikolopoulos and Schulz (1979). The values proposed in these references are:

$$T_l = 1690\ \text{K}\ (1417°\text{C}) \qquad (6)$$
$$T_s = 1680\ \text{K}\ (1407°\text{C})$$

Linear thermal expansion

The thermal expansion is here described by a strain parameter. The correlation implemented in TRANSURANUS is proposed by Gehr (1973).

Table 5: 15-15Ti steels linear thermal expansion correlation.

[t]	[ζ]	Reference
°C	–	Gehr, 1973

Correlation
$\zeta = -0.0003101 + 0.00001545\ t + 0.00000000275\ t^2$

In general, there is a good agreement between literature data, with no strong dependence on the chemical composition of the steel (around reference values) or on the thermo-mechanical process (cold working, aging). In Figure 6, the 1.4970 data reported in Rudtsch *et al.* (2005) are compared with the correlation implemented in the *LFR-oriented version*.

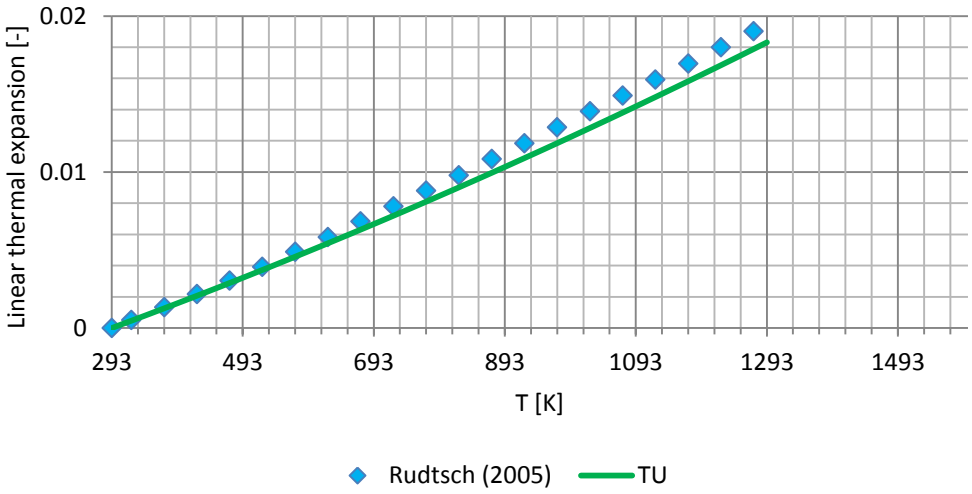

Figure 6: Comparison between the Rudtsch et al. (2005) data for linear thermal expansion and the correlation implemented in TRANSURANUS.

Density

The TRANSURANUS routine RO calculates the density of the steel as a function of temperature using the linear expansion correlation. The relation between these two quantities is straightforward:

$$\rho(T) = \rho_0 \left(\frac{1}{1+\zeta(T)}\right)^3 \qquad (7)$$

Therefore, only the value ρ_0 at a certain reference temperature is needed. Equation (7) is implemented in TRANSURANUS (Schumann, 1970), and results in good agreement with the value proposed by Rudtsch *et al.* (2005).

$t = 20$ [°C] (8)

$\rho_0 = 7900$ [kg m^{-3}]

An explicit fit for $\rho(T)$ is represented in Figure 7. This correlation does not present validity range problems.

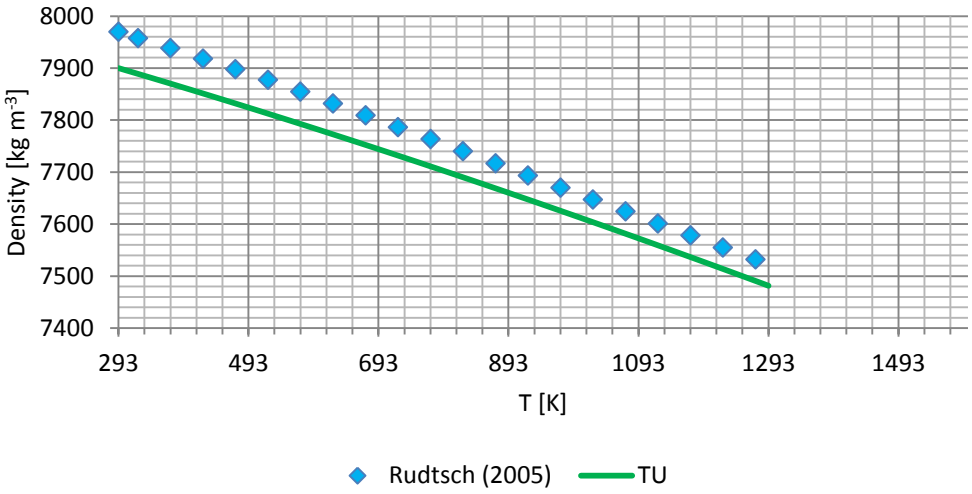

Figure 7: Comparison between the Rudtsch et al. (2005) data for density and the correlation implemented in TRANSURANUS.

Specific heat

Specific heat measurements have been carried out in the range 20÷1000°C (293÷1273 K). In Figure 8, the correlation proposed by Banerjee *et al.* (2007) is compared with the 1.4970 data reported in Rudtsch *et al.* (2005). The former correlation has been selected and implemented in the *LFR-oriented version*.

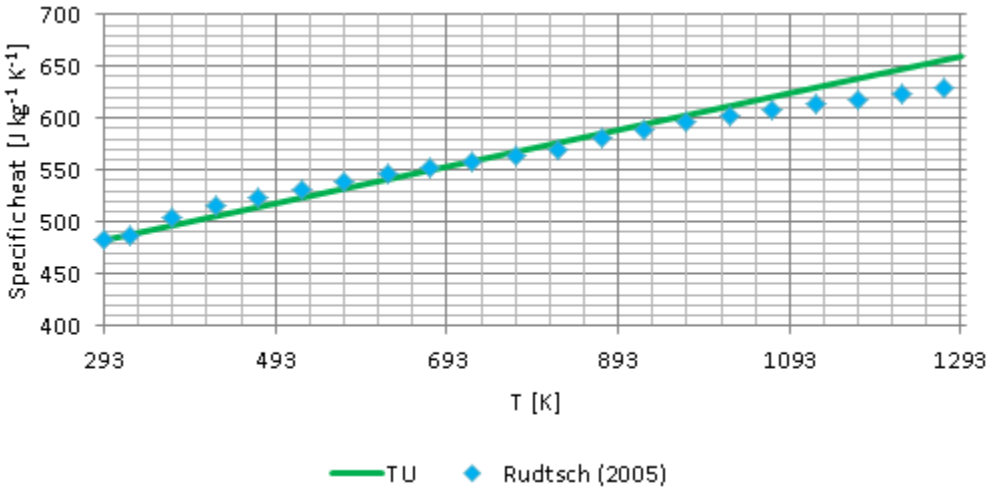

Figure 8: Specific heat correlation compared with recent experimental data for 1.4970 steel (Rudtsch et al., 2005).

In Table 6, the correlation plotted in Figure 8 is reported.

Table 6: 15-15Ti steels specific heat correlation.

[T]	[c_p]	Reference
K	J $kg^{-1}K^{-1}$	Banerjee, 2007

Correlation
$c_p = 431 + 0.177\ T + 0.0000872\ T^{-2}$

Thermal conductivity

The thermal conductivity of the cladding material is a fundamental property because it determines the temperature gradient across the cladding, controlling thermal stress and temperature levels (which determine all the other mechanical properties). Therefore, it is fundamental to have a reliable correlation implemented in the routine LAMBDA of TRANSURANUS code.

It should be noticed that the cold work treatment slightly alters the thermal conductivity (especially over 900 K, region in which also the measurement uncertainty grows). Therefore, the degree of cold work should be specified. In Figure 9, the correlation proposed by Tobbe (1975) and implemented in the *LFR-oriented version* is reported and compared with the data from Rudtsch *et al.* (2005) 20% cold worked 1.4970 steel.

Table 7: 15-15Ti steels thermal conductibility correlations.

[T]	[λ]	Reference
°C	W $m^{-1}K^{-1}$	Többe, 1975

Correlation
$\lambda = 13.95 + 0.01163t$

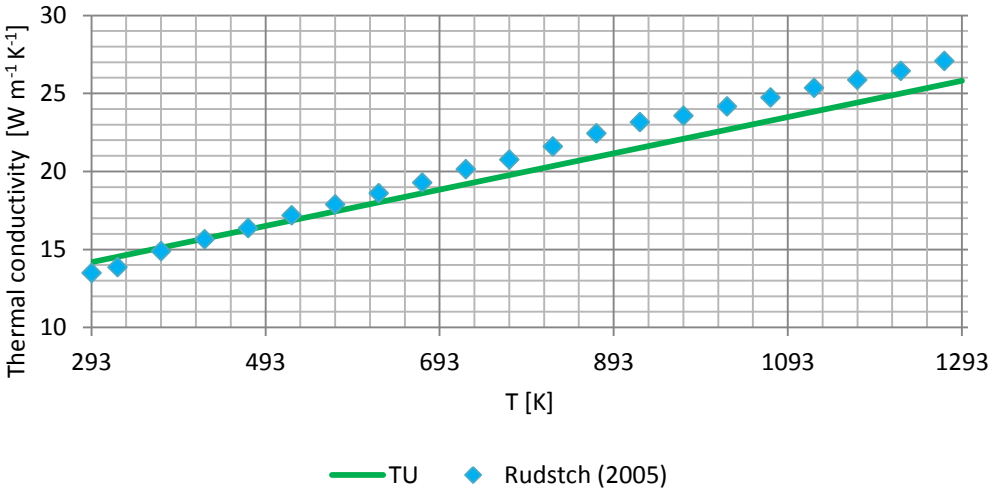

Figure 9: Comparison between correlation and experimental data for thermal conductivity of a Ti stabilized 20% cold worked austenitic stainless steel.

3.2 Mechanical properties

This subsection presents the most relevant mechanical properties of the 15-15Ti austenitic stainless steels. Thermal creep and swelling phenomena will be treated separately. All the properties presented here are intended out-of-pile, therefore only the dependence on temperature is considered. The properties already implemented in the *v1m3j12 version*, and also adopted in the *LFR-oriented version*, will be discussed and compared with data and correlations found in literature, pointing out the critical issues.

Young's modulus

There are very few data available in the open literature about the Young's modulus of a 15-15Ti steel (or about similar austenitic stainless steels). The only data found in literature come from Bergmann (1988) for 1.4970 steel. It is in general stated that the Young's modulus does not depend on the cold work degree. In Figure 10, the correlation proposed by Többe (1975) is plotted and compared with the data from Bergmann (1988).

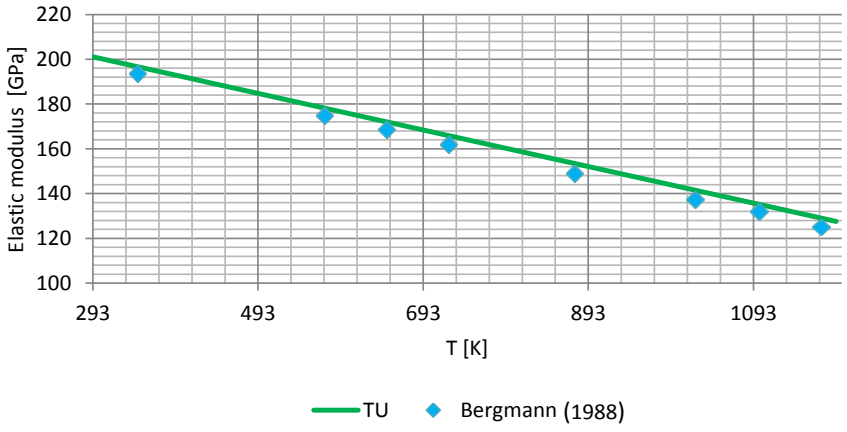

Figure 10: Comparison between correlation and experimental data for the elastic modulus of 15-15Ti stainless steel.

In Table 8, the correlation plotted in Figure 10 is reported. The range of validity should be the one explored in Bergmann experiment, 20÷800 °C (293-1073 K).

Table 8: 15-15Ti steels Young's modulus correlation.

[t]	[E]	Reference
°C	GPa	Többe, 1975

Correlation
$E = (202700 - 81.67t)/1000$

The correlation implemented in TRANSURANUS overestimates the elastic modulus in all the range of temperatures.

Yield strength and ultimate tensile strength

These properties are discussed together because they represent the basic parameters of the stress-strain diagram of a steel (along with rupture strain discussed in the next subsection and the Young's modulus). Moreover, it is important to notice that for these properties there is a quite strong disagreement between what reported in Filacchioni *et al.* (1990) and what implemented in TRANSURANUS (Többe, 1975). The data reported in Filacchioni *et al.* (1990) refer to the DS3, a 15-15Ti austenitic steel close to the AIM1. The discrepancies between the data and the correlation can be explained with the relevance of the alloying element for these properties. Accordingly, different steels of the 15-15Ti family can show very different behavior. It is important to remind that every property has to be intended out-of-pile.

According to the literature data, measurements have been carried out until roughly 1100 K (≈ 850°C) and therefore correlations are reliable until this temperature with around 10% of uncertainty. Nevertheless, the range of validity of these correlations is suitable for the fuel performance analysis of the LFR in operational cases.

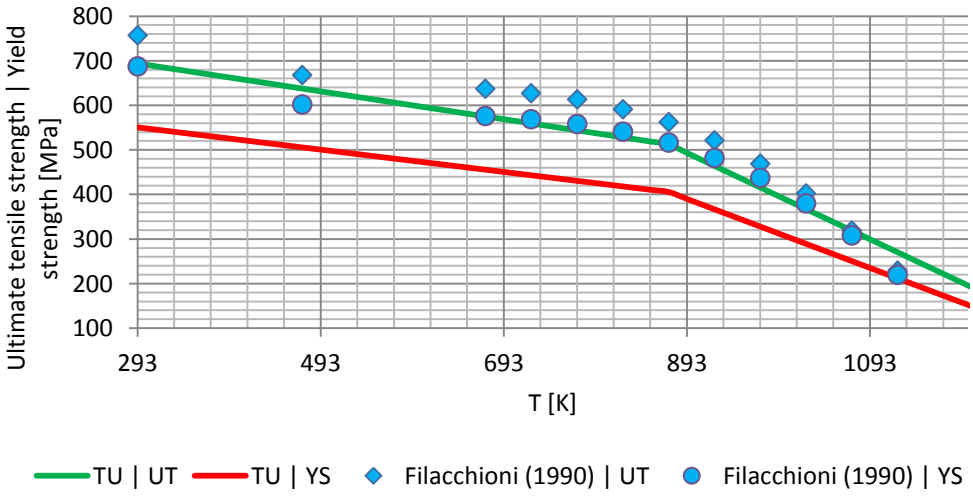

Figure 11: Correlations for ultimate tensile strength (UT) and yield strength (YS) are here plotted together.

In Table 9, the correlations plotted in Figure 11 are reported.

Table 9: 15-15Ti steels yield strength and ultimate tensile strength correlations.

[t]	[E]	Reference
°C	MPa	Többe, 1975

Correlation

$$\sigma_{Y,0.2\%} = \begin{cases} 555.5 - 0.25 \cdot T[°C] & if\ T < 600°C \\ 405.5 - 0.775 \cdot (T[°C] - 600) & if\ 600°C < T < 1000°C \\ 345.5 - 0.25 \cdot T[°C] & if\ T > 1000°C \end{cases}$$

$$\sigma_{UT} = \begin{cases} 700 - 0.3125 \cdot T[°C] & if\ T < 600°C \\ 512.5 - 0.96875 \cdot (T[°C] - 600) & if\ 600°C < T < 1000°C \\ 437.5 - 0.3125 \cdot T[°C] & if\ T > 1000°C \end{cases}$$

The third segment of the correlation implemented in TRANSURANUS has a slope which is less than the second segment, bringing to higher values of ultimate tensile strength at high temperature, not supported by open literature data.

Rupture strength is calculated from the rupture strain in TRANSURANUS, and therefore no specific correlation is implemented. Actually, also the rupture strain presents the same criticalities as the quantities described in this subsection.

Rupture strain

For the elongation at break it is fundamental to understand if the Többe (1975) data are reliable. There is disagreement between the correlation implemented in TRANSURANUS and the data proposed by Filacchioni *et al.* (1990) on DS3, similar to AIM1. Once again, this behavior can be explained with the different composition of the alloying element that dramatically influences some properties. In addition, this is the only property whose modeling in TRANSURANUS considers also the in-pile behavior: when neutron fluence exceeds 10^{22} n cm^{-2}, the rupture strain is set at 6%. A conversion factor of 2 10^{21} n cm^{-2} = 1 dpa is assumed. In Figure 12, the correlations are plotted. In Table 10, the out-of-pile correlation plotted in Figure 12 is shown.

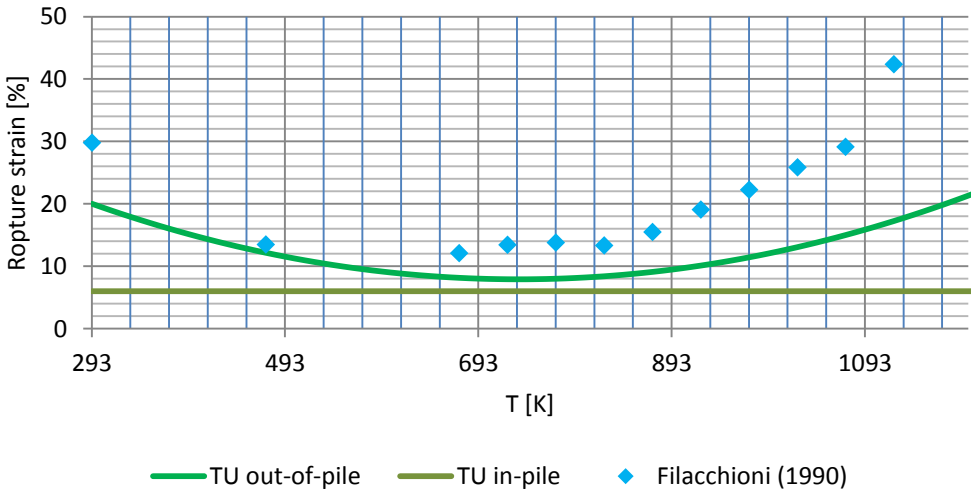

Figure 12: The mismatch between correlation and open literature data for the rupture strain of the 15-15Ti austenitic stainless steel is here clearly shown.

Table 10: 15-15Ti steels elongation at break correlations.

[t]	[EAB]	Reference
°C	%	Többe, 1975

Correlation

$$EAB = 8 + 0.00474\,(t - 500) + 0.000062\,(t - 500)^2$$

3.3 Swelling

Void swelling is a critical phenomenon for a cladding material to be used in a fast reactor. In particular, the risk of gap reopening and subsequent "thermal feedback" has to be avoided. Therefore, particular attention has been paid in adopting an austenitic stainless steel able to resist in an environment characterized by a fast neutron spectrum. Steels can be resistant to swelling in two ways: having long incubation time or having little swelling rates.

In principle, swelling depends also on stress, because the stress field influences the distribution of radiation induced point defects responsible of the phenomenon. A review of these effects can be found in Hübner (2000).

In order to implement swelling correlations in TRANSURANUS, it is necessary to consider both the dependence on temperature and the dependence on fast neutron fluence[2]. In this work, the subroutine SWELOC has been updated with two correlations concerning two class of austenitic stainless steels. The first, called "Specific AIM1", refers to the most advanced steel irradiated in Phénix (AIM1 austenitic stainless steel). The second, called "Generalized 15-15Ti", refers to an older version of the steel. In Figure 13, both these correlations are plotted.

"Specific AIM1"

$$\frac{\Delta V}{V}(\%) = 1.3\cdot 10^{-5} \exp\left[-\left(\frac{T(°C) - 490}{100}\right)^2\right]\Phi^{3.9} \qquad (9)$$

"Generalized 15-15Ti"

$$\frac{\Delta V}{V}(\%) = 1.5\cdot 10^{-3} \exp\left[-2.5\left(\frac{T(°C) - 450}{100}\right)^2\right]\Phi^{2.75} \qquad (10)$$

Φ is the fast neutron fluence divided by 10^{22} n cm^{-2}, while the conversion between fluence and dpa is $2\cdot 10^{21}$ (n cm^{-2})/dpa.

According to the data plotted in Figure 14, it seems reasonable to assume a best estimate incubation time in the order of 60 dpa, while for the worst case a reasonable incubation time could be around 20 dpa.

[2] There is an intrinsic relation between the swelling and the creep phenomena. Different approaches to consider this interaction have been proposed (Hübner, 2000), but they are not applied in the present work because of lack of data.

Before reporting the correlations implemented in the TRANSURANUS, it must be said that discrepancies in available data are very strong, that leads to the necessity of a sensitivity analysis for this important phenomenon. In any case, Dubuisson (2013) and Bergmann *et al.* (2003) are considered to be reliable data references.

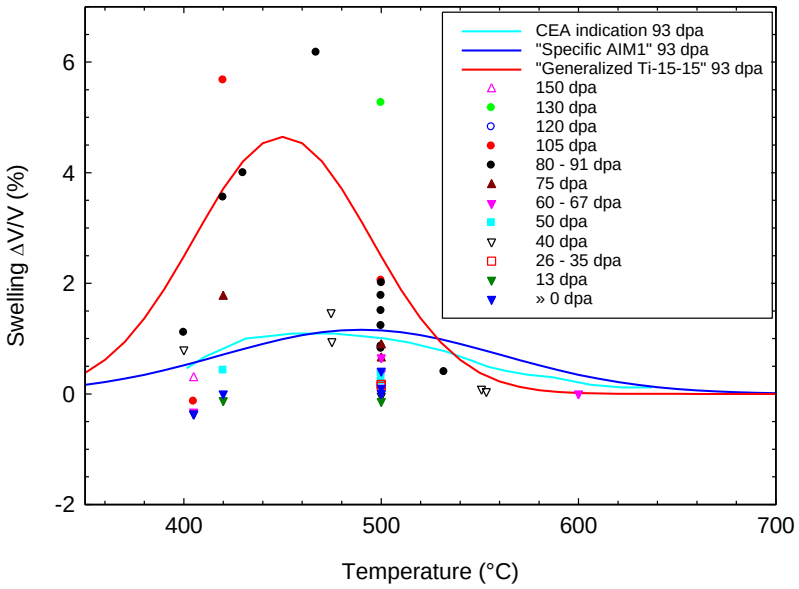

Figure 13: Comparison between experimental data and the "Specific AIM1" and "Generalized 15-15Ti" correlations for the cladding steel swelling as a function of temperature.

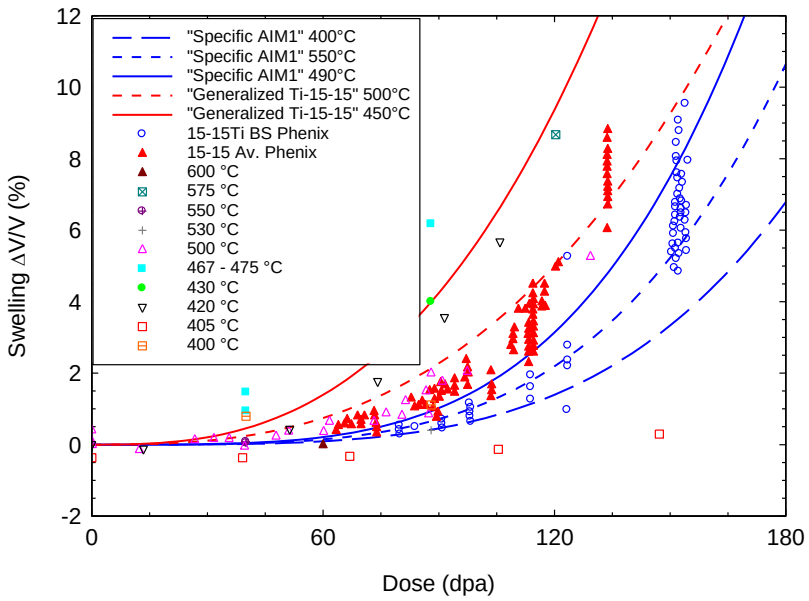

Figure 14: Comparison between experimental data and the "Specific AIM1" and "Generalized 15-15Ti" correlations for the cladding steel swelling as a function of dpa.

3.4 Thermal creep strain rate

Thermal creep is a critical phenomenon for the cladding steel. The different chemical composition in terms of alloying elements plays a fundamental role in determining the creep strain rate of a steel.

Therefore, in the *LFR-oriented version* two specific correlations for 1.4970m and AIM1 steels have been included.

1.4970m creep strain rate

For the 1.4970m specific steel of the 15-15Ti class, Többe (1975) correlation, already present in the *v1m3j12 version*, has been adopted in the *LFR-oriented version* for the thermal creep strain rate (Table 11). The structure of this correlation is a Nabarro-Herring equation, different from the typical Arrhenius equations used in creep strain rate modeling. In Figure 15, the correlation is plotted.

Table 11: 1.4970m thermal creep strain rate correlation.

[ε̇]	[σ]	[T]	Reference
% h^{-1}	MPa	K	Többe, 1975

Correlation
$\dot{\varepsilon} = 7.49\ 10^{+15}\ e^{-\frac{91000}{1.986\ T}} \sinh\frac{57.46\ \sigma}{1.986\ T}$

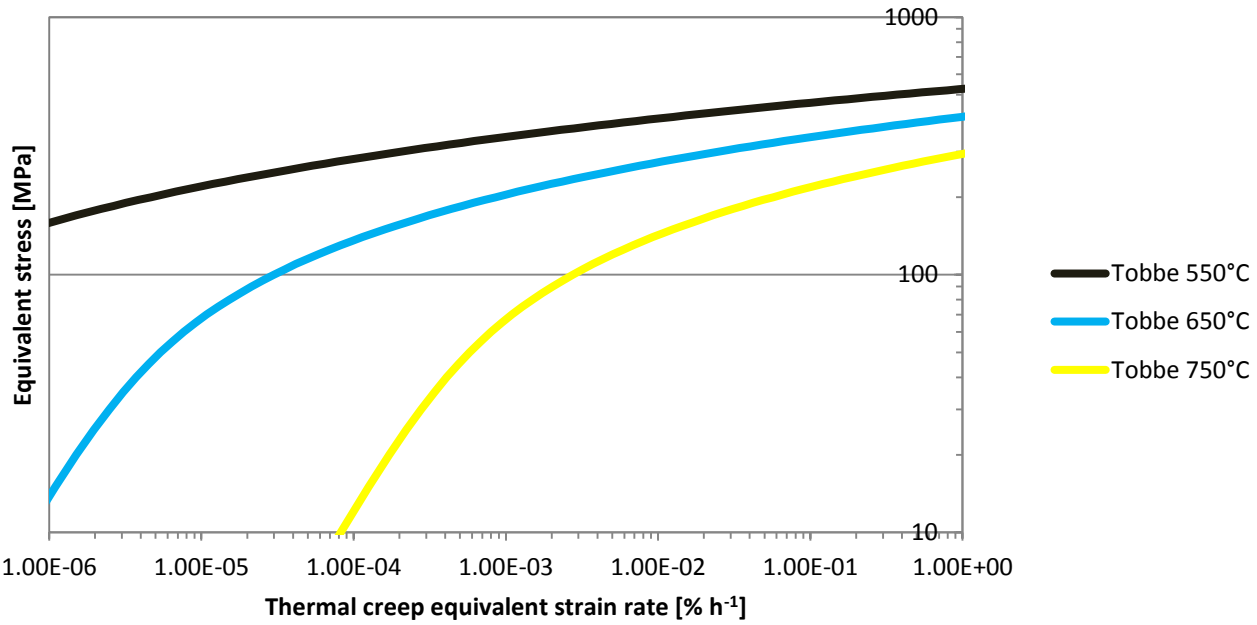

Figure 15: Többe correlation for the thermal creep strain rate of 1.4970m steel.

AIM1 creep strain rate

For the AIM1 specific steel of the 15-15Ti class, a modified version of the Többe correlation is adopted (Table 12), fitting Gavoille et al. (2013) data. This correlation is implemented in the LFR-oriented version of TRANSURANUS. In Figure 16, the correlation is compared also with experimental data from Filacchioni et al. (1990). Also this correlation presents a Nabarro-Herring structure.

Table 12: AIM1 thermal creep strain rate correlation.

[$\dot{\varepsilon}$]	[σ]	[T]	Reference
% h^{-1}	MPa	K	Gavoille *et al.*, 2013 (data)

Correlation
$\dot{\varepsilon} = 2.30\ 10^{+14}\ e^{-\frac{84600}{1.986\ T}} \sinh \frac{39.72\ \sigma}{1.986\ T}$

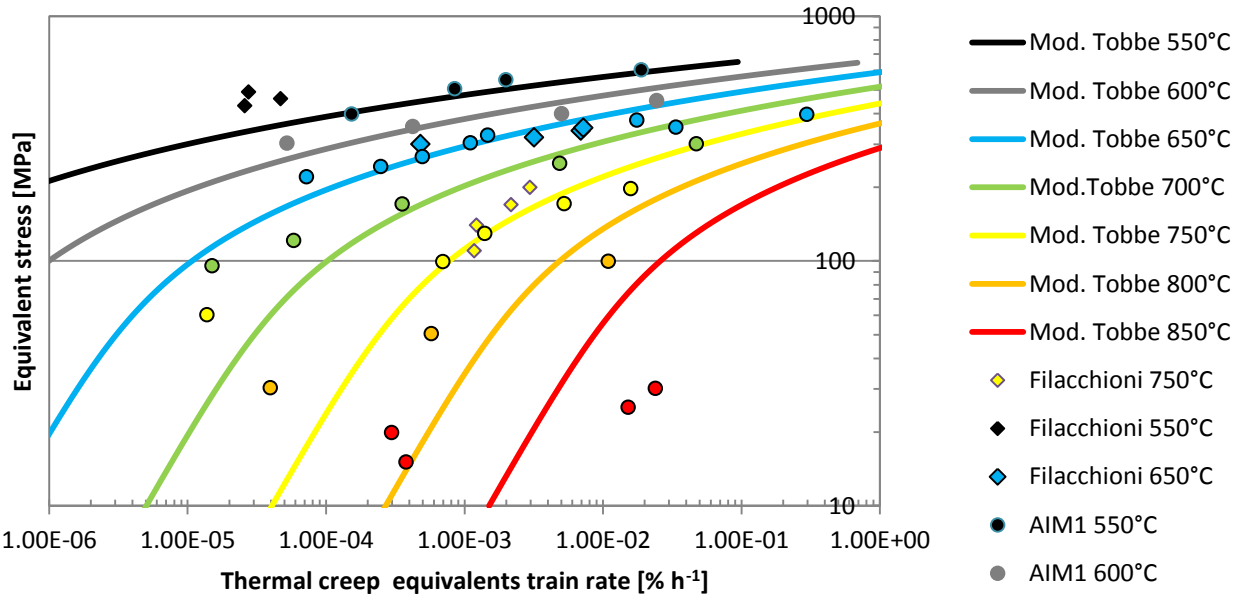

Figure 16: Modified Többe correlation for the thermal creep strain of the AIM1 steel. The fit is made on Gavoille data, Filacchioni data are reported for comparison.

3.5 Cumulative Damage Function

In order to model the thermal creep behavior of the cladding steel, a Cumulative Damage Function (CDF) approach has been implemented in the *LFR-oriented version* of TRANSURANUS. A CDF is a creep failure criterion widely used and validated for a lot of different steels (Waltar *et al.*, 2011). In Table 13, two possible definitions are reported. If the value of CDF exceeds unity, it is assumed that the steel has accumulated an amount of strain which leads to rupture. In this work, a CDF defined with rupture time has been implemented in the *LFR-oriented version*. At each time step, thermal creep rupture time is calculated and the CDF value is proportionally increased. It is important to notice that the rupture time changes at each time step, depending on the combination of stress and temperature in the cladding.

In order to calculate the cladding CDF, the following process is applied: first of all, a parameter condensing temperature and rupture time (i.e., the Larson-Miller parameter) is calculated from the equivalent (Von Mises) stress through an experimental correlation; secondly, the rupture time is calculated from the temperature through the condensed parameter; the rupture time is used to calculate the CDF increase. This process relies on the possibility of using just two relatively simple correlations to handle a phenomenon with three variables. One of these correlations is the definition of the condensed parameter, the other one is the stress-parameter relation.

Table 13: Cumulative Damage Function (CDF) possible definitions[3]**.**

Based on rupture time	Based on rupture strain
$\mathrm{CDF} = \sum_i \frac{\Delta t_i}{t_{R,i}}$	$\mathrm{CDF} = \sum_i \frac{\Delta \varepsilon_i}{\varepsilon_{th,R,i}}$

Definition of the Larson-Miller Parameter (LMP)

The Larson-Miller parameter definition derives from modeling the creep mechanism, by means of a threshold type equation. In particular, the creep rate temperature dependence can be expressed with an Arrhenius equation. Supposing that the dependence on temperature of the activation energy of the process is very little, the Larson-Miller parameter can be defined as:

$$\mathrm{LMP} \equiv T(C + \mathrm{Log}\ t_R) \qquad (11)$$

where T is temperature in Kelvin, C is a constant depending on the material considered, and t_R is the rupture time in hours. Larson-Miller parameter is assumed to be function of the stress. This allows the use of this parameter to calculate rupture time from stress and temperature, which is fundamental in evaluating the CDF.

The assumption of a low dependence of the activation energy on the temperature is not exactly verified. Therefore, other models have been developed for high temperature regime. Moreover, at high temperature, the physical microscopic phenomena which lead to creep are different, requiring a different modeling approach.

A different parametric approach for 15-15Ti steels

The effort of introducing a new parameter is justified because the creep mechanism of the 15-15Ti steels is not well described by an Arrhenius equation (Többe, 1975). The difference in the thermal

[3] According to Waltar *et al.* (2011), a FAE (Fuel Adjacency Effect) coefficient can be added at the denominator, allowing for the chemical interaction between fuel and cladding (e.g., JOG formation). This interaction is neglected in the present work, because the mechanism of interaction between MOX fuel and austenitic cladding steel is still under investigation.

creep mechanism should lead to the use of a different parameter. Indeed, Larson-Miller parameter is by definition nonphysical for this class of steels.

The creep mechanism of the 15-15Ti steels can be described by means of a Nabarro-Herring equation (the same form of Többe correlation), which introduces a change in the creep behavior at high temperature. Two equations are in general used for Nabarro-Herring creep rate modeling, one being the approximation of the other:

$$\dot{\varepsilon} = \mathrm{A}e^{-\frac{\Delta H}{RT}} \sinh \frac{B\sigma}{RT} \simeq \mathrm{A}e^{-\frac{\Delta H}{RT}} \frac{B\sigma}{RT} \tag{12}$$

In Equation (12), A and B are constants depending on the material, R is the perfect gas constant and σ represent the equivalent Von Mises stress applied to the material. The stress is involved in the creep mechanism because Nabarro-Herring thermal creep is interpreted by the migration of point defects in the metal lattice, which is governed by stress level. The hyperbolic sine term becomes important at high temperature.

In analogy with the definition of Larson-Miller parameter, from Equation (12) it is possible to define a parameter P merging temperature and rupture time as follows:

$$P \equiv T\left(C + \log \frac{t_R}{T}\right) \tag{13}$$

Comparing this result with Larson-Miller parameter, it can be noticed how the presence of an high temperature effect is translated in a rescaling of the rupture time. In this subsection, both LMP and P parameters are used to construct stress-parameter diagrams interpolating creep data of few stabilized austenitic stainless steels. What is expected is that, at high temperature and for steel of the 15-15Ti class, P would be more reliable than LMP.

It is useful to summarize all the hypotheses made in the definition of P. Some of them are in common with Larson-Miller parameter, some others are specific.

1) Creep rate can be modeled by a Nabarro-Herring equation (13).

   This means that the creep phenomenon has to be governed by point-like entities (defects or little precipitates) in the lattice, at high temperature.

2) Activation energy of the creep phenomenon can be assumed independent of temperature and stress.

3) Stress variation effect is little compared with temperature effect.

   This is in general not true, particularly when strong stress gradients are presents and creep is originated from vacancies flow.

Hypothesis 3) is critical and should always be checked. In general, if stresses are intense, it is possible to go further in Mc Laurin expansion, Equation (12), adding higher order terms. This results in a parameter that has the same functional structure of P, with more free parameters that have to be set.

Rupture time correlation for 1.4970m

The thermal creep strain for 1.4970m is calculated by means of Többe correlation, which has a Nabarro-Herring structure. This suggests that the correlation for rupture time should be based on P parameter. Indeed, a single stress-LMP correlation is not able to follow temperature changes. In Figure 17, the stress-P correlation implemented in the *LFR-oriented version* of TRANSURANUS, based on Bergmann (1988) data, is reported.

$$P = T\left(20 + \mathrm{Log}\frac{t_R}{T}\right) \tag{14}$$

$$P = 0.01892153\,\sigma^2 - 24.19134\,\sigma + 21761.81 \quad \text{if } \sigma < 395$$
$$P = -6.017016\,\sigma + 17535.01 \quad \text{if } \sigma \geq 395 \tag{15}$$

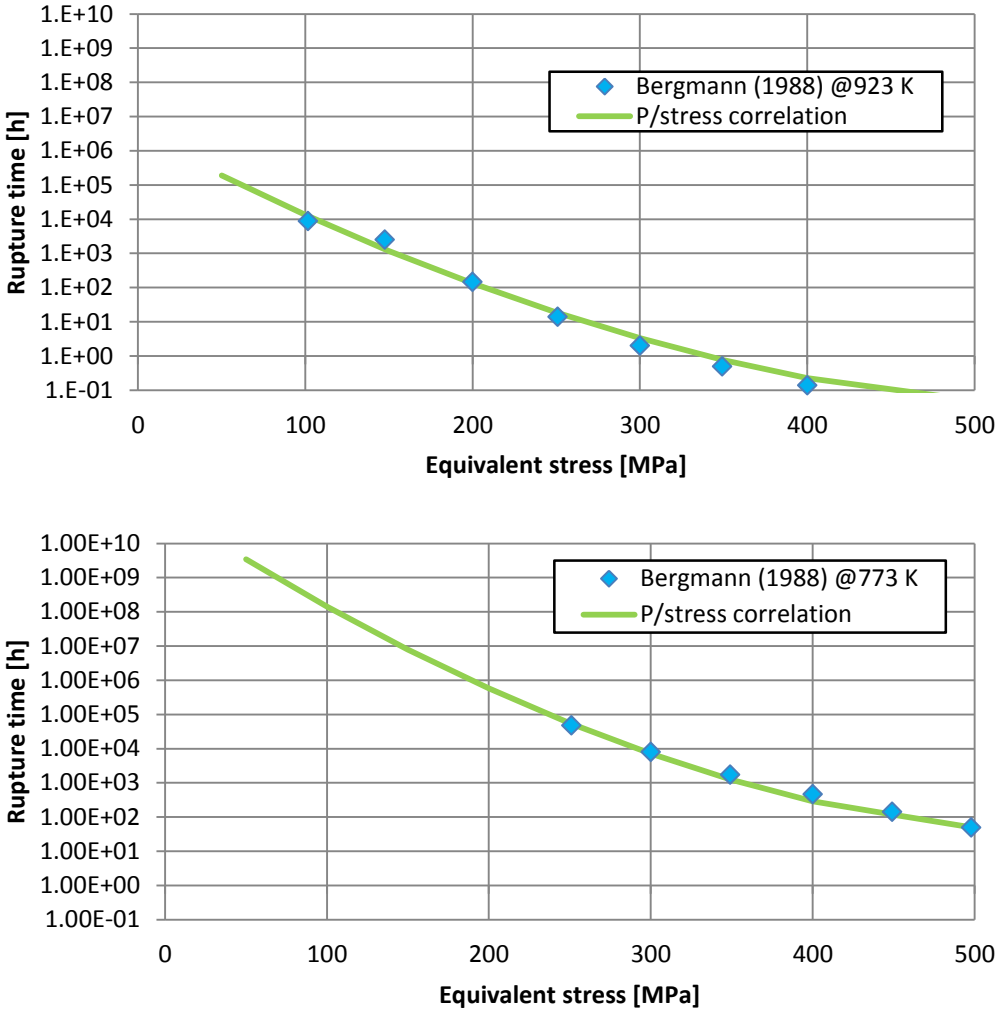

Figure 17: P/stress correlation for 1.4970m steel. Rupture time is calculated from equivalent stress, at different temperatures.

Rupture time correlation for AIM1

The thermal creep strain for AIM1 is calculated by means of the modified Többe correlation, which has a Nabarro-Herring structure. This suggests that the correlation for rupture time should be based on P parameter. Nevertheless, according to Filacchioni *et al.* (1990), in this particular case the classical LMP is sufficient. Therefore, a correlation based on the Larson-Miller parameter has been implemented. Of course, also a stress-P correlation can be used, but where possible LMP is here preferred because it is usually adopted in the literature. The correlation implemented in the *LFR-oriented version* of TRANSURANUS is the following:

$$\mathrm{LMP} = \mathrm{T}\,(17.125 + \mathrm{Log}\,\mathrm{t_R}) \tag{16}$$

$$\mathrm{LMP} = \frac{2060 - \sigma}{0.095} \tag{17}$$

In Figure 18, the correlation is compared with Filacchioni (1990) data.

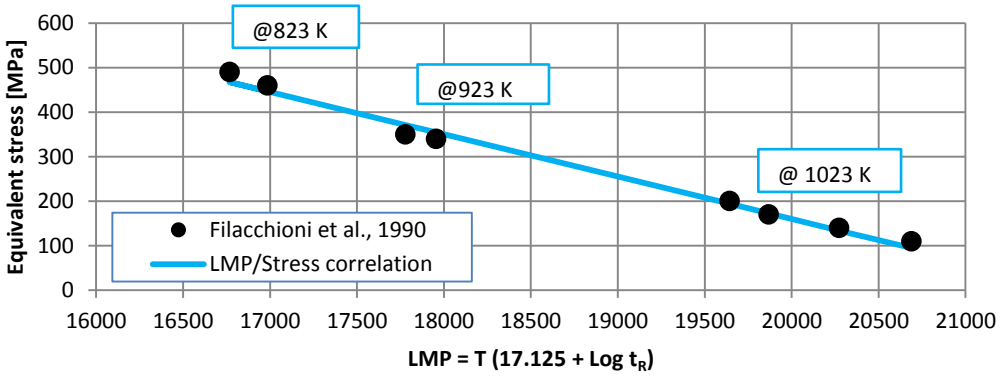

Figure 18: LMP/stress correlation for AIM1.

3.6 Irradiation creep

The irradiation creep of the 15-15Ti austenitic steels depends on the neutron flux and on the mean neutron energy, along with the stress. The correlation proposed by Többe (1975), reported in Table 14, is already implemented in TRANSURANUS (*v1m3j12*).

Table 14: 15-15Ti steels irradiation creep correlation.

[σ]	[φ]	[$\bar{E}$]	[$\dot{\varepsilon}$]	Reference
MPa	n cm^{-2} s^{-1}	MeV	% h^{-1}	Többe, 1975

Correlation
$\dot{\varepsilon} = 3.2\ 10^{-24}\ \bar{E}\ \varphi\ \sigma$

The treatment of the irradiation creep in TRANSURANUS

The correlation for the irradiation creep rate can be expressed in the following general form:

$$\dot{\varepsilon} = A^* \cdot \varphi \cdot \sigma \tag{18}$$

where A* is a constant in MPa^{-1} n^{-1} cm^2 s h^{-1} (the unit of measurement is unusual since some conversions have been applied).

A similar approach is already adopted in TRANSURANUS for other materials (TRANSURANUS Handbook, 2013; Többe, 1975). In these routines, the irradiation creep rate is proportional to the flux, and not to the fluence. Obviously, to calculate the irradiation creep, the time integration is needed:

$$\varepsilon_{n+1} = \varepsilon_n + \Delta\varepsilon_n = \varepsilon_n + \dot{\varepsilon}\Delta t \tag{19}$$

For this reason, the irradiation creep rate is expressed in h^{-1}.

The Equation (18) has been implemented following the literature for what concerns the cladding in Liquid Metal Reactors (Frost, 1994; Kohno *et al.*, 1999; Toloczko *et al.*, 1996; Toloczko *et al.*, 1998). The relation indicated by the literature reads:

$$\dot{\varepsilon}/_{\sigma} = B_0 + D \cdot \dot{S} \tag{20}$$

Where

$\dot{\varepsilon}$ is the irradiation creep rate in dpa^{-1}
B_0 is the creep compliance in dpa^{-1} MPa^{-1}
D is the swelling enhanced coefficient in MPa^{-1}
$\dot{S}$ is the volumetric swelling rate dpa^{-1}

Nevertheless, because of the high uncertainty of the swelling behavior, the approach proposed does not consider the coupling with the swelling - i.e., the second term of the Equation (20). In order to implement this relation in TRANSURANUS, the irradiation creep rate has to be converted from dpa^{-1} in h^{-1} (i.e., from unit of "dose" to unite of time) according to the following relation:

$$K \cdot d = \varphi \cdot t \cdot 3600 \tag{21}$$

Where

K is the conversion factor between fluence and "dose" in n cm^{-2} dpa^{-1} (a typical value for fast reactor is $2 \cdot 10^{21}$)

d is the "dose" in dpa

t is the time in h (3600 is the conversion from hours to seconds)

Even if the fluence appears in the previous relation, only the flux is present in the Equation (18) since the irradiation creep has to be expressed per unit of time.

By means of some substitutions, it is possible to derive the initial equation, Equation (18), where

$$A = \frac{B_0}{K} \cdot 3600 \tag{22}$$

and the irradiation creep rate is proportional to the flux and stress.

REFERENCES

Agosti, F., Botazzoli, P., Di Marcello, V., Pastore, G., Luzzi, L., 2013. Extension of the TRANSURANUS code to the analysis of cladding materials for liquid metal cooled fast reactors: a preliminary approach. Technical Report, CESNEF-IN-02-2013 (public version).

Aït Abderrahim, H., Baeten, P., De Bruyn, D., Fernandez, R., 2012. MYRRHA – A multi-purpose fast spectrum research reactor. Energ. Convers. Manage. 63, 4–10.

Alemberti, A., Frogheri, M., Mansani, L., 2013. The Lead Fast Reactor: Demonstrator (ALFRED) and ELFR Design. In: Proceedings of the IAEA International Conference on Fast Reactors and Related Fuel Cycles: Safe Technologies and Sustainable Scenarios (FR13), Paris, France, March 3-4.

Banerjee, A., Raju, S., Divakar, R., Mohandas, E., 2007. High temperature heat capacity of alloy D9 using drop calorimetry based enthalpy increment measurements. Int. J. Thermophys. 28 (1), 97–108.

Bergmann, H.J., 1988. Projekt-Materialdatenhandbuch IV KNKII/3, Revisionsstand 04/88, INTERATOM Bericht/Report 55.07148.1.B.

Bergmann, H.J., Dietz, W., Ehrlich, K., Mühling, G., Schirra, M., 2003. Entwicklung des Werkstoffs X10CrNiTiB 15 15 als Strukturmaterial für Brennelemente. Wissenschaftiche Berichte FZKA 6864, FZK, Karlsruhe.

Cacuci, D.G., 2011. Chapter 23: Lead-Cooled Fast Reactor (LFR) Design: Safety, Neutronics, Thermal Hydraulics, Structural Mechanics, Fuel, Core, and Plant Design. In: Handbook of Nuclear Engineering, Volume 4, ed. Springer, Boston.

Cheynet, B., Dubois, J.D., Milesi, M., 1996. Données thermodynamiques des éléments chimiques, Techniques de L'Ingénieur, Matériaux métalliques, No. M153, Form M64.

Dubuisson, P., 2013. Core structural materials - feedback experience from Phénix. IAEA TECDOC 1689, pp. 235-247.

Filacchioni, G., De Angelis, U., Ferrara, D., Pilloni, L., 1990. Mechanical and structural behaviour of the second double stabilized stainless steels generation. In: Proceedings of the International Conference on Fast Reactor Core and Fuel Structural Behaviour, Inverness, London, UK, June 4-6, pp. 255-261.

Friedland, A.J., 1966. Coolant Properties, Heat Transfer and Fluid Flow of Liquid Metals. In: Fast Reactor Technology: Plant Design, J.G. Yevick (Ed.), Chapter. 2, The M.I.T. Press, Cambridge (MA), USA.

Frost, B.R.T., 1994. Nuclear Materials, Volume 10B, ed., Materials Science and Technology Series, VCH Verlagsgesellschaft GmbH and VCH Publishers, Inc, Weinheim.

García Ferré, F., Ormellese, M., Di Fonzo, F., Beghi, M.G., 2013. Advanced Al_2O_3 coatings for high temperature operation of steels in heavy liquid metals: a preliminary study. Corros. Sci. 77, 375–378.

Gavoille, P., Courcelle, A., Seran, J.L., Averty, X., Bourdiliau, B., Provitina, O., Garat, V., Verwaerde, D., 2013. Mechanical Properties of Cladding and Wrapper Materials for the ASTRID Fast-Reactor Project. In: Proceedings of the IAEA International Conference on Fast Reactors and Related Fuel Cycles: Safe Technologies and Sustainable Scenarios (FR13), Paris, France, March 3-4.

Gehr, H.L., 1973. Datensammlung zur Kernelementauslegung. Interatom - Technischer Bericht 73.30.

GIF, 2002. A Technology Roadmap for Generation IV Nuclear Energy Systems. Technical Report GIF-002-00.

Gurvich, L.V., Veyts, I.V., 1991. Thermodynamic Properties of Individual Substances, 4th ed., Vol. 2, Parts 1 and 2, Hemisphere Pub. Corp., New York.

Hübner, R., 2000. Das Bestrahlungverhalten des austenitischen Stahls DIN 1.4970, FZK, Karlsruhe.

Hultgren, R., Desai, P.D., Hawkins, D. T., Gleiser, M., Kelley, K.K., 1973. Selected Values of the Thermodynamic Properties of Binary Alloys. ASM, Metals Park, Ohio, USA.

http://www.leader-fp7.eu/ (accessed 06.08.2014).

Iida, T., Morita, Z., Takeuchi, S., 1975. Viscosity Measurements of Pure Liquid Metals by the Capillary Method. J. Japan Inst. Metals 39, 1169–1175.

Kirshenbaum, A.D., Cahill, J.A., Grosse, A.V., 1961. The density of liquid lead from the melting. J. Inorg. Nucl. Chem. 22, 33–38.

Kohno, Y., Kohyama, A., Hirose T., Hamilton, M.L., Narui, M., 1999. Mechanical property changes of low activation ferritic/martensitic steels after neutron irradiation. J. Nucl. Mater. 271-272, 145–150.

Kutateladze, S.S., Borishansky, V.M., Novikov, I.I., Fedyaskii, O.S., 1959. Liquid-metal Heat Transfer Media. At. Energ., Suppl. 2. (Transl. Cons. Bur. Inc., New York, 1959).

Kyrillov, P.I., Deniskina, N.B., 2000. Thermophysical Properties of Liquid Metal Coolants. Tables and Correlations, Review FEI-0291, IPPE, Obninsk.

Lombardi, C., 2006. Impianti nucleari, Cusl, Milano.

Lucas, L.D., 1984, Données physico-chimiques des principaux métaux et métalloïdes. Techniques de l'Ingénieur, Matériaux métalliques, N° M153, Form M65a.

Lyon, R.N. (Ed.), 1954. Liquid Metals Handbook, 2nd Ed., Report NAVEXOS P-733, Atomic Energy Commission and Dept. of the Navy, Washington, USA (rev. 1954).

Nikolopoulos, P., Schulz, B., 1979. Density, thermal expansion of stainless steel and interfacial properties of UO_2-stainless steel above 1690 K. J. Nucl. Mater. 82, 172–178.

OECD-NEA, 2007. Handbook on Lead-Bismuth Eutectic Alloy and Lead properties, Materials Compatibility, Thermal-hydraulics and Technologies.

Rudtsch, S., Ebert, H.P., Hemberger, F., Barth, G., Brandt, R., Groß, U., Hohenauer, W., Jaenicke-Roessler, K., Kaschnitz, E., Pfaff, E., Pößnecker, W., Pottlacher, G., Rhode, M., Wilthan, B., 2005. Intercomparison of thermophysical property measurement on an austenitic stainless steel. Int. J. Thermophys. 26 (3), 855–867.

Ruppersberg, H., Speicher, W., 1976. Density and Compressibility of Liquid Li-Pb Alloys. Z. Naturforsch. 31 a, 47–52.

Schumann, U., 1970. MAPLIB, A program system for provision of material property data to computer programs. KFK 1253.

Smithells Metals Reference Book (8th edition), 2004. Gale W.F., Totemeier T.C. (Eds.), Elsevier, Amsterdam.

Többe H., 1975. Das Brennstabrechenprogramm IAMBUS zur Auslegung von Schellbrüter – Brenn - stäben, Technischer Bericht, ITB 75.65.

Toloczko, M.B., Garner, F.A., 1996. Irradiation Creep and Void Swelling of two LMR Heats of HT9 at ≈ 400°C and 165 dpa. J. Nucl. Mater. 233-237, 289–292.

Toloczko, M.B., Garner, F.A., Eiholzer, C.R., 1998. Irradiation Creep of Various Ferritic Alloys Irradiated at ≈ 400°C in the PFR and FFTF Reactors. J. Nucl. Mater. 258-263, 1163–1166.

TRANSURANUS Handbook, 2013. European Commission, JRC, Institute for Transuranium Elements, Karlsruhe.

Ushakov, P.A., Zhukov, A.V., Matyukhin, N.M., 1977. Heat transfer to liquid metals in regular arrays of fuel elements. Translated from Teplofizika Vysokikh Temperatur 15 (5).

Waltar A.E., Todd D.R., Tsvetkov, P.V. (Eds), 2011. Fast Spectrum Reactors, Springer, New York.

Weisenburger, A, Heinzel, A., Muller, G., Muscher, H., Rousanov, A., 2008. T91 cladding tubes with and without modified FeCrAlY coatings exposed in LBE at different flow, stress and temperature conditions. J. Nucl. Mater. 376, 274–281.

4 Conclusion and future work

The present work has been dedicated to the extension of the TRANSURANUS code for analyzing the fuel pin behavior of innovative LFRs, with reference to the materials adopted in the ALFRED design. The material properties of lead as well as of 15-15Ti austenitic cladding steels have been implemented in the *LFR-oriented version*.

The main outcomes of this report may be summarized as follows:

- The properties of lead have been updated in the TRANSURANUS code. The OECD-NEA Handbook has been used as summarized and reasoned reference. In particular, the correlations concerning specific heat capacity, dynamic viscosity, density, heat transfer, boiling temperature, thermal conductivity, enthalpy, boiling pressure, heat of evaporation and corrosion have been updated.
- A critical review of the main properties of 15-15Ti steel has been performed, with the description of the out-of-pile correlations implemented in the TRANSURANUS code. The properties of the austenitic steels are compared with other literature data in order to assess their validity. Beside this purpose, the comparison has been useful to understand the critical properties which are strongly dependent on the alloying elements and to underline the different behavior of the various steels of the 15-15Ti family (AIM1, 1.4970, D9). In this sense, yield strength, ultimate tensile strength, rupture strain, swelling and thermal creep are features that strongly depend on the composition.
- The Banerjee correlation for the heat capacity of the 15-15Ti steel has been implemented in the code.
- New correlations for the swelling, the thermal creep strain and the Cumulative Damage Function (CDF, with the introduction of the P parameter) of 15-15Ti cladding steels have been implemented in the *LFR-oriented version*. This crucial aspect was totally absent in TRANSURANUS before this work. In particular, specific correlations for the 1.4970m and the AIM1 steels have been proposed.

As natural continuation of this work, we envisage in the future to adopt the *LFR-oriented version* for analyzing the fuel pin integral behavior of the ALFRED reactor. To this purpose, the capabilities of the TRANSURANUS integral performance code will be exploited to evaluate (on the basis of power history simulations) the synergy of the phenomena occurring throughout the fuel pin life in reactor and their impact on the fuel pin design improvement.

In particular, the following results are expected to be suitable for giving important feedbacks to the reactor designers during the conceptual design of ALFRED reactor (see also Figure 1, in Introduction):

- critical analysis of the fuel pin behavior in reactor, along with a sensitivity analysis on the models affected by more uncertainty so as to identify a worst case scenario for the fuel pin performance;
- careful evaluation of the PCMI dynamics, both in normal operation and accident conditions, due to the closing process of the fuel pin gap;

- optimization of the fuel pin design and performance, in order to achieve enlarged safety margins;
- identification of the most adequate FA geometrical configuration from the thermo-mechanical point of view;
- identification of the main issues on which the R&D activities and efforts should be focused in the near future as far as the behavior of the materials (lead, AIM1 cladding steel, coating, MOX fuel) is concerned.

All these future activities are expected to give useful indications for the design of the ALFRED reactor and, more in general, for improving the intrinsic safety features of innovative lead cooled FBRs.

Part2

Modeling and analysis of nuclear fuel pin behavior for innovative lead cooled FBR: MOX conductivity models

CONTENTS

1 Introduction

1.1 Objective of the activity

Among the parameters that governs the myriad of processes that occurs during irradiation of fuels rods, the fuel temperature, is by far the most important one (i.e. it dominates the FGR and swelling mechanisms) [1].

The correct prediction of the fuel temperature profile is therefore the basis for the simulation of integral fuel rods by means of fuel performance codes. The present report aims to assess the correlations implemented in TRANSURANUS code to simulate conductivity of MOX fuels comparing them with correlations available from open literature.

1.2 Thermal conductivity of ceramic fuel

Thermal conductivity is a property representing the ability of a solid material to transfer heat. There are three phenomena considered when modelling thermal conductivity. Lattice vibrations, radiation heat transfer and electronic conductivity[2].

Lattice vibration thermal conductivity (k_{latt}) is modelled by assuming the solid to be an ideal gas consisting of phonons. Phonons are quasi particles representing the wave nature of the vibrating solid in the lattice. They tend to collide with each other and with defects in the crystal with a certain mean free path. They transport their energy as they translate in the medium from the hot side to the cold one. Thermal conductivity depends on the amount of energy a phonon can carry and the mean free path of the phonon[3]. Phonon's mean free path should be inversely proportional to the temperature. Due to the presence of point defects in the crystal solid that acts as a barrier to phonon's mobility, the mean free path cannot keep monotonically increasing as the temperatures gets lower[3]. This requires that the mean free path is inversely proportional to temperature plus an extra constant term representing phonon scattering with defects. Being proportional to the mean free path of the phonon, k_{latt} would be written as:

$$k_{latt} = \frac{1}{A + BT} \qquad \text{Eq.1}$$

Where A, and B are constants, and T is the temperature in (K).

Heat is conducted as well with radiation on the form of electromagnetic waves. Energy is transported due to the movement of charged particles (protons and electrons) which emit some of their energy on the form of electromagnetic radiation[3][4]. Radiation term of thermal conductivity (K_{rad}) is written on the form of a constant times the cube of temperature:

$$k_{Rad} = CT^3 \qquad \text{Eq.2}$$

At temperatures high enough, energy is sufficient to generate an amount of electron-hole pairs that contribute to thermal conductivity (K_{el})[3].

$$k_{el} = 2\left(\frac{K_b}{e}\right)^2 T\left[\sigma + \frac{2\sigma_e\sigma_h}{\sigma}\left(\frac{E_g}{2K_bT} + 2\right)\right] \qquad \text{Eq.3}$$

Where:

k_{el}= electronic contribution to thermal conductivity.

K_b= Boltzmann constant, 1.38x10^{23} (J/K)

e= electron charge, 1.6x10^{-19} (Coul)

$\sigma_{e/h}$= electron/hole contribution to electrical conductivity ($\frac{1}{\Omega}m$)

$\sigma \quad = \sigma_e + \sigma_h$ ($\frac{1}{\Omega}m$)

E_g = energy gap between conduction and valence bands (J)

Where the first term on the RHS is the conductivity effect of holes and electrons separately. The second term represents the ambipolar effect, which is the release of the kinetic energy of both the electron and hole when they recombine together plus the release of their generation energy at areas of lower temperature leading to the transfer of heat electronically.

This equation can be simplified using some experimental data and assumptions to be written on the form:[2]

$$k_{el} = D\frac{e^{\frac{-E}{T}}}{T^n} \qquad \text{Eq.4}$$

Where D,E and n are constants, it should be noted that n differs from one model to another.

These physical principles of heat conduction and their equation forms are generally taken into account in the models even if they can be implemented in different ways. Most of these models account only for the first two thermal conductivity principles.

1.3 Effect of temperature

Thermal conductivity of UOx and MOX is a property that depends on temperature. It has been noted experimentally that the thermal conductivity decreases with temperature until a plateau is reached in the range between 1500 to 2000 ^{0}C. This decrease is due to the lattice vibration conductivity, which is inversely proportional to the temperature. At temperatures above the plateau range, the thermal conductivity begins to rise again. This is attributed to either of the two other components of the thermal conductivity. Radiation heat conduction takes place above the plateau temperature even though it is not that much significant. Electronic term of the thermal conductivity is the second term that is responsible for the increase of thermal conductivity.

The lattice vibration mechanism is included in all the models. As usual, it takes into consideration other factors that affect the heat conductivity other than temperature (e.g. burn up rate, deviation from stoichiometry, etc). Some models, take the radiation conduction term into consideration to explain the increase of thermal conductivity at higher temperatures, while others relate that increase to the electronic conduction term.

1.4 Effect of stoichiometry

The theoretical oxygen to metal ratio (O/M) between Uranium or Plutonium oxide (U-Pu)O_2 is two. Deviation from this value are generally adopted by design and are also induced in the nuclear fuel aseffect of irradiation. The deviation can lead to hyper (>2) or hypo (<2) stoichiometric state of the fuel[6].

The effect of deviation from stoichiometric is generally modeled by assuming that this deviation causes more defects in the lattice. This perturbation is included in the constant A in Eq.1 which represents the phonon-defect interaction in the lattice and determined originally for stoichiometric fuel conditions.

The modification of due to deviation from stoichiometry can be written as

$$k_{latt} = \frac{1}{A_0 + \mathrm{Cx} + BT} \qquad \text{Eq.5}$$

Where A_0 is the constant A for stoichiometric fuel and C is a constant multiplied by x which is the deviation form stoichiometry (O/M-2)).

1.5 Effect of burn up

The irradiation process that takes place in a nuclear reactor leads to various changes in the properties of the fuel rod. Defects in the lattice, porosity increase, deviation from stoichiometry and fuel cracking with irradiation leads to degradation of the thermal conductivity. This effect is important in fast reactors since burn up can reach to more than 10% of the original weight content of the uranium and plutonium[6]. Solid fission products have different effects on thermal conductivity. In general, those that are dissolved tend to decrease the thermal conductivity, while those that are precipitated tends to increase it. The integral effect is however a degradation of conductivity with increasing burn-ups.

1.6 Effect of fuel porosity

The presence of voids in the solid fuel pin leads to degradation of its thermal conductivity. A poreless fuel is required to obtain the maximum thermal conductivity. On the other side, the presence of pores in the fuel pin is important to accommodate the release of fission gases that are formed during irradiation. Theses fission gases can cause internal pressure of the fuel pin to increase leading to deformation and swelling of the fuel. This effect is more important for fast reactors than thermal reactors because the higher power density leads to more generation of fission gases[6].

The porosity (P) is defined as the volume of the pores inside the fuel divided by the total volume of the fuel this can be written as:

$$P = 1 - \frac{\rho}{\rho_{TD}} \qquad \text{Eq.6}$$

Where ρ is the actual density of the fuel, and ρ_{TD} is the theoretical density of the fuel's material without pores. The effect of porosity on thermal conductivity is considered by using a correction factor of the thermal conductivity. This factor has many formulations but the most used are the modified Loeb formula:

$$k = k_{TD}(1 - \alpha P) \qquad \text{Eq.7}$$

or the Maxwell-Eucken formula:

$$k = k_{TD}\frac{1-P}{1+\beta P} \qquad \text{Eq.8}$$

Where k_{TD} is the thermal conductivity of the poreless fuel. α and β are constants. Theoretically, the values of α is 1 and β is 0.5. Experimentally, the noticed values of these factors are higher than what the theory predicts. This is due to the fact that the pores are not randomly distributed in the lattice which is theoretical assumption[7]. The wide range of values used for the constants α and β shows that they are in fact variables that depend on the pore shape. The values assigned to them represents an average of the porosity effect.

1.7 Effect of Plutonium content

The effect of Plutonium on the constants A and B in the lattice vibration thermal conductivity term has been carefully studied. Evidence does not show any systematic trend for the variation of the constant A, while it shows a systematic increase of the constant B. Overall the effect of increasing Plutonium's content in the fuel is a decrease of the thermal conductivity of MOX fuel[3]. This decrease reaches up to 15% for a plutonium content of around 25 wt.%.

2 TRANSURANUS thermal conductivity models

This section provides an assessment and a comparison of the correlations adopted in TRANSURANUS to simulate MOX fuel conductivity.

2.1 Correlation 31-Van Uffelen and Schubert

This correlation is based on the data obtained experimentally by Duriez et.al where the laser flash technique was used to measure the thermal diffusivity of MOX fuel. The Pu content of the fuel was between 3-15%.wt, O/M ratio between 1.95-2.0 and in the temperature range between 700-2300 K[9]. The the thermal conductivity was modeled by using values of the heat capacity calculated from Kopp's law[8]. The ambipolar electronic thermal conductivity term is based on the work of Ronchi et.al in which they measured the thermal diffusivity and the heat capacity of UO_2 for a temperature range between 500 and 1900 using an advanced laser-flash technique that gave better results than conventional laser flash methods at high temperatures[9]. The correlation gives the thermal conductivity of MOX as a function of temperature and burn-up:

$$k_{100} = \frac{1}{a + a_1 bu + bT + b_1 bu\, T_p} + \frac{c}{T^2} e^{-\frac{d}{T}} \qquad \text{Eq.9}$$

Where

a=0.0308
a1 =5.498x10^{-3}
b=2.515 x10^{-4}
b1= -2.498 x10^{-6}
c= 4.715x x10^{9}
d=16361

T is in K and T_p = min(1923,T), bu is the local burn up in $\frac{MWd}{kgHM}$

The porosity effect can be taken into account using the following correction formula

$$k_P = k_{100}(1 - P)^{2.5} \qquad \text{Eq.10}$$

This correlation has been assessed assuming different conditions. Due to the lattice vibration term, the correlation predicts a decrease of thermal conductivity for 0 $\frac{MWd}{kgHM}$ fuel with temperature until it reaches a minimum around 2000 ^{0}K and then begins to rise again due to the electronic heat conduction as shown in Fig.1. This figure assumes a fuel of 95% theoretical density and includes different level burn-ups.

The effect of burn up on the thermal conductivity is more important at lower temperature. As can be seen in Fig.1, at 800 K the thermal conductivity decreased by 60% of its original value for un-irradiated fuel when the burn up reached 100 $\frac{MWd}{kgHM}$. For 2000 K, the thermal conductivity for the same range of burn up decreases only by 10%. It is noticed as well that the higher burn-up, the lower the rate of change of thermal conductivity with temperature. Also as the burn-up increases, the lower the temperature for which the thermal conductivity reaches its minimum before it increases again. At burn up of 100 $\frac{MWd}{kgHM}$, the thermal conductivity is slightly changing with

temperature until the temperature is above 1500 K where the effect of the ambipolar term of thermal conductivity starts to rise. This behavior is explained by the increase of the defects in the solid due to irradiation. As consequence of this the phonon-defect interaction in the fuel dominates with respect to hte temperature dependent phonon-phonon interaction term.

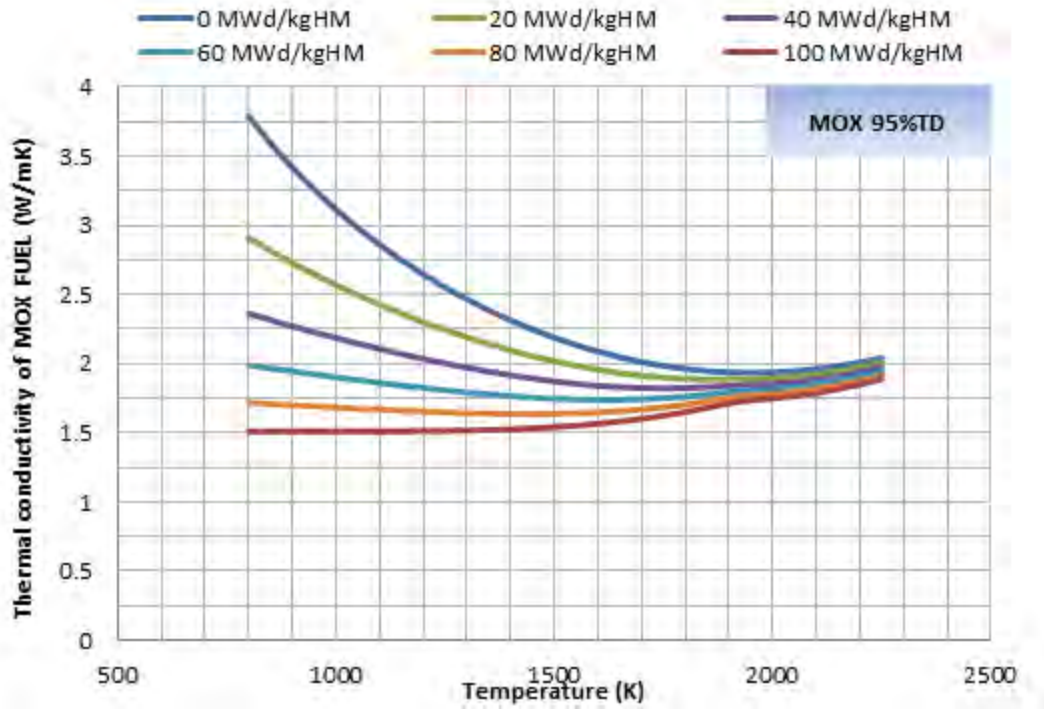

Fig.1 - Thermal conductivity as a function of temperature for different burn ups, correlation 31.

The effect of porosity is analyzed in Fig.2 (under the assumption of un-irradiated fuel). The correlation predicts a decrease of thermal conductivity with porosity. This decrease is linear and the rate of decrease is constant over the whole range of temperatures. It is between 20 to 25% in thermal conductivity when the porosity increase from 0 to 10%.

In Fig.3, The contributions of the lattice vibration and the ambipolar thermal conductivity are plotted according Van Uffeleln & Schubert correlation. This is done for this correlation only to illustrate what was explained before in theory related to the dominating contribution of lattice vibration term at low temperatures. At low temperatures the main contribution to the total thermal conductivity is the one related the lattice vibration. As the temperature increases, this term keeps decreasing combined with the increase of the electronic term. When the rate of increase of electronic thermal conductivity dominates the rate of decrease due to lattice vibration the thermal conductivity begin to rise again. This domination takes place in the temperature range between (1600-2000 K).

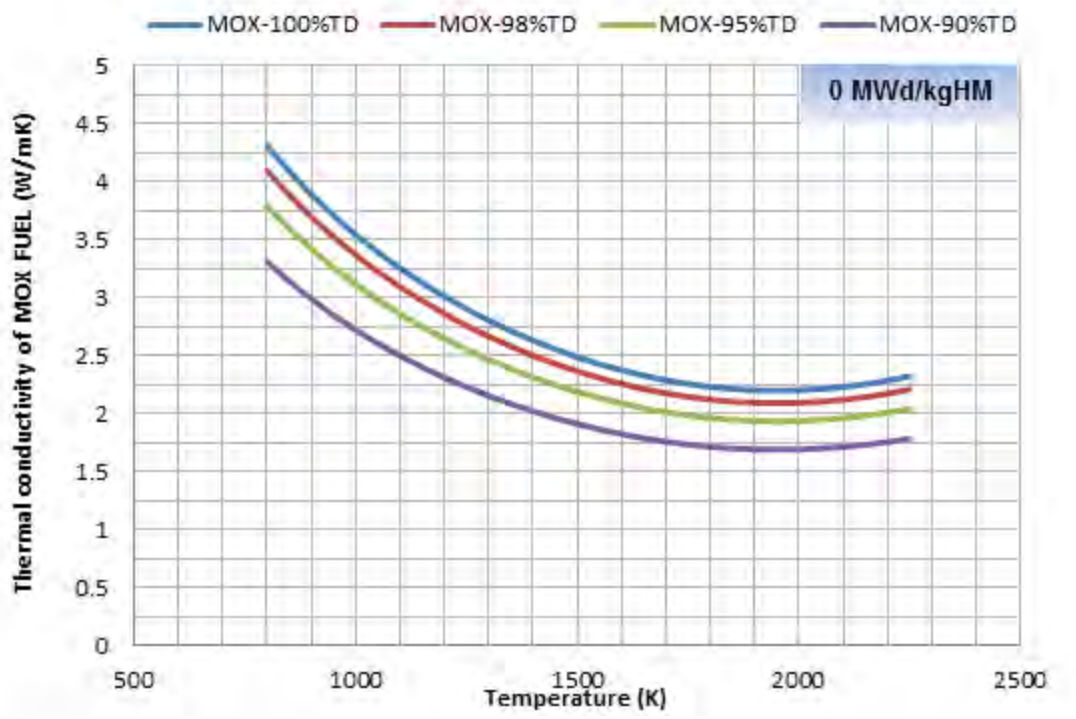

Fig.2 - Effect of fuel porosity on thermal conductivity, correlation 31.

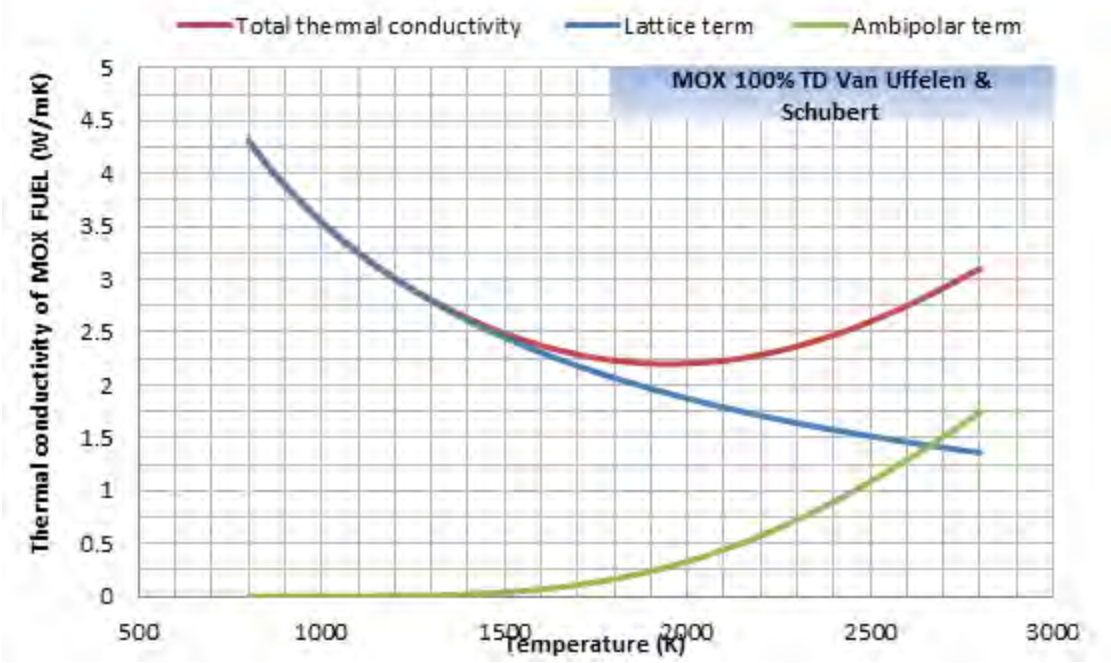

Fig.3 - Comparison between the lattice and the ambipolar contribution to the total thermal conductivity.

2.2 Correlation 32-Carbajo

This correlation is based on the work of Carbajo et.al. that take basis for best value estimation of data available from open literature available recommendations given in other works. The physically based correlation by Lucuta et.al was recommended. It gives the thermal conductivity as a function of temperature, burn-up, deviation from stoichiometry along with a porosity correction. The

correlation takes the fuel irradiation into account as well as the effect of dissolved and precipitated solid fission fragments as a separate function from the un-irradiated fully dense fuel element**Errore. L'origine riferimento non è stata trovata.**.
The thermal conductivity for a 100%TD MOX fuel is given by

$$k_{100} = 1.158x\left(\frac{1}{a_0 + a_1X + (b_0 + b_1X)t_k} + \frac{c}{t_k^{2.5}}e^{-\frac{d}{t_k}}\right)x\, FD(bu,T)xFP(bu,T)xFR(T)\ \frac{W}{mK} \quad \text{Eq.11}$$

Where

a_0=0.035, a_1=2.85, b_0 =0.286, b1= -0.715, c= 6400 and d=16.35
X is the deviation from stoichiometry,
t_k=$\frac{T}{1000}$ and T is the temperature in [K]

The factor FD represnts the negative effect of dissolved fission fragments on the thermal conductivity and is defined as:

$$FD(bu_{at},T) = \omega\left[\arctan(\frac{1}{\omega})\right] \quad \text{Eq.12}$$

For bu_{at} >0 and

$$FD(0,T) = 1 \quad \text{Eq.13}$$

where

$$\omega = \frac{1.09}{bu_{at}^{3.265}} + 0.0643\left(\frac{T}{bu_{at}}\right)^{1/2} \quad \text{Eq.14}$$

bu_{at} is the burnup in at.%

The factor FP represents the increase in thermal conductivity due to the precipitaed solid fission products:

$$FP(bu_{at},T) = 1 + \frac{0.019bu_{at}}{(3 - 0.019\ bu_{at})\left[1 + exp\left(-\frac{T-1200}{100}\right)\right]} \quad \text{Eq.15}$$

.
The factor FR accounts for radiation effects. It is important below 900 K and reaches near unity rapidly above 900K and does not play a significant role above that temperautre.

$$FR(T) = 1 - \frac{0.2}{1 + exp\left(\frac{T-900}{80}\right)} \quad \text{Eq.16}$$

The porosity effect is modelled using the Maxwell-Euckman correction formula

$$k_P = k_{100}(\frac{1-P}{1+2P}) \quad \text{Eq.17}$$

The correlation predicts a decrease of thermal conductivity with temperature due to lattice vibration until it reaches a minimum around 2000 K. Then, it begins to rise again due to the electronic heat conduction as shown in Fig.4 for a 95%TD fuel at different burn ups. The same is true for different values of fuel porosity. It can be noticed as well the decrease of thermal conductivity with burn up. The effect of burn up on the thermal conductivity is more important at lower temperature. As can be seen from Fig.4, at 800 K, the thermal conductivity decreased by 40% of its original value for un-irradiated fuel when the burn up reached 10 at.%. For 2000 K, the thermal conductivity for the same range of burn up decreases by 15%.

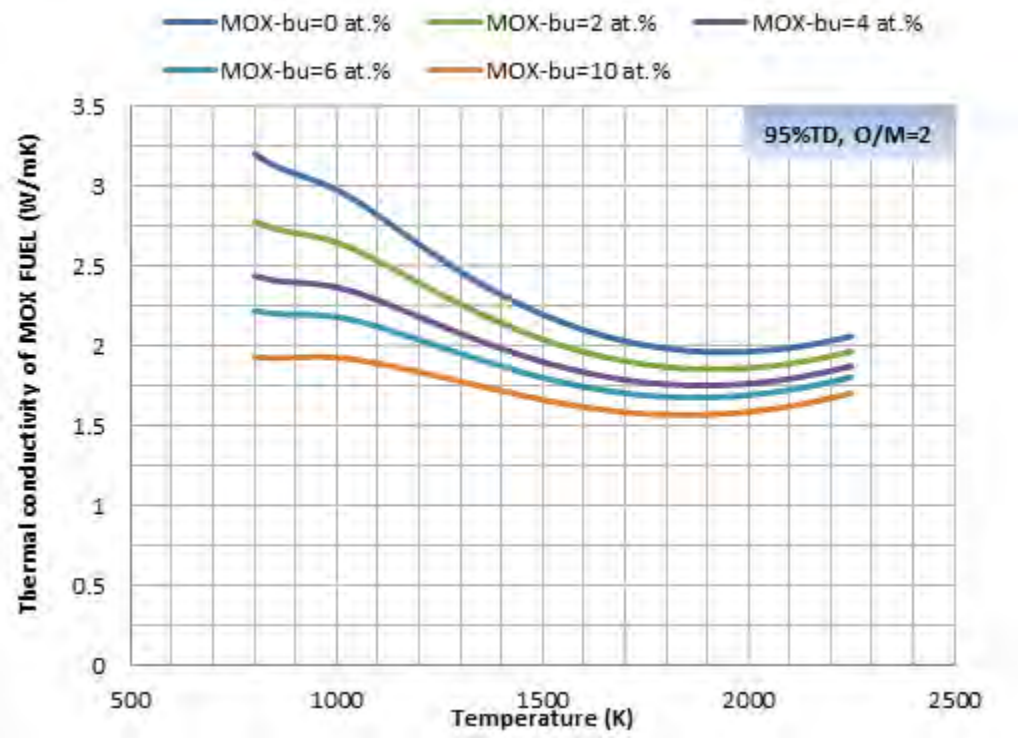

Fig.4 - Thermal conductivity as a function of temperature for different burn ups, correlation 32.

The effect of porosity is analyzed inFig.5 (for un-irradiated MOX). The decrease of conductivity with increased porosity is linear and the rate of decrease is constant over the whole range of temperatures. It is between 20 to 25 when the porosity increase from 0 to 10%.

The effect of O/M is reported in Fig.6 and *Fig.7* (for un-irradiated MOX). The correlation is physical for the hypostoichiometric section while, for the deviation in the direction of hyperstoichiometry, the correlation does not give physical results since it predicts the increase of thermal conductivity, Fig.6 (that is in contradiction with the theoretical and experimental finding that hilight a maximum of condutivity for O/M = 2 and lower values for all the other ratios). Due to this reason, further analyses are conducted only up to O/M = 2, *Fig.7*. It sholud be pointed out that the code recommends the use of these correlations only for O/M up to 2. It can be noticed that the lower the temperature, the higher the degradation of thermal conductivity with deviation from stoichiometry. For 800 K the thermal conductivity decreases by 30% for a deviation from stoichiometry of 0.05. At 2000 K for the same range of deviations, the decrease of thermal conductivity is around 8% and decreases more as the temperature goes higher.

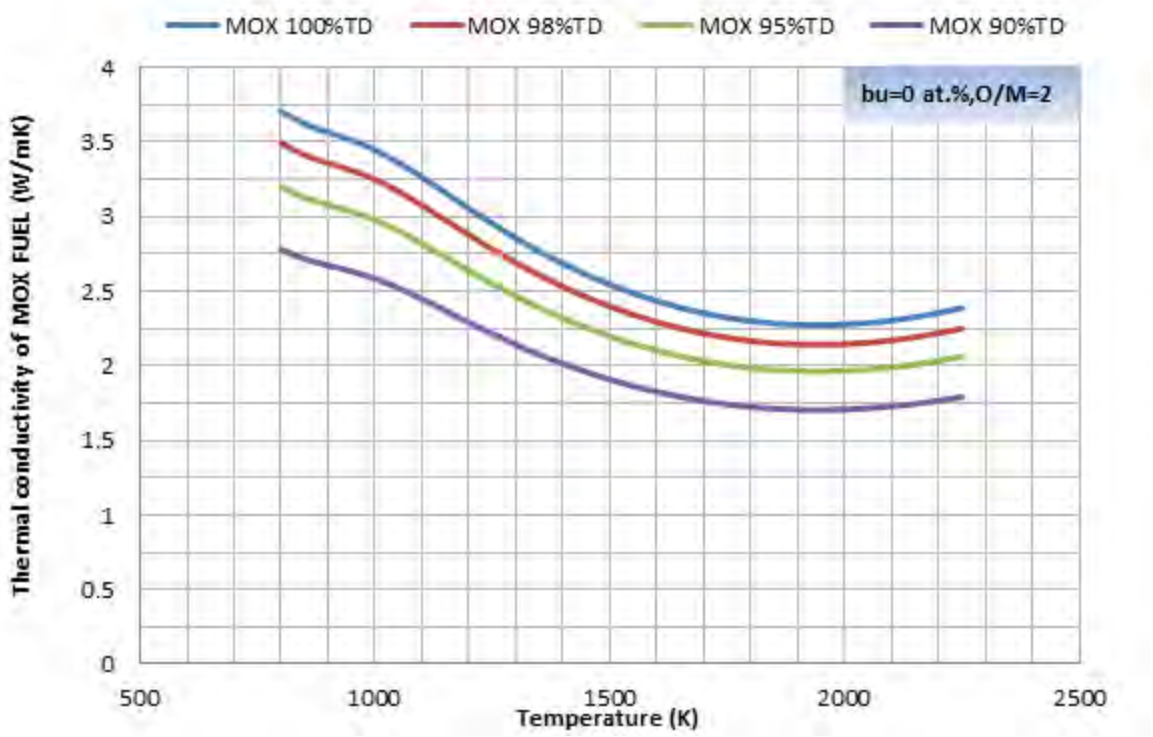

Fig.5 - Effect of fuel porosity on thermal conductivity, correlation 32.

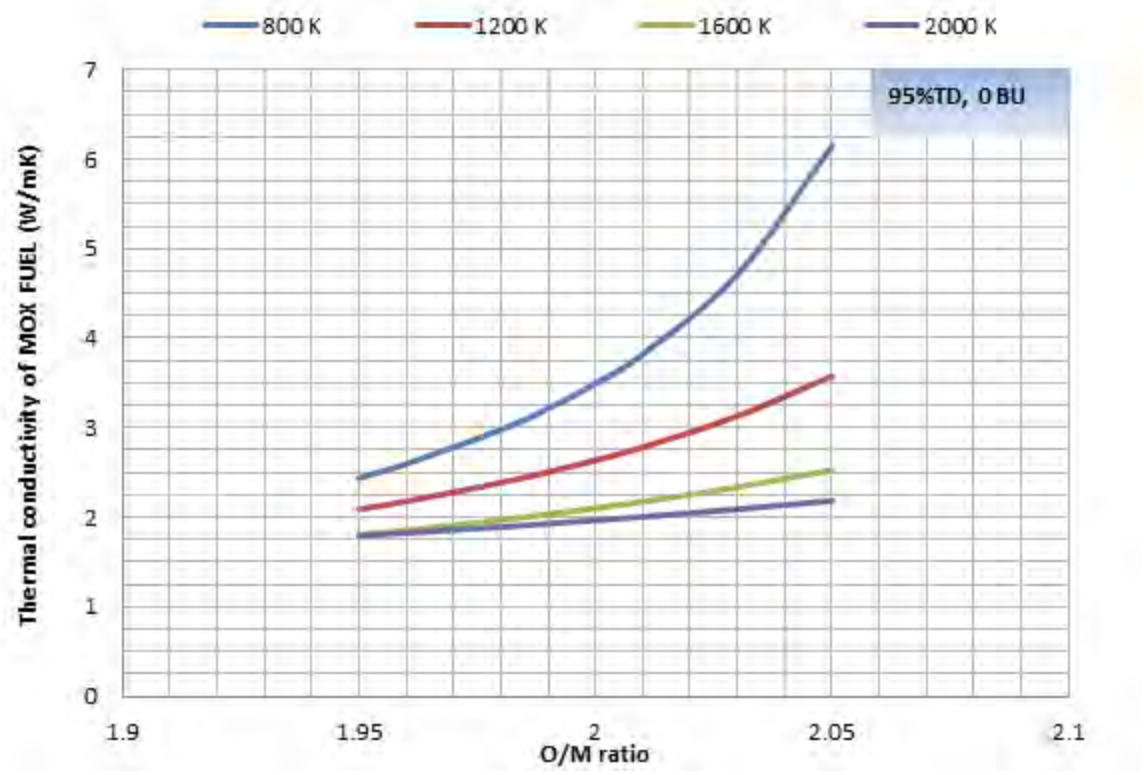

Fig.6 - effect of deviation from stoichiometry on thermal conductivity at different values of temperature, correlation 32.

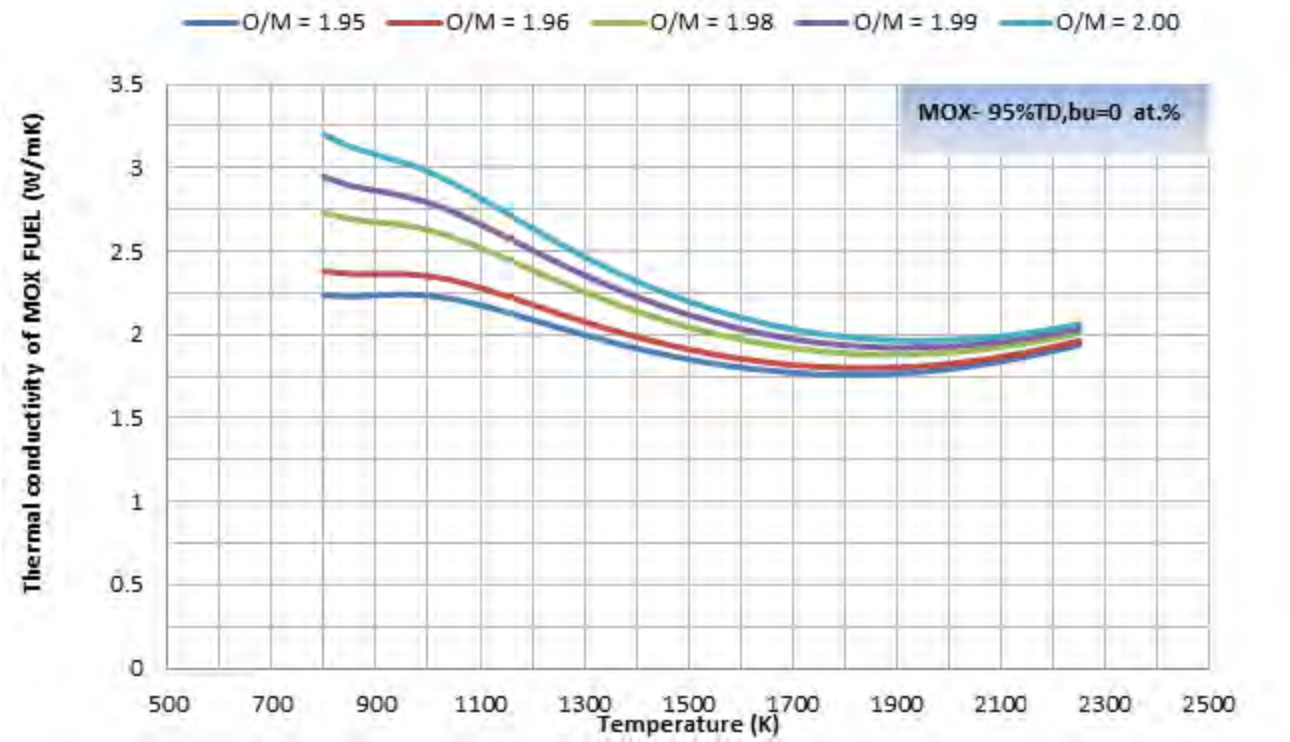

Fig.7 - Thermal conductivity as a function of temperature for different burn ups, correlation 32.

2.3 Correlation 33-Lanning and Beyer

This correlation gives the thermal conductivity for 95%TD MOX according to Lanning and Beyer. The correlation is based on the work of Duriez et al.[8] It gives the thermal conductivity as a function of temperature, burn up and deviation from stoichiometry included in the lattice vibration term and another term for ambipolar thermal conductivity that is a function of temperature only.

The thermal conductivity for MOX 95%TD is given by:

$$k_{95} = \frac{1}{(A(X) + B(X)T + f(bu) + (1 - 0.9e^{-0.04bu})xg(bu)xh(T))} + \frac{C_{mod}}{T^2}e^{-\frac{D}{T}} \qquad \text{Eq.18}$$

Where:

X is the deviation from stoichiometry and

$A(x) = 0.035 + 2.85X$

$B(X) = (2.86 - 7.15X)x10^{-4}$

$f(bu) = 1.87x10^{-3}xbu$

$g(bu) = 0.038xbu^{0.28}$

$h(T) = \frac{1}{1 + 396e^{\frac{-6380}{T}}}$

$C_{mod} = 1.5x10^{9}$

$D = 13520$

T is in K and the burn up is in $\frac{MWd}{kgHM}$.

A porosity correction term according to Lucuta applies to obtain the thermal conductivity at different real densities. The porosity correction is on the form of Maxwell-Euckman formula:

$$k_p = k_{95} x 1.0789 x \left(\frac{d}{1 + 0.5(1 - d)}\right) \qquad \text{Eq.19}$$

The correlation predicts decrease of thermal conductivity with temperature until it reaches a minimum between 1850 and 1900 K then begins to rise again due to the electronic heat conduction as shown in *Fig.8* for a 95%TD of the fuel at different burn-ups. The same is true for different values of fuel porosity. It can be noticed as well that the decrease of thermal conductivity with burn-up which is consistent with the other MOX correlation used in TRANSURANUS and the theoretical expectations. Again, the effect of burn-up on the thermal conductivity is more important at lower temperature as can be seen from *Fig.8* being the degradation of conductivity in the order of 40% at 800K (in the range 0 – 100MWd/kgHM). At 2000 K, the thermal conductivity for the same range of burn-up decreases by 18%.

Porosity effect is given in *Fig.9*. The decrease is linear and the rate of decrease is constant over the whole range of temperatures (it is about 15% when the porosity increase from 0 to 10%).

Deviation from stoichiometry is accounted in *Fig.10* and *Fig.11*. The more hypostoichiometric the fuel, the higher the decrease of the thermal conductivity. For a change of O/M from 2 to 1.95, the decrease in thermal conductivity can reach upto 30% at 800 K. This effect gets lower as the temperature goes high. At 2000 K and the reduction in thermal conductivity on the same range of change of O/M ratio is about 8%, as noticed in *Fig.10*.

It is known that the thermal conductivity decreases with temperature to a minimum then increases again. It can be notice from *Fig.10*. that the more hypostoichiometric the fuel is the lower the temperature for which the thermal conductivity reaches that minimum.

As in the previous case, the correlation is non physical for hyperstoichiometry since it predicts the increase of thermal conductivity with hyperstoichiometry which contradicts the experimental findings. It sholud be pointed out that the code recommends the use of these correlations only for O/M up to 2. The lower is the temperature, the higher is the degradation of thermal conductivity with the hypostoichiometry, *Fig.11*. For 800 K the thermal conductivity decreases by 30% for a deviation from stoichiometry of 0.05. At 2000 K for the same range of deviations the decrease of thermal conductivity is around 8% and decreases more as the temperature goes higher.

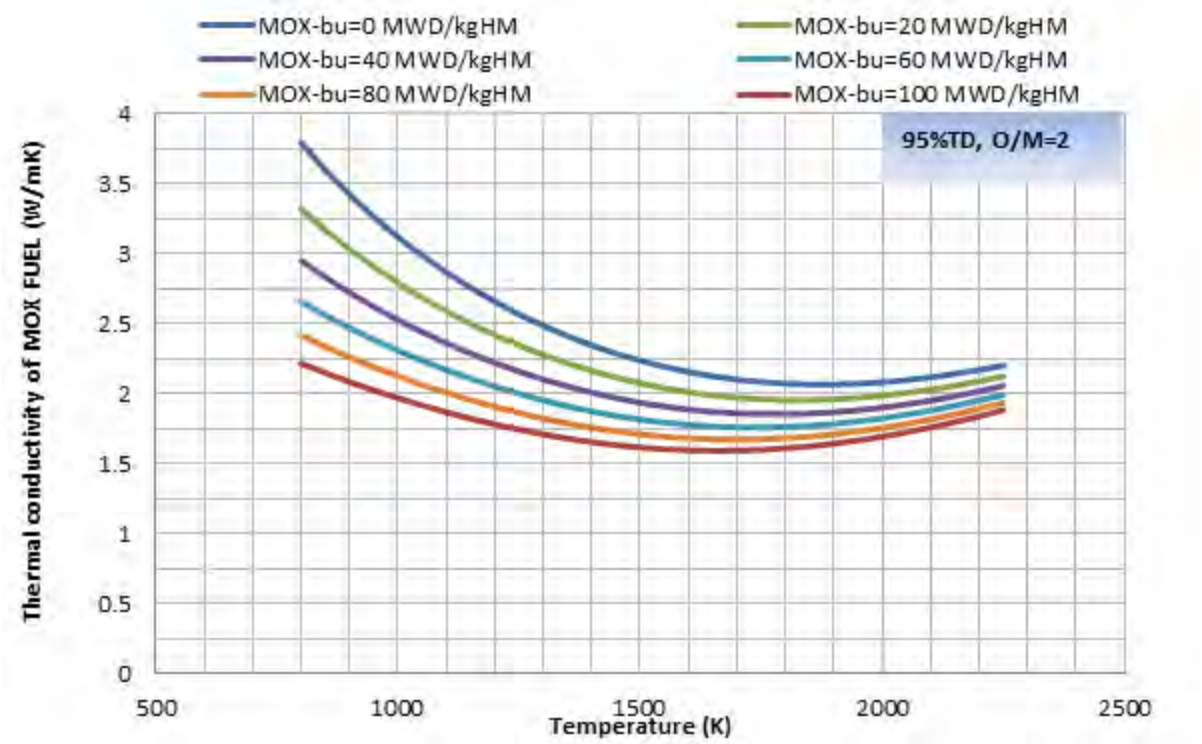

Fig.8 - Thermal conductivity as a function of temperature for different burn ups, correlation 33.

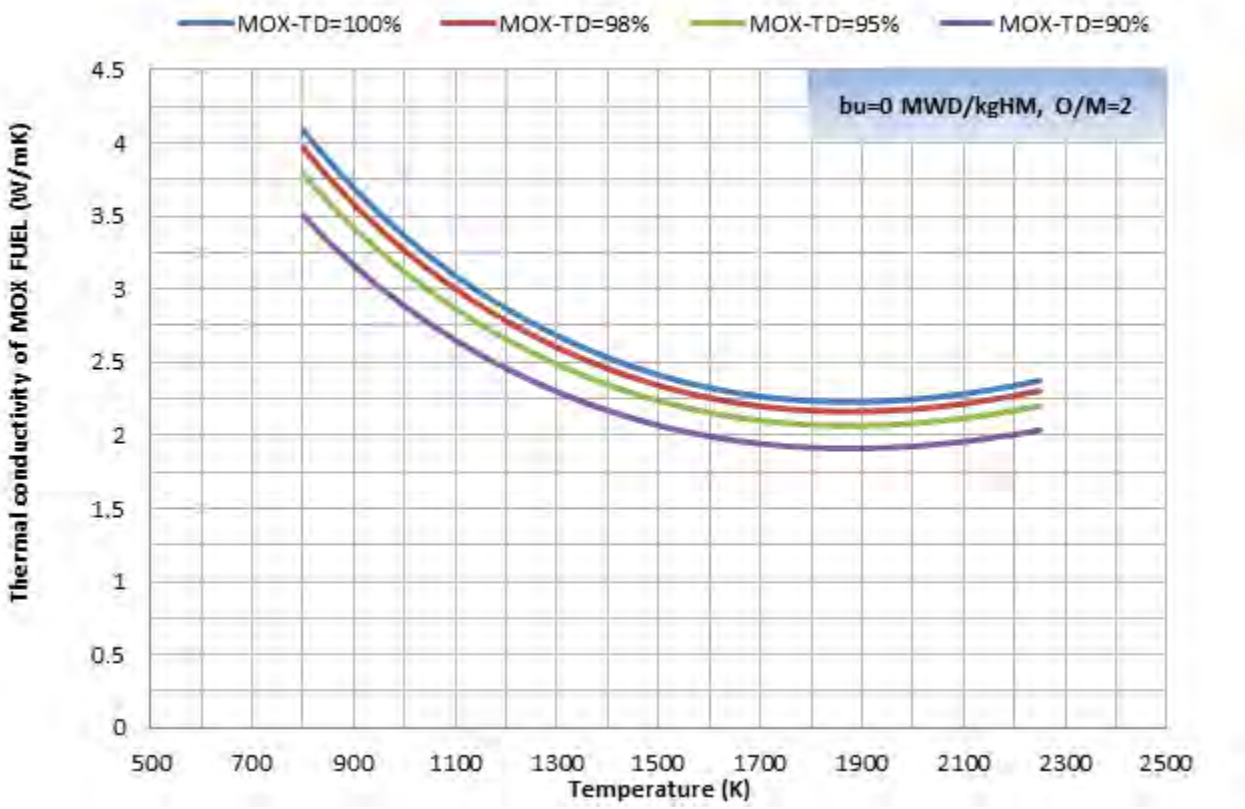

Fig.9 - Effect of fuel porosity on thermal conductivity, correlation 33.

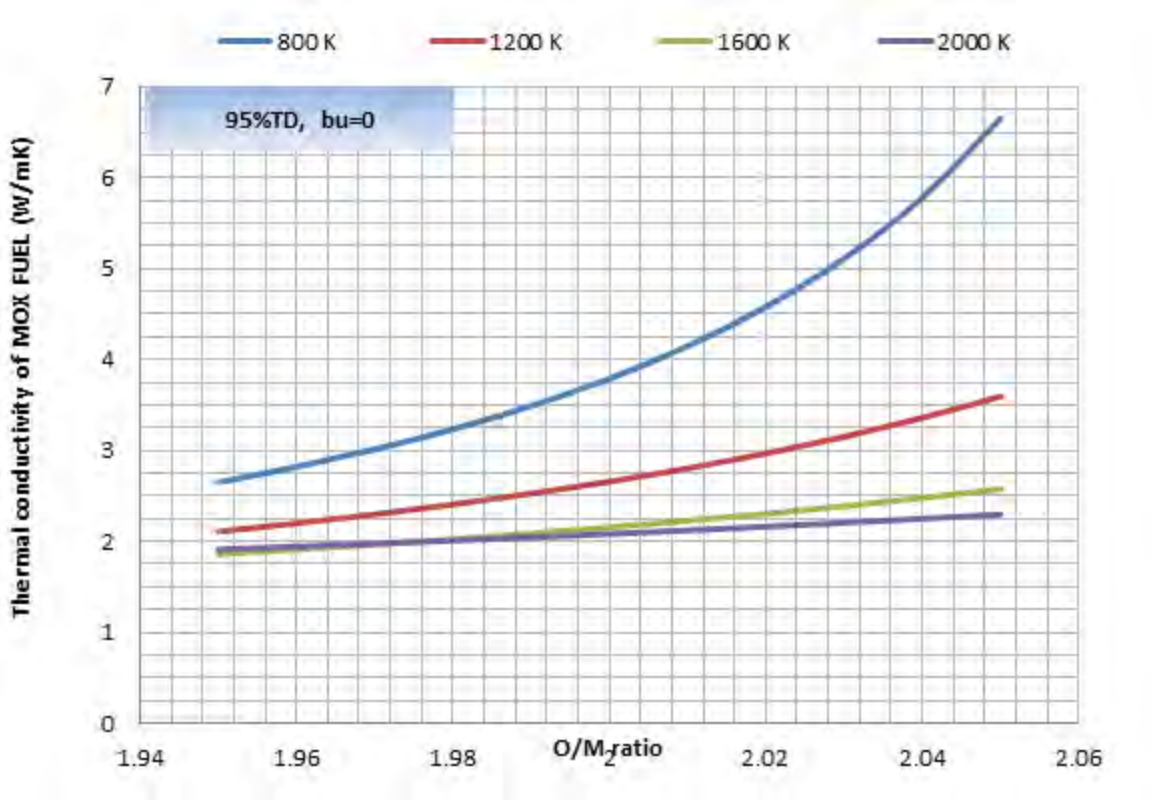

Fig.10 - Effect of deviation from stoichiometry on thermal conductivity at different values of temperature, correlation 33.

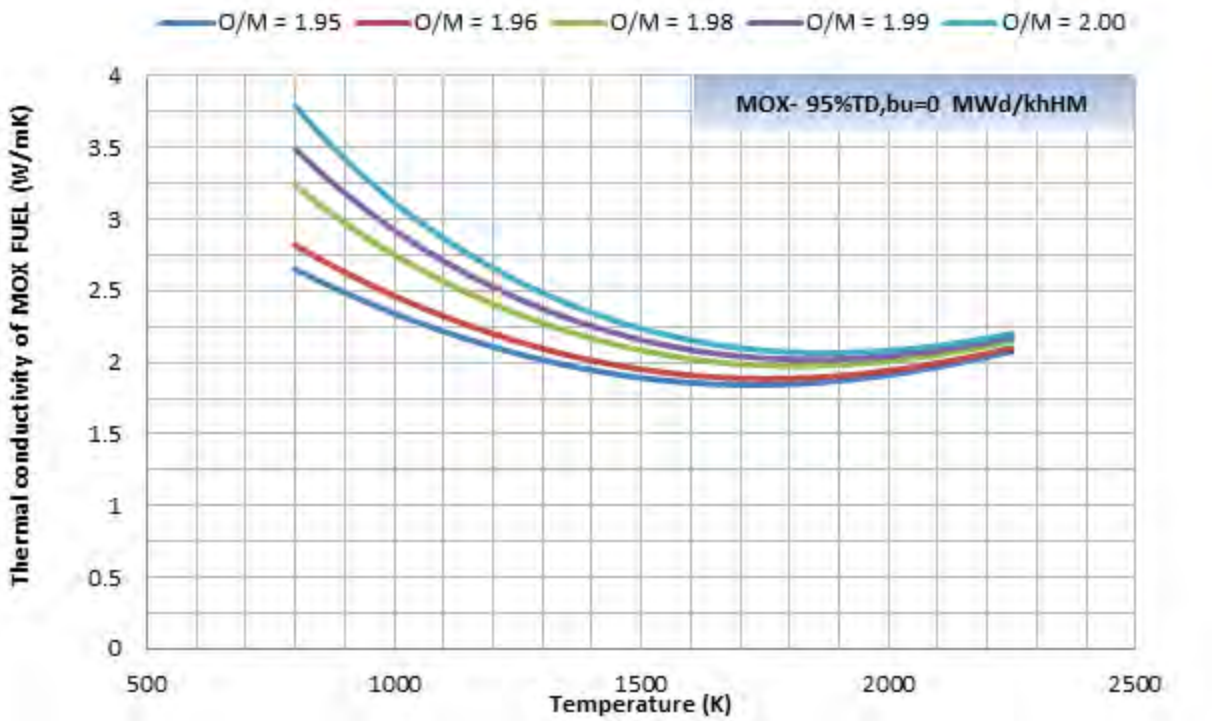

Fig.11 - Thermal conductivity as a function of temperature for different burn ups, correlation 33.

2.4 Correlation 34, Wiesenack.

Correlation 34 is the original Wiesenack's correlation that is developed for UO_2 fuel. In order to apply it for MOX, the correlation is multiplied by a correction factor of 0.92. The original correlation gives the thermal conductivity of MOX as a function of temperature and burn-up on the form:

$$k_{95} = \frac{1}{A_0 + A_1 bu + Bxmin\{1650, \vartheta\} + B_2 buxmin\{1650, \vartheta\}} + Ce^{D\vartheta} \left[\frac{W}{mK}\right] \qquad \text{Eq.20}$$

Where:

$A_0 = 0.1148$
$A_1 = 0.0035$
$B = 2.475x10^{-4}$
$B_2 = -8.24175x10^{-7}$
$C = 0.0132$
$D = 0.00188$

And ϑ is the temperature in [^{0}C] and bu is the burn up in $\frac{MWd}{kgUO2}$
There is no specific equation for porosity correction given for this model so the original MATPRO-11 porosity correction is used:

$$k_P = k_{95} \frac{1 - \beta P}{1 - 0.05\beta} \qquad \text{Eq.21}$$

Where P is the porosity and $\beta = 2.58 - 0.58x10^{-3}\vartheta$

The correlation predicts a decrease of thermal conductivity with temperature until it reaches a minimum between 1700 and 1900 K. For un-irradiated fuel, the minimum of thermal conductivity is reached at 1900 as shown in *Fig.12*. The correlation indicates that as the burn up of the fuel increases, that minimum in thermal conductivity is reached at a lower temperature. The minimum in thermal conductivity at burn up of 100 $\frac{MWd}{kgUO2}$ is reached at a temperature range between 1500 to 1600. It can be noticed as well that the higher the burn up the flatter the curve of thermal conductivity at lower temperature before it increases rapidly again at higher temperature. This gives an indication that the phonon-phonon lattice vibration term is not effective and that the constant term related to the phonon-defect interaction is the dominant one leading to almost constant thermal conductivities at the range in which the thermal conductivity is more dependent on lattice vibration rather than electronic conductivity. The thermal conductivity begins to rise again in the range of temperature in which the ambipolar conductivity is dominant. The effect of burn up on the thermal conductivity is higher at lower temperature as shown in *Fig.12* At 800 K the thermal conductivity decreased by 55% of its original value for unirradiated fuel when the burn up reached 100 $\frac{MWd}{kgHM}$. For 2000 K, the thermal conductivity for the same range of burn-up decreases by 25%. The burn up at temperatures higher than 2000K seems to have a constant effect. The amount of thermal conductivity decrease is the same regardless of the initial level of thermal conductivity. The curves appear to be parallel to each others as can be seen in *Fig.12*.

The correlation predicts (*Fig.13*) a decrease of thermal conductivity with porosity. This decrease in thermal conductivity is about 22% at low temperature (800 K) when the porosity increases from 0%

to 10%. On the same range of variation of porosity, as the temperature increases to 1900 the decrease of thermal conductivity with porosity decreases to 11%.

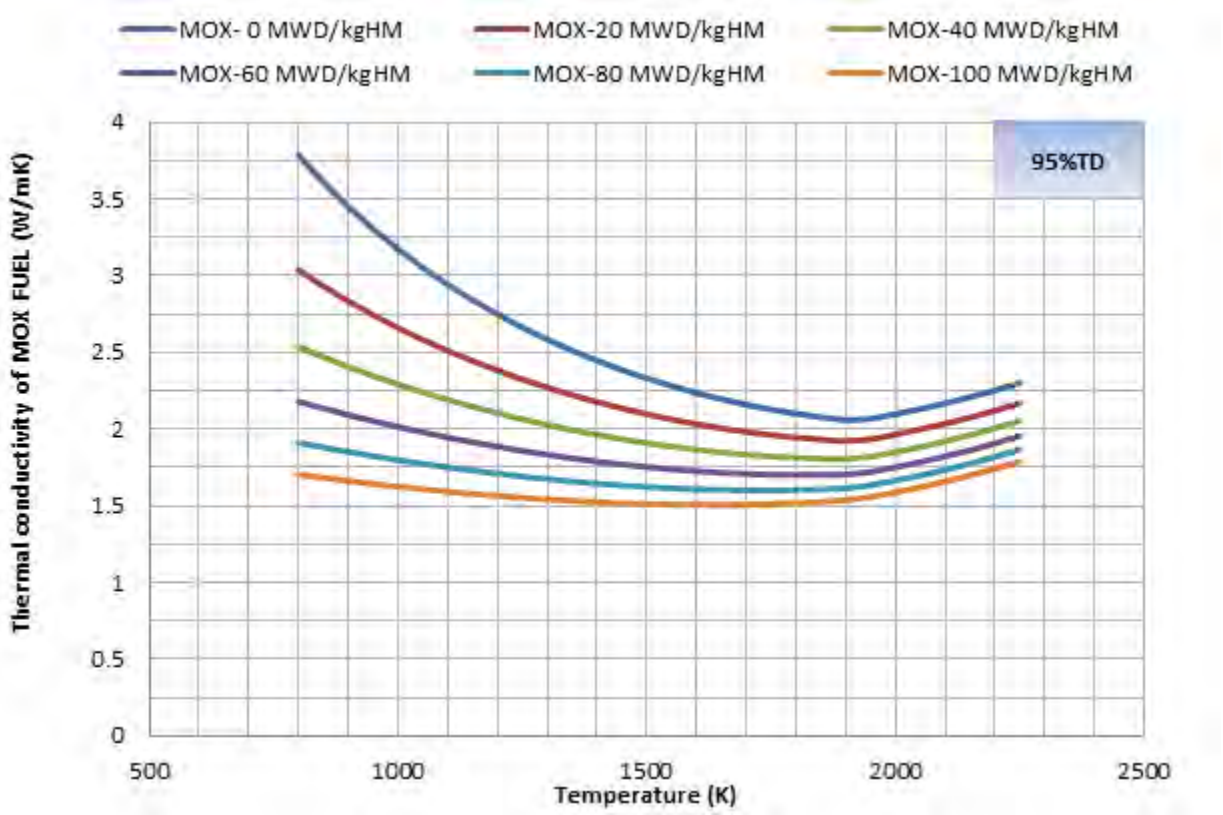

Fig.12 - Thermal conductivity as a function of temperature for different burn ups, correlation 34.

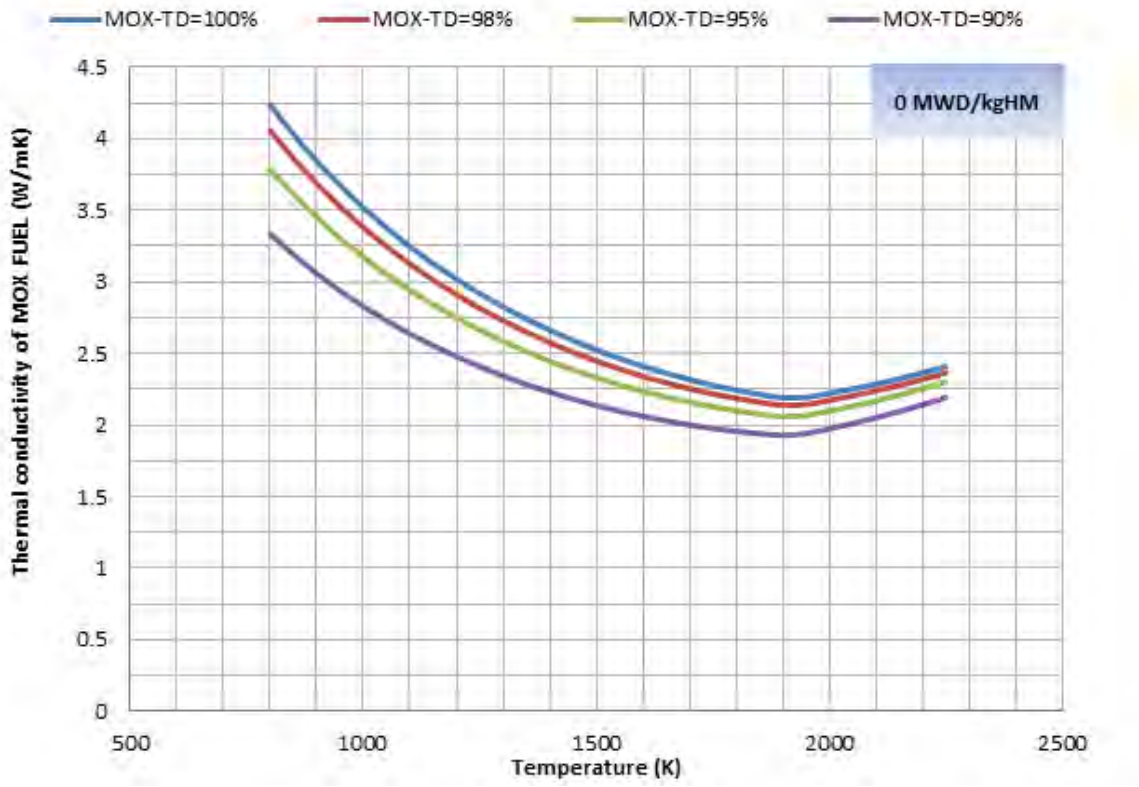

Fig.13 - Effect of fuel porosity on thermal conductivity, correlation 34.

2.5 Comparison among TRANSURANUS models

The correlations implemented in TRANUSURANUS code described above are compared in Fig. 14 and Fig.15. The thermal conductivity change with temperature for un-irradiated 95% TD MOX fuel is given in Fig. 14. The two correlations that has the effect of deviation from stoichiometry as variables are ploted for two limits of 2 (stoichiometric condition) and 1.96 to see the range of changes due to deviation from stoichiometry.
One can notice from Fig. 14 that the highest predicted thermal conductivity for the whole temperature range is that for the Weisenak correlation (correlation 34) that is originally developed for UO_2 fuel with a correction factor to make it applicable for MOX. Lanning and beyer's correlation for stoichiometric condition gives values that are comparable to that of the modified Weisenak correlation. The more hypostyoichiometric the fuel becomes, the higher deviation between the two correlations exists. Correlation 31 according to Van Ufflen and Schubert is identical to that of Lanning and Beyer (correlation 33) at lower temperature. As the ambipolar thermal conductivity term begins to dominate, Correlation 33 deviates to a lower values from that of Correlation 31 which is similar with the thermal conductivity according to Carbajo (correlation 32). Correlation 32 gives a lower value of thermal conductivity from the other correlations at stoichiometric conditions. At temperatures below 1000 K then, it becomes similar with them in the intermediate temperature range then follow the same path as correlation 31 and deviates again to lower values than that of correlation 32 and 34.

For the same theoretical density and with burn-up up to 100 $\frac{MWd}{kgHM}$, the rate of degradation of thermal conductivity according to correlation 34 is the highest for most of the temperature range of interest leading to higher decrease of thermal conductivity. The thermal conductivity by that correlation is now comparable to those for the hypo-stoichiometric (O/M =1.96) correlations. Stoichiometric correlations 32 and 33 have the lowest rate of decrease of thermal conductivity with burn up and at the level of 100 $\frac{MWd}{kgHM}$ they predict the highest thermal conductivities among all the correlations.

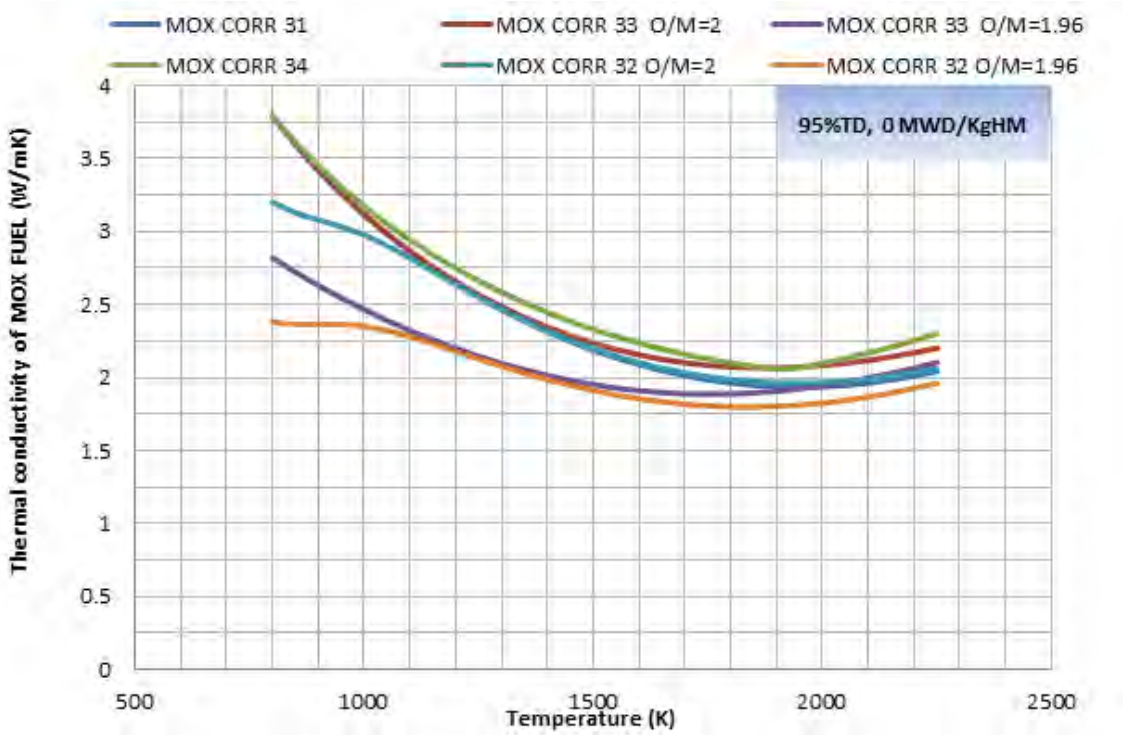

Fig.14 - Thermal conductivities from TRANSURANUS correlations.

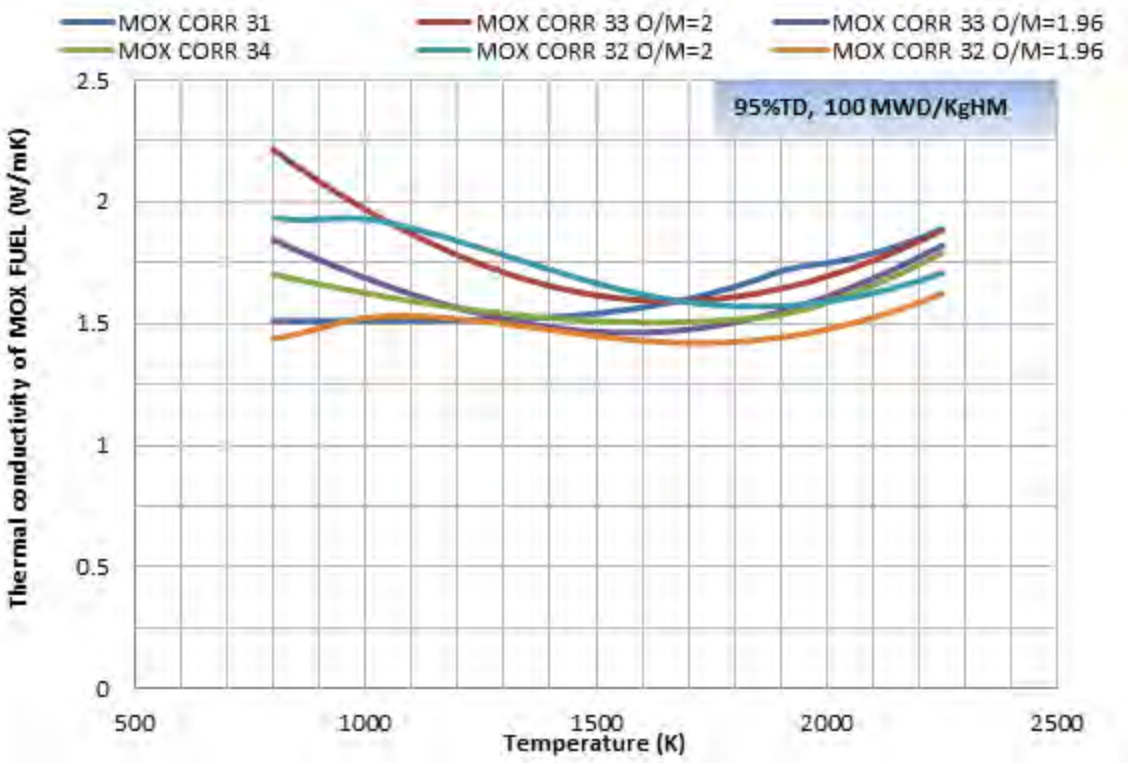

Fig.15 - Thermal conductivities from TRANSURANUS correlations.

3 Analysis of MOX conductivity models from open literature

In this section, several open literature correlations are described along with the variables that are considered. The form of the equation for each model along with comments on the results obtained from these correlations are included.

3.1 D.G Martin review 1982

In this work Martin did a re-appraisal of four thermal conductivity correlations (Washington, Anscough, Killeen and Brandt) and chose one of them to do some ammendments to it instead of producing a new independent correlation. The correlation chosen was that based on Washington's review in 1973. Even though the correlation by Killeen was the most correlation based on theory for stoichiometric fuel, There were no theoretical knowledge sufficient enough to apply it with certainity on non-stoichiometric fuel. The two correlations (*Fig.16*) are close to each other at low and high temperature range, and even in the intermediate one, the deviation of Washington's correlation from that of Killeen should not cause great errors.[7]

The data available were reappraised and the few new data that appeared since the work of Washington were added to the review. The correlation seemed to be giving satisfactory results for UO_2 and MOX as a function of temperature and O/M ratio.

The amended correlation can be written for hypostoichiometric MOX as:

$$K_{100} = \frac{1}{0.037 + 3.33X + 2.37.10^{-4}T} + 78.9.10^{-12}T^3 \qquad \text{Eq.22}$$

The original correlations were tailored for UO2 and were projected to MOX by assuming a correction factor of 0.95.The new correlation neglected the effect of irradiation in the temperature range of (500-2800 ^{0}C) and the effect of plutonium content. It took the O/M ratio into account in the lattice vibration term. The porosity correction was based on a modified Loeb forumula for porosity level between (0<P<0.1) and based on Maxwell-Euckman formula in the range of (0.1<P<0.2). The effect of porosity is a linear decrease of thermal conductivity as the porosity increases. This decrease reaches to 42% for a porosity increase from 0 to 20% as shown in *Fig.17*

The effect of deviation from stoichiometry is a degradation of the thermal conductivity. This effect is predicted from this correlation as shown in fig. to be from 42% at temperature of 800 K and decreases with temperature to a value of 18% at 2000K for a stoichiometry change between (2 and 1.95). The effect of stoichiometry keeps decreasing with temperature but it can be considered important on the whole range of normal operation of a fast breeder reactor fueled with MOX.

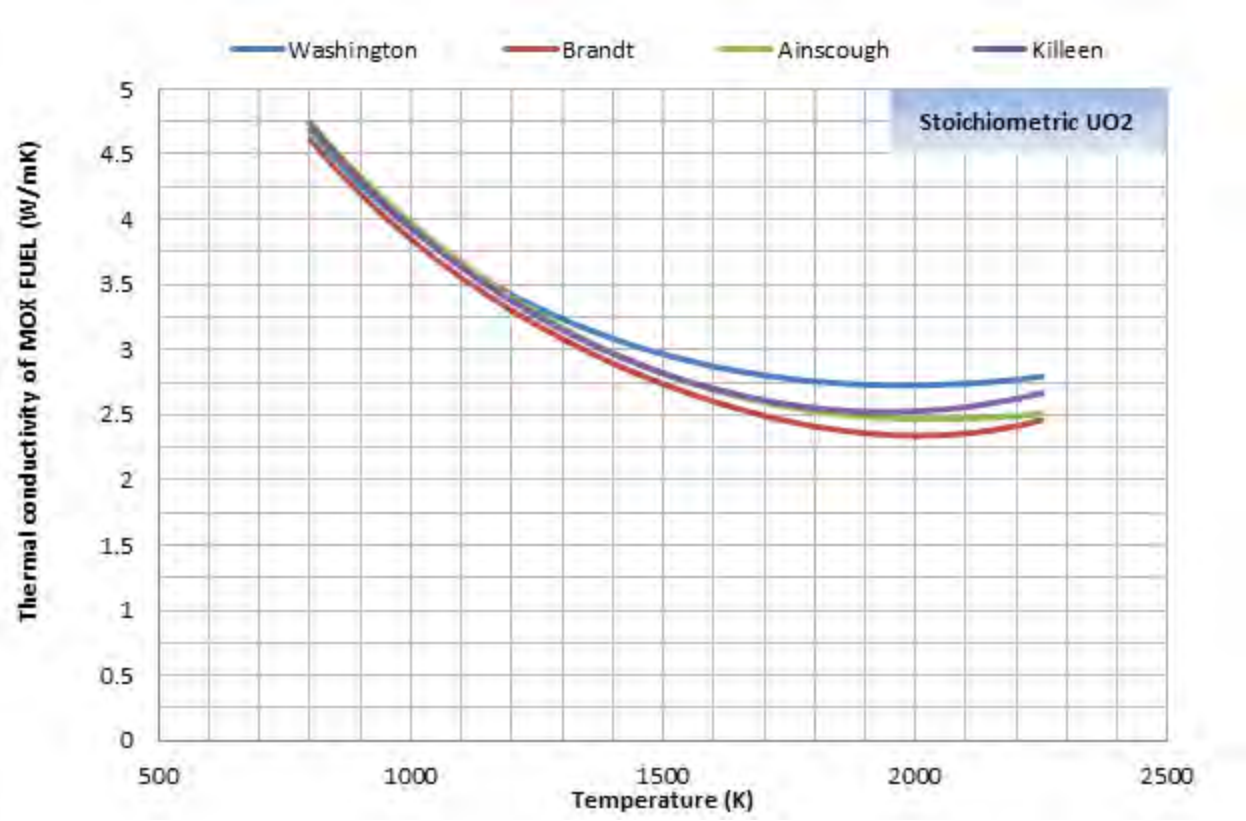

Fig.16 - Thermal conductivity according to the four re-appraised models by Martin.

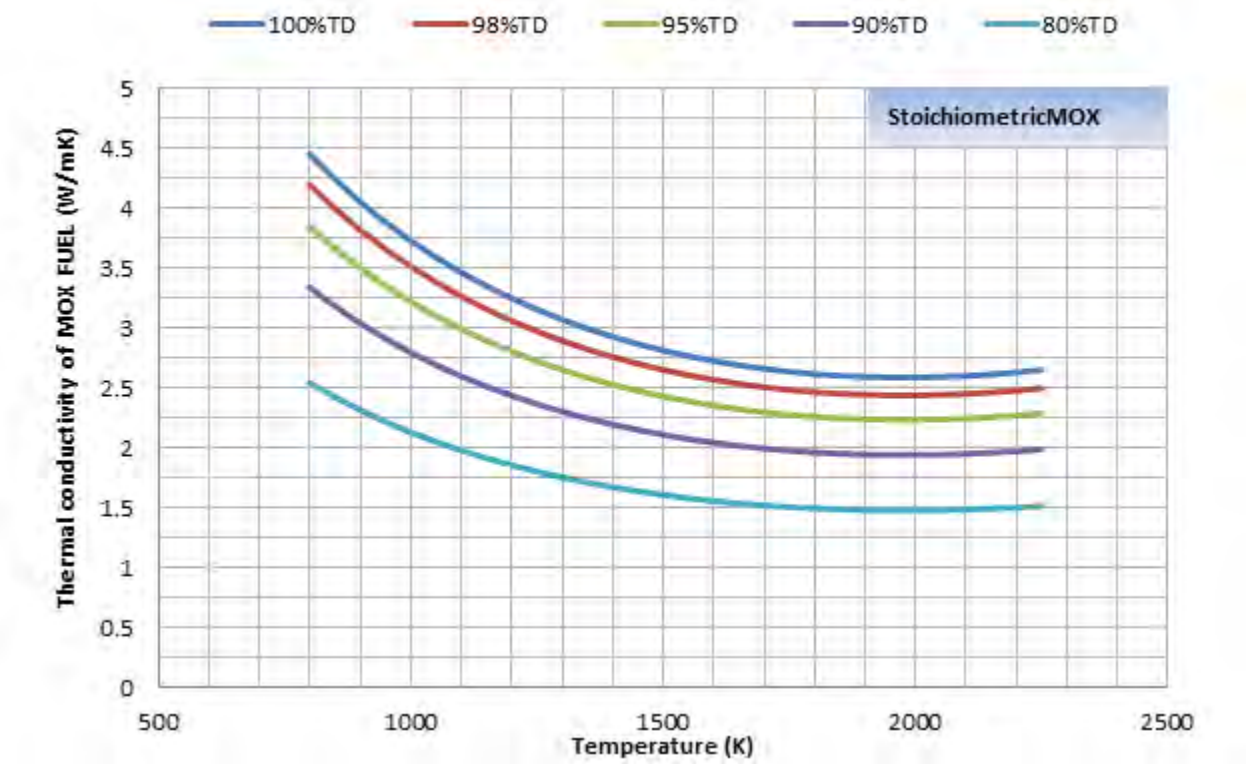

Fig.17 - Effect of fuel porosity on thermal conductivity, Martin.

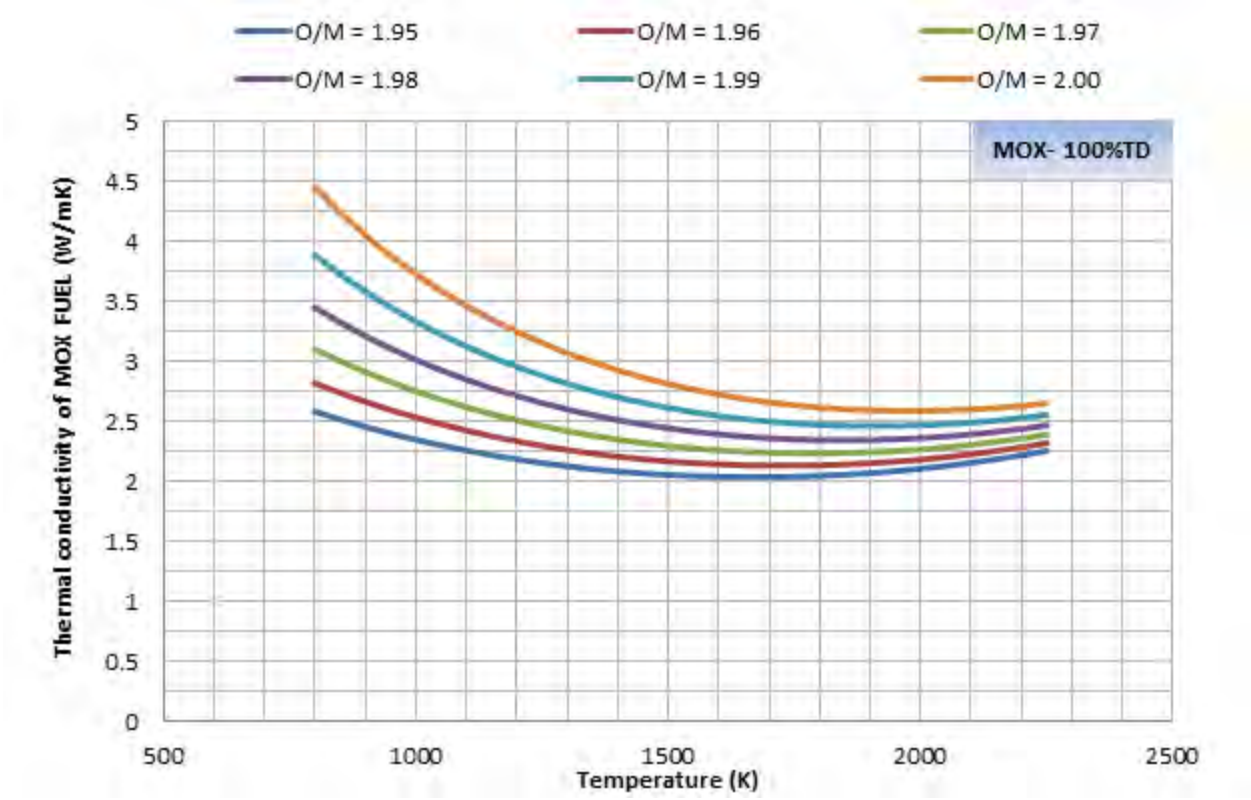

Fig.18 - Thermal conductivity as a function of temperature for different stoichiometries, Martin.

3.2 FTHCON subscode-MATPRO

The correlation used by the FTHCON subroutine determines the thermal conductivity of uncracked UO_2 and MOX fuels as a function of temperature, O/M ratio and plutonium content of a solid fuel. It uses a porosity correction based on the Maxwell-Eucken relation. The burn-up is used only to calculate the melting temperature of the fuel. Interpolation is used to remedy the discontinuity of the slope in the temperature range between (1364-2300 K).

The correlation can be written as follows for Solid fuel:

$$= \left[\frac{D}{1+(6.5-0.00469T'(1-D)}\right]\left[\frac{C_V}{(A+BT'')(1+3e_{th})}\right] + 5.2997\text{x}10^{-3}\text{Te}^{\left[-\frac{13358}{\text{T}}\right]}\left\{1+0.169\left[\frac{13358}{\text{T}}+2\right]^2\right\} \quad \text{Eq.23}$$

Where:

K = Thermal conductivity (W/m.K)
D = fractional theoretical density
C_V= Phonon contribution to the specific heat at constant vlume (J/kg.K). MATPRO correlation for specific heat is used to calculate this factor
e_{th}= Linear strain caused by thermal expansion for temperatures above 300 K. MATPRO correlation for linear strain is used to calculate this factor for uranium and plutonium then the value is weighted according to the percentage of Plutonium in the fuel.
A = a factor represents the point defect contribution to the phonon's mfp. = 0.339 + 12.6X where X is the absolute value of the deviation from stoichiometry

B= a factor representing the phonon-phonon scattering contribution to the thermal conductivity. = 0.06867(1 + 0.6238 PU) where PU is the weight fraction of the plutonium content of the fuel.
T = Fuel temperature in (K)
T' = Fuel temperature if <1364.
For temperature higher than 1834 then $D\{1 + [6.5 - 0.00469T']\} = -1$
For intermediate range (1364<T<1834), linear interpolation is used to obtain the value of T'
T'' = Fuel temperature if T<1800
2050 if T> 2300
Between (1800<T<2300)Linear interpolation is used to obtain the value of T''

The expected standard error for this correlation is as follows

$$UK = [0.2(1 - PU) + 0.7PU](1 + [2 - O/M]10)$$

Even though the deviation from stoichiometry is included in the model as a parameter determining thermal conductivity, the model does not show any sensible change of thermal conductivity with deviation from stoichiometry. *Fig.19* shows the magnitude of difference of thermal conductivity for a deviation from stoichiometry of 0.05. The maximum change of thermal conductivity at temperature of 500 K is less than 2% and decreases more with temperature to reach less than 0.3% at 3000 K.

The model (*Fig.20*) predicts a change of thermal conductivity between (12 to 9)% with the plutonium content (0 to 30%.wt) between 500K and 2250 K respectively. This shows a rate of decrease of (0.4 to 0.3%) for every 1%.wt increase in Plutonium content. The results shows that the Thermal conductivity of The model is more dependent on Plutonium content than on deviation from stoichiometry.

In *Fig.21*, the thermal conductivity is plotted as a function of temperature for different values of plutonium content for stoichiometric fuel at 95%.TD. The figure shows the results that were illustrated in *Fig.20* as a function of temperature.

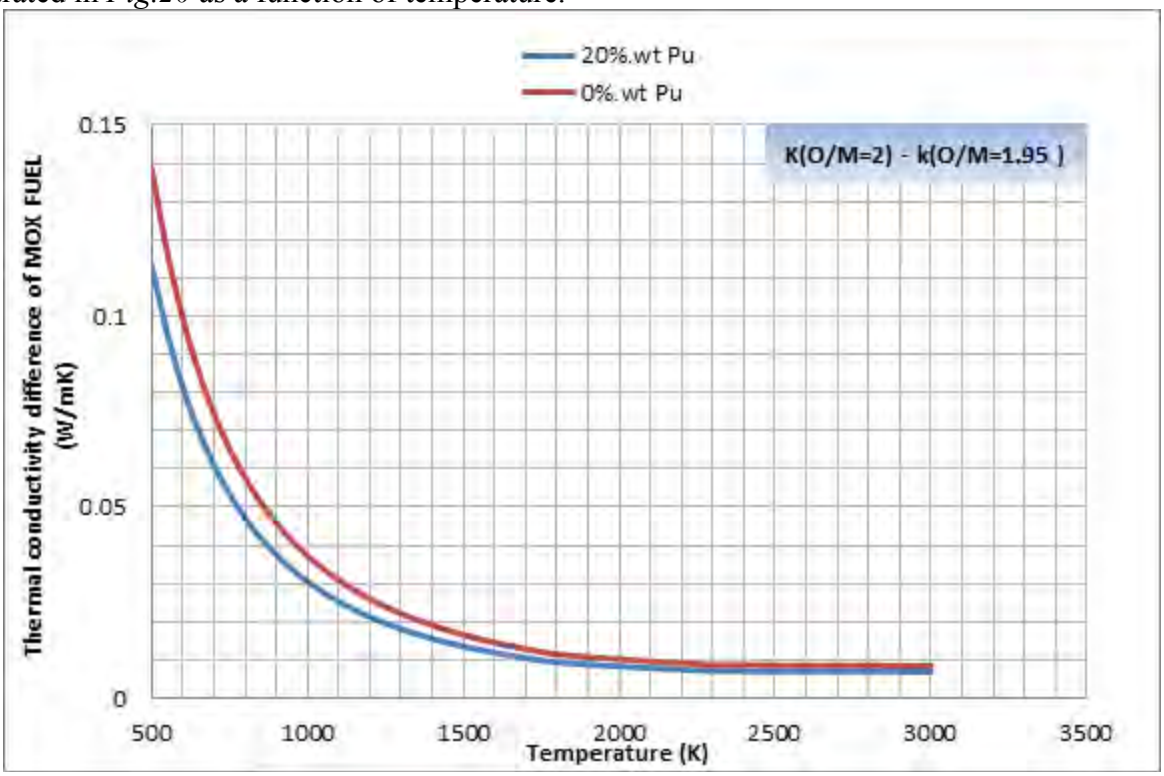

Fig.19 - Difference between thermal conductivities measured at O/M 0f 2 and 1.95 plotted as a function of temperature.

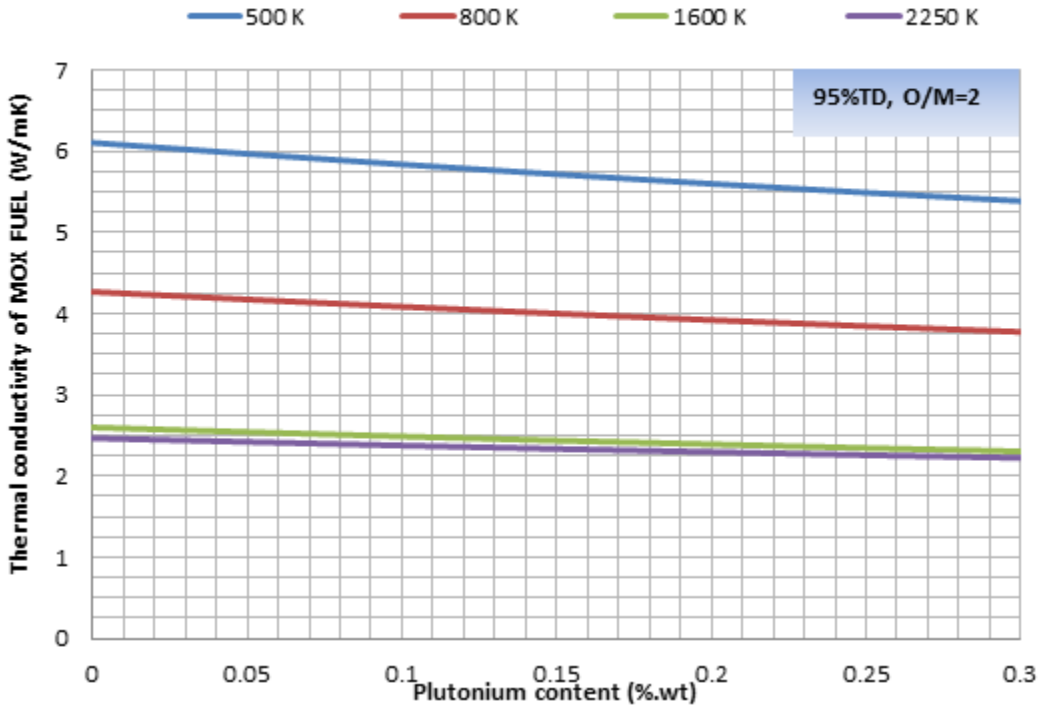

Fig.20 - Thermal conductivity as a function of plutonium content of the fuel.

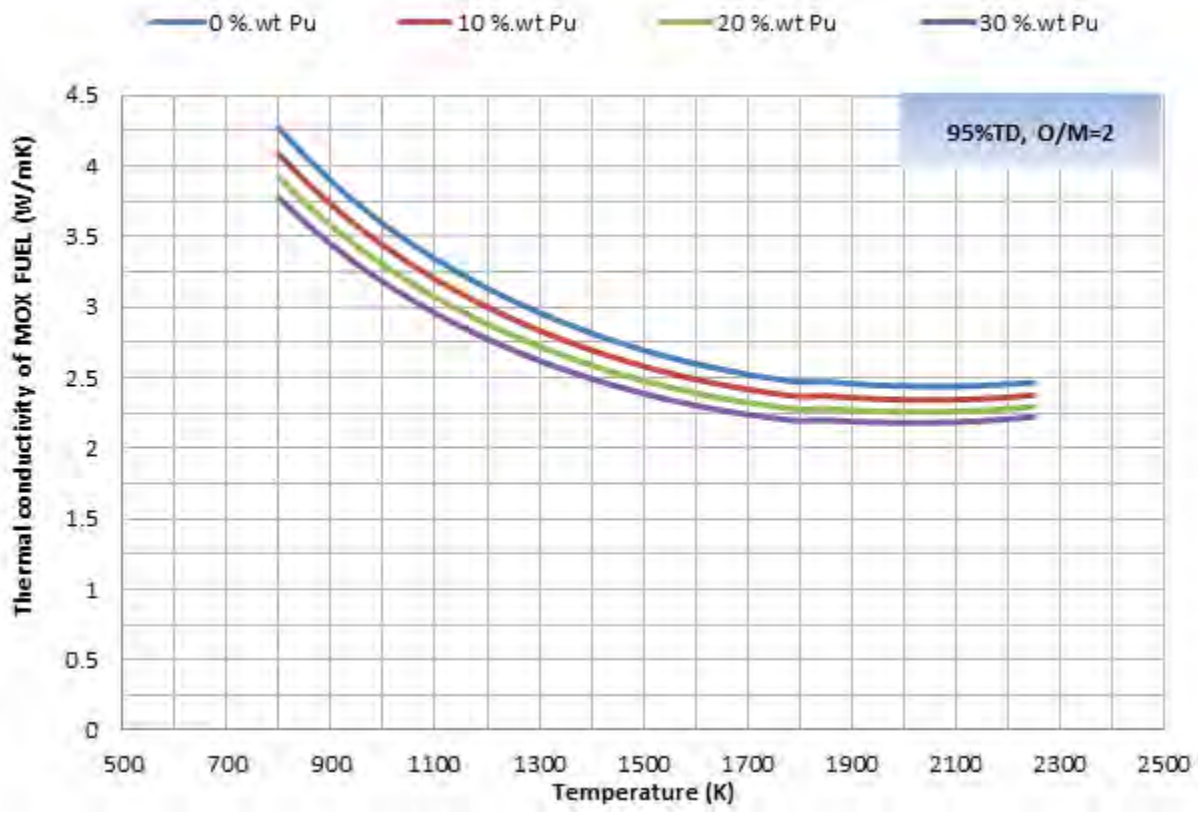

Fig.21 Thermal conductivity as a function of temperature for different Plutonium contents.

3.3 The COMETHE formulation-1982

This formula is used for UO_2 and MOX fuels. It gives thermal conductivity of 95%TD fuel. A porosity correction is used to give the thermal conductivity at different porosities. It was enhanced to take the plutonium weight percentage into account based on the data from Gibby, Van Craey and weilbacher.[11] The formula is written as follows

$$K_{95TD} = \frac{A_0}{A_1+A_2X+(1+B_0q)T} + CT^3 \qquad (\text{Eq.24}$$

Where
T = temperature (K)
X = absolute value of deviation from stoichiometry
q= Plutonium content
A_0 = 40.05
A_1 = 129.4
A_2 = 16020
B_0 = 0.8
C = 0.6416×10^{-12}

The model predicts (*Fig.22*) a decrease in thermal conductivity at lower temperature of about 0.5% for every 1%.wt increase in the Plutonium content for stoichiometric fuel. The rate of decrease slightly decreases at 2000 K but still in the same range of 0.5% per 1%.wt increase in Pu content implying a constant effect of plutonium content on the whole temperature range of interest under normal operations.
The effect of deviation from stoichiometry (from 2 to 1.95) is illustrated in Fig.23. The decrease of thermal conductivity with hypo-stoichiometry can reach up to 42% decrease in thermal conductivity at lower temperatures (800 K). This effect decreases with temperature to reach around 18% decrease with stoichiometric decrease from 2 to 1.95. For the whole range of temperatures of interest the change of thermal conductivity with deviation from stoichiometry is higher than that due to increase of plutonium content of the fuel.

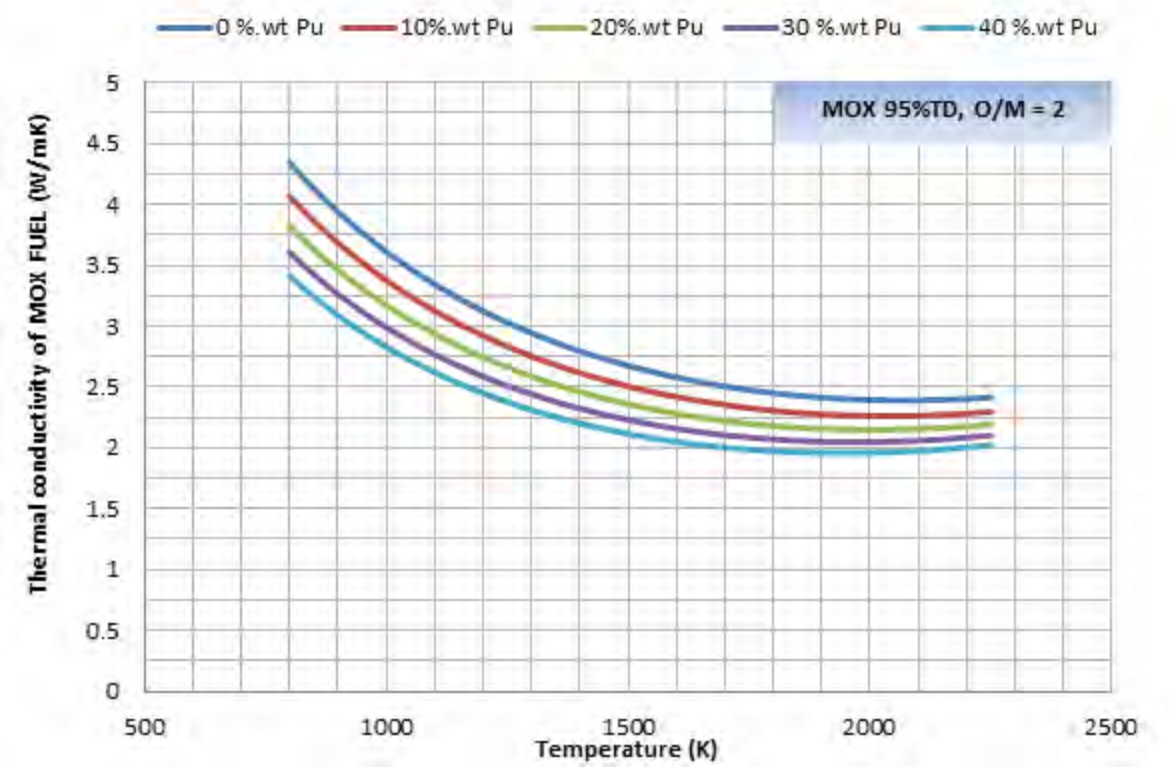

Fig.22 - Thermal conductivity as a function of temperature for different plutonium contents.

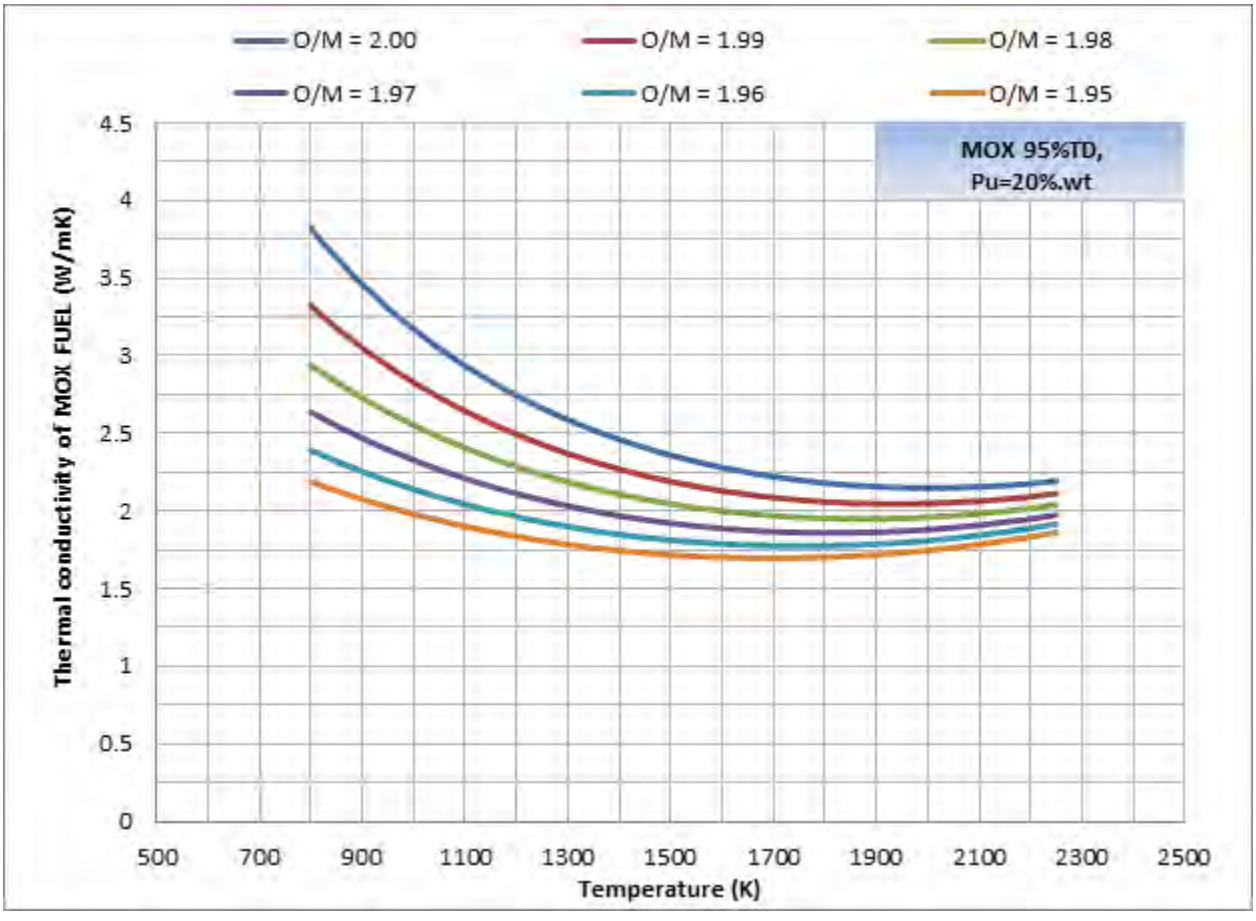

Fig.23 - Thermal conductivity as a function of temperature for different O/M ratios.

3.4 Baron Hervè- 1995 Model

The model is a modification of the same model that originated in 1994. The modification concerns the high temperature term. It included originally a term relating high temperature conductivity to radiation. The modification substituted this term by another one that considers electronic thermal conductivity instead. This was done based on the work be Delette and Charles.[11] The model takes the temperature, deviation from stoichiometry, plutonium and Gadolinium content as variables. In order to apply this model to MOX fuel, The Gadolinium content should be set to zero.

$$K(T) = \frac{1}{A_0 + A_1 x + A_2 g + A_3 g^2 + (B_0(1 + B_1 q) + B_2 g + B_3 g^2)T + \frac{C + Dg}{T^2}\exp(-\frac{W}{kT})} \qquad \text{Eq.25}$$

Where:

k=Boltzmann constant ($1.38.10^{-23}$ J/K)
W= $(1.41*1.6)*10^{-19}$ J
A_0=$4.4819.10^{-2}$(m.K/W), A_1=4, A_2=0.611 (m.K/W), A_3=11.081(m.K/W)
B_0= $2.4544.10^{-4}$(m/W) , B_1=0.8, B_2=$9.603.10^{-4}$(m/W), B_3=$-1.768.10^{-2}$(m/W)
C=$5.516.10^{9}$(W.K/m)
D=$-4.302.10^{10}$(W.K/m)
And, T is temperature in K up to 2600 K, x is the absolute value of deviation from stoichiometry, q is the plutonium weight content, and g is the Gadolinium weight content.

The model predicts the same effect of Plutonium as in the Comethe formulation. In *Fig.24* a decrease in thermal conductivity at lower temperature of about 0.5% for every 1%.wt increase in the Plutonium content for stoichiometric fuel. The rate of decrease slightly decreases at 2000 K but still in the same range of 0.5% per 1%.wt increase in Pu content implying a constant effect of plutonium content on the whole temperature range of interest under normal operations.

The effect of deviation from stoichiometry (from 2 to 1.95) is illustrated in Fig.25. Similar to the COMETHE formulation, the decrease of thermal conductivity with hypostoichiometry can reach up to 42% decrease in thermal conductivity at lower temperatures (800 K). This effect decreases with temperature to reach around 18% decrease with O/M ratio decrease from 2 to 1.95. For the whole range of temperatures of interest, the change of thermal conductivity with deviation from stoichiometry is higher than that due to increase of plutonium content of the fuel.

Comparing the COMETHE formulation and Baron-Hervè model, the values of thermal conductivity at temperatures up to 2000K are comparable. Above 2000 K, It can be noticed that the thermal conductivity increases on a higher rate for Baron-Hervè model than for COMETHE formulation.

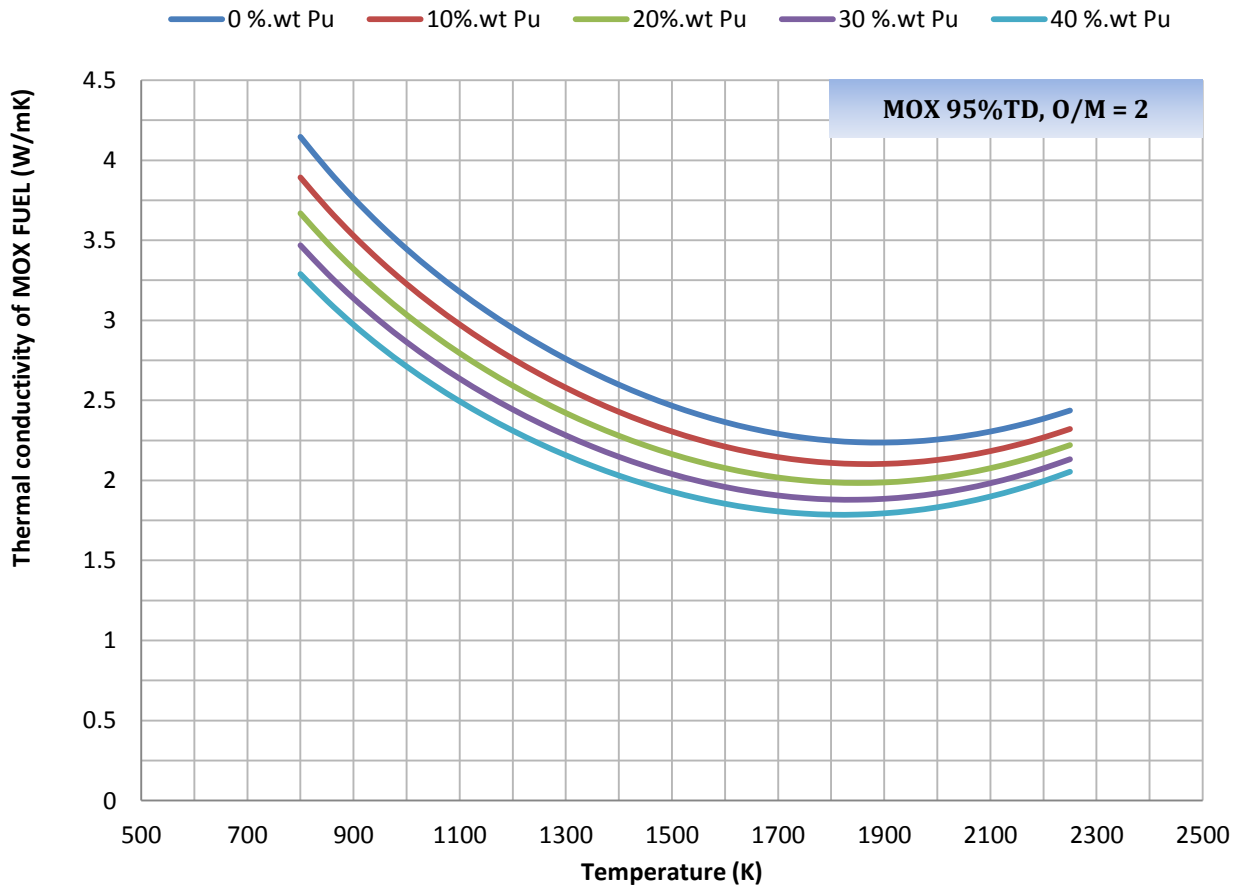

Fig.24 - Thermal conductivity as a function of temperature for different plutonium contents.

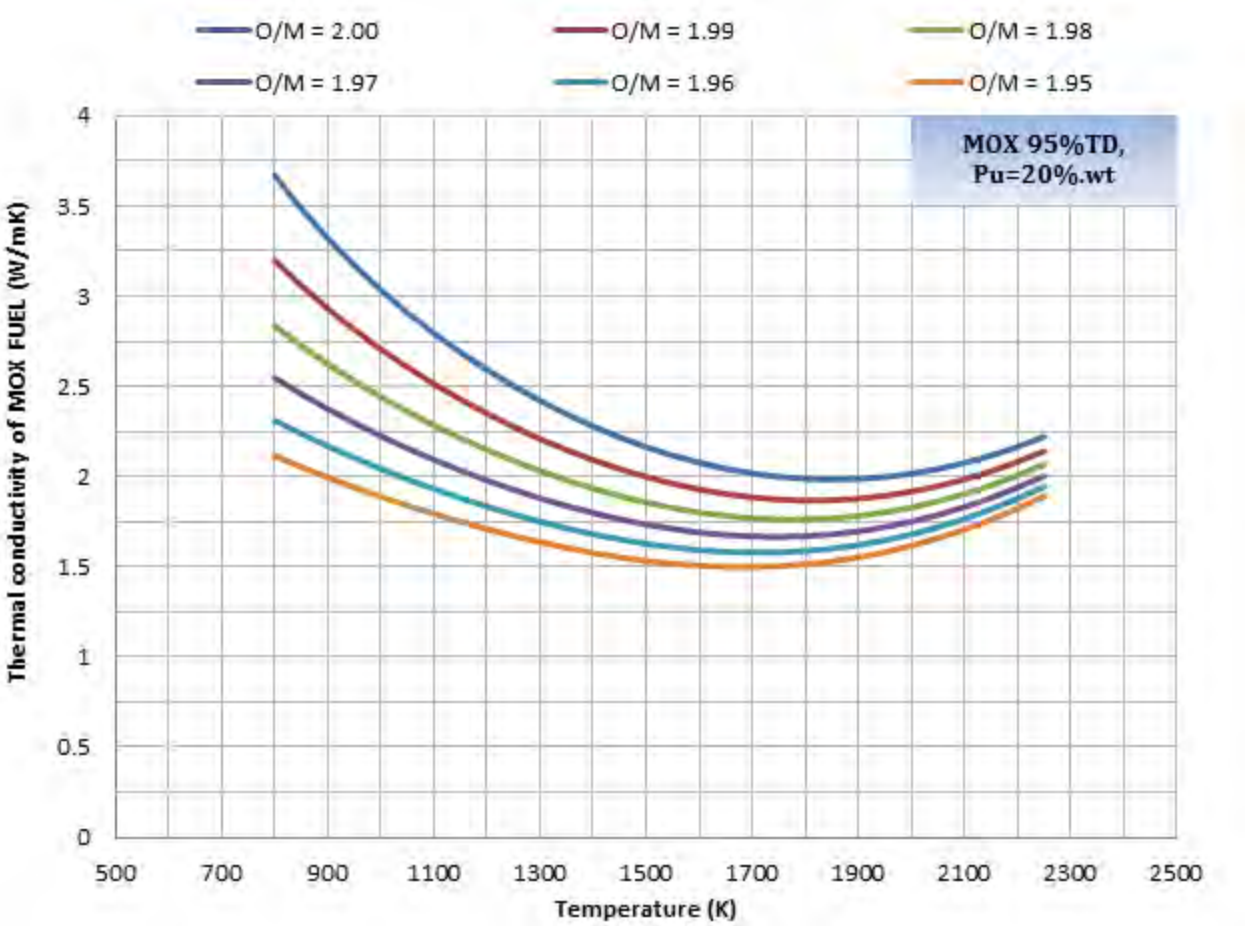

Fig.25 - Thermal conductivity as a function of temperature for different O/M ratios.

4 Comparison between the studied models.

In *Fig.26*, All the studied models are plotted together. For the models that include the deviation from stoichiometry as a variable, the correlations are plotted for fresh fuel, for two limits of stoichiometry (2 and 1.96). This is due to the significant effect of deviation from stoichiometry on thermal conductivity. Meanwhile there are models that do not consider this effect, so it was needed to see the prediction of both types of models together and how the deviation from stoichiometry leads to higher variability between the models.

In *Fig.26*, The TRANSURANUS models are plotted with solid lines while the open literature correlations are in dashed lines at O/M ratio of 2. The open literature correlations are plotted with dots at O/M=1.96.

FOR (O/M=2), It can been seen that MATPRO at 20%.wt Plutonium and Martin's values of thermal conductivity are higher than TRANSURANUS models for all values of temperatures considered. The values of COMETHE formulation for 20%.wt Plutonium is following Wiesenack's correlation upto 1600K then becomes slightly higher than it, then becomes lower again at 2100K. The COEMTHE formulation gives higher thermal conductivities than the rest of TRANSURANUS correlations for the shown range of temperature, except at 2200K when Lanning and beyer's correlations starts to give higher values of thermal conductivities.

Baron and hervè's correlation for 20%.wt Pu gives lower values than TRANSURANUS correlations except Carbajo's correlation upto 1100K where it becomes slightly lower but comparable to Carbajo and (Van Uffelen and Schubert) upto 1800 K where it starts to give higher values than both of them but still lower than Wiesenack and (Lanning and Beyer). At 2200K, it starts to become higher than Lanning and beyer but still lower than Weisenack.

In *Fig.27*, The same plot as in *Fig.26* is done but the Plutonium content was reduced to 10%.wt. TRANSURANUS correlations do not consider Pu content so they remain the same. The situation is the same for Martin's review. As for MATPRO correlation an expected increase in Thermal conductivity occurs. The rate of increase of thermal conductivity for COMETHE formulation is stronger than for MATPRO. The thermal conductivities predicted by COMETHE is now higher than Martin's and almost comparable to MATPRO below 1000K. With more decrease of Pu content, COMETHE becomes higher than MATPRO for temperature upto 1100 for pure UO_2.

For Baron-Hervè correlation, As the Pu content increase, thermal conductivity increases and follows Martin's at temperature upto 1100 K then follows Weisenack's correlation for the rest of the temperature range.

In *Fig.26* when O/M ratio is reduced to 1.96. It is obvious at lower temperatures that the open literature correlations, except MATPRO, predict a higher degradation with deviation from stoichiometry than TRANSURANUS correlations that takes O/M ratio into account (Carbajo-Lanning and beyer). At 1700 K it can be noticed that Martin review and COMETHE formulation begins to follow Carbajo's correlation. For the whole range of temperature, Baron and hervè's correlation is lower than all the others except below 950 K where it is slightly higher than Martin's review.

With O/M and Pu content decreased to 1.96 and 10%.wt *Fig.27*, the open literature correlations that takes Pu content into account are still lower than Transuranus correlations in general. COMETHE

formulation is higher than Carbajo for T<900 K then decreases up to 1600 where it becomes higher than Carbajo again but still lower than Lanning and beyer for the whole range of temperature. Baron and Hervè's correlation becomes higher than Martin's up to 1300 K. It decrease again upto 2150 K where it increases again.

It this section there were no need to plot another figure at higher burn-up value since this was done in section 2.5 for TRANSURANUS correlations. The open literature correlations that were studied here do not have burn-up as a variable. So the figure is expected to be a plot where TRANSURANUS predicted thermal conductivites degrade with burn-up for the same porosity and stoichiometry level and the open literature remains in their high level.

It is important to note that even if the open literature models do not take burn-up as an explicit variable affecting thermal conductivity, it does not mean that the thermal conductivity would not degrade with irradiation. It means that with irradiation, the fuel structure would change and it would have different level of porosity and stoichiometry and that would lead to a degradation of thermal conductivity with burn-up.

So, in order to compare TRANSURANUS correlations that takes burn-up as an explicit variable with the considered open literature correlations at higher burn-up, one must compare them with open literature correlations at a different level of porosity and stoichiometry corresponding to the new level of burn-up which is out of the scope of this study for now.

Finally a comparison is made between Martin's review and COMETHE formulation and the physically based correlation of Killeen. This is done for stoichiometric fuel with 20%.wt Pu content. This is justified by what Martin recommendations in his paper[7] that Killeen's equation is more preferred but due to lack of knowledge of how to project this correlation to non-stoichiometric fuel, Washington's recommendation was considered a suitable substitute.

It can be noticed from *Fig.28* that COMETHE formulation is consistent with Washington's equation at lower temperature range upto 1000K where there is a slight deviation between the two upto 1300K. Then the COMETHE formulation follows Killeen's model better than the review of Martin. From 2300 K both correlations deviates from Killeen's model. COMETHE correlation has larger deviation from Martin's review than Martin's at high temperatures.

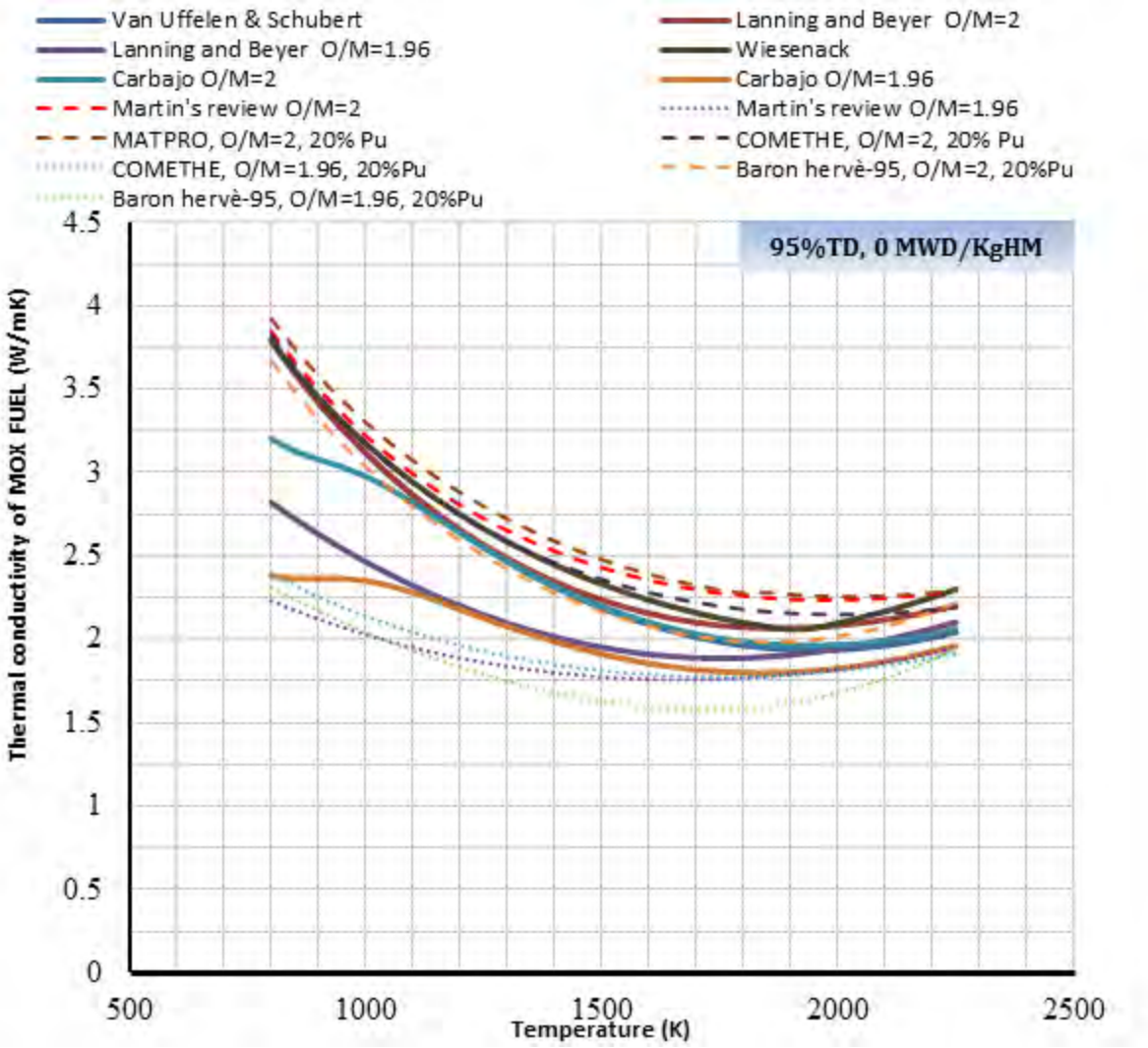

Fig.26 - Thermal conductivity models of TRANSURANUS and open literature models at 20%.wt Pu.

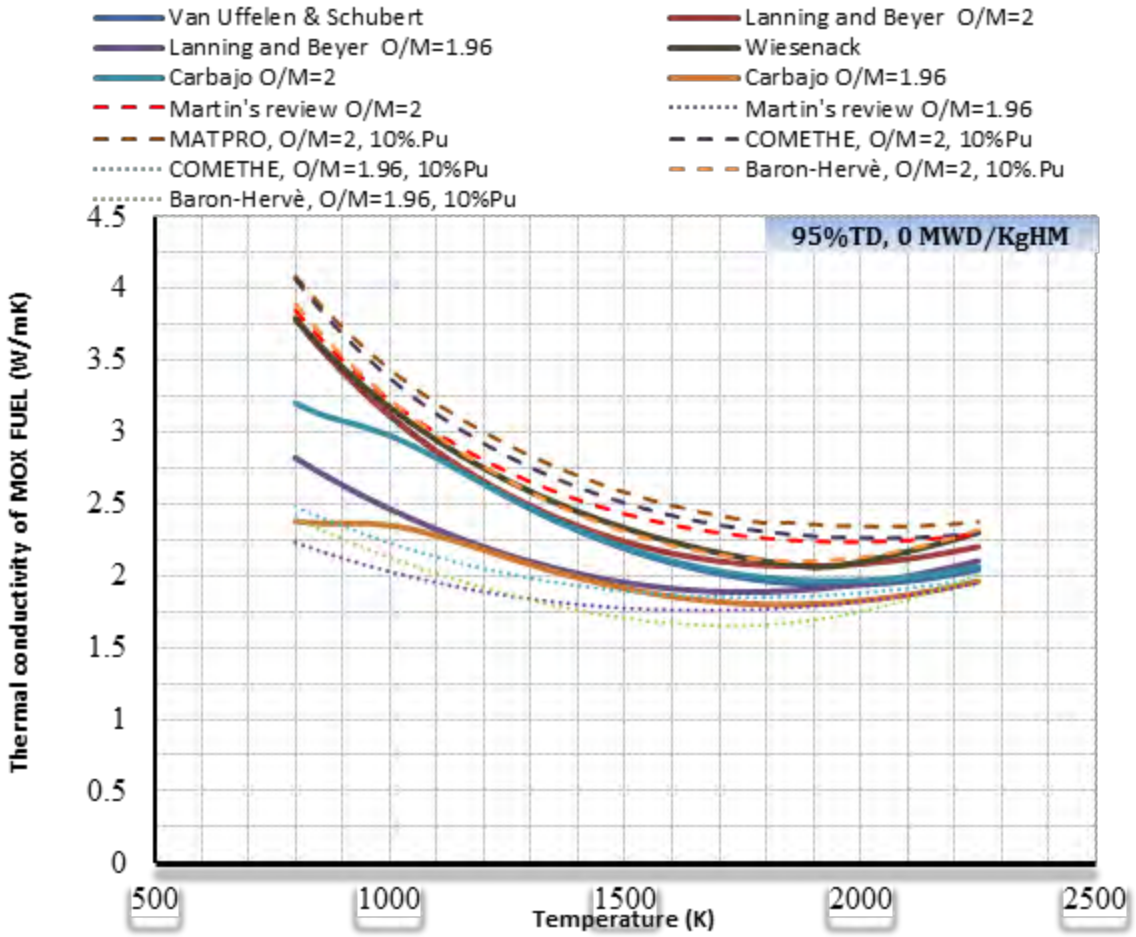

Fig.27 - Thermal conductivity models of TRANSURANUS and open literature models at 10%.wt Pu.

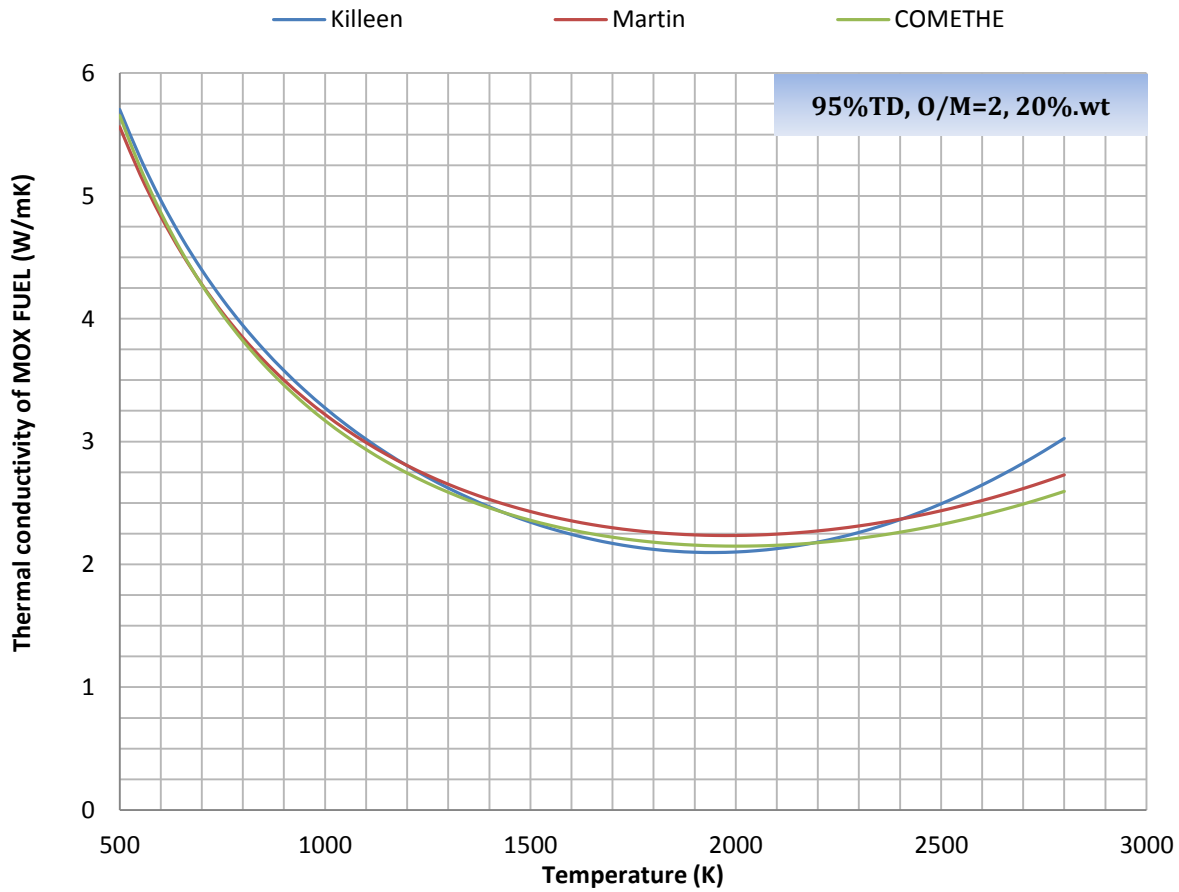

Fig.28 - Thermal conductivities of the Killeen, Martin and COMETHE correlations.

REFERENCES

[1] *Rozzia Davide, Del Nevo Alessandro,* **Modeling of FGR in nuclear reactor UO_2 fuel and its extension to MOX fuel.**

[2] *G.J.Hyland,* **Thermal conductivity of solid uo2: critique and recommendation 1982.** *J. Nuclear Materials 113 (1983) 125-132*

[3] *D. R. Olander,* **Fundamental Aspects of Nuclear Reactors Fuel Elements**. Department of Nuclear Engineering University of California, Berkeley, 1976.

[4] *http://en.wikipedia.org/wiki/Heat_transfer#Radiation,* Last check 22-09-2014

[5] **SCDAP/RELAP5/MOD3.1 Code manual volume4: MATPRO—A library of materials properties for light water reactor accident analysis.**

[6] *Neil E. Todreas, Mujid S. Kazimi,* **Nucleaer Systems I, thermal Hydraulic Fundamentals 1st edition.** Massachusetts Institute of Technology, 1990.

[7] *D.G. Martin*, **A reappraisal of the thermal conductivity of UO_2 and mixed (U,Pu) oxide fuels.** Journal of Nuclear Materials 110 (1982) 73-94.

[8] *Christian Duriez, Jean-Pierre Alessandri, Thierry Gervais, and Yannick Philipponneau,* **Thermal conductivity of hypostoichiometric low Pu content $(U,Pu)O_{2-x}$ mixed oxide.** J. Nuclear Materials 277 (2000) 143-158.

[9] *C.Ronchi, M. Sheindlin, M. Musella, and G.J. Hyland,* **Thermal conductivity of uranium dioxide up to 2900 K from simulations measurement of the heat capacity and thermal diffusivity.** J. Applied Physics 85, 776 (1999)

[10] Juan J. Carbajo, Gradyon L.Yoder, Sergey G. Popov, and Victor K. Ivanov, **A review of the thermophysical properties of MOX and UO_2 fuels.** J. Nuclear Materials 299 (2001) 181-198

[11] *Daniel Baron,* **Fuel thermal conductivity: A review of the modeling available for UO_2, $(U\text{-}Gd)O_2$ and MOX fuel.** Thermal performance of high burn-up LWR fuel, seminar proceddings Cadarache, France 3-6 March, 1998.